International
Progress Report

IPR-02-11

Äspö Hard Rock Laboratory

Estimation of rock mass strength and deformation in three dimensions for four 30m cubes located at a depth region of 380-500m at Äspö HRL

Pinnaduwa H.S.W Kulatilake
Jinyong Park
Jeong-Gi Um

Kulatilake & Associates

March 2002

Svensk Kärnbränslehantering AB
Swedish Nuclear Fuel
and Waste Management Co
Box 5864
SE-102 40 Stockholm Sweden
Tel +46 8 459 84 00
Fax +46 8 661 57 19

Äspö Hard Rock
Laboratory

Report no.	No.
IPR-02-11	F102K
Author	Date
Kulatilake, Park, Um	01-12-03
Checked by	Date
Christer Andersson, Rolf Christiansson	02-04-03
Approved	Date
Christer Svemar	02-04-09

Äspö Hard Rock Laboratory

Estimation of rock mass strength and deformation in three dimensions for four 30m cubes located at a depth region of 380-500m at Äspö HRL

Pinnaduwa H.S.W Kulatilake
Jinyong Park
Jeong-Gi Um

Kulatilake & Associates

March 2002

Keywords: 3DEC, Rock block strength, Rock block deformability

Abstract

The location of a rock mass volume termed the NGI's (Norwegian Geotechnical Institute's) box in the three-dimensional (3-D) space at the ASPO Hard Rock Laboratory was shown in a previous report (Kulatilake and Um, 2001). The NGI box was divided into 480 blocks of 30m cubes. The same previous report provides details pertaining to selection of the following four 30m cubes from the NGI box, each having a different lithology: (a) NGI block number 409---Aspo diorite; (b) NGI block number 169----Smaland granite; (c) NGI block number 5---fine grained granite; (d) NGI block number 49----a mixed lithology consisting of about 49% Smaland granite, 22% Aspo diorite, 15% greenstone and 14% fine grained granite. Development and validation of a stochastic 3-D fracture network model for each of the selected 4 NGI blocks are also addressed in the same previous report. This report covers the procedures developed to estimate rock block strength and deformability in three-dimensions for the selected four 30m cubes of the NGI box and the results obtained.

The mean intact rock strength at the 4 NGI blocks studied lie between 267 and 303 MPa. These values indicate that the intact rock is strong. For NGI block #s 409, 169, 5 and 49 the ratio of mean rock mass strength/mean intact rock strength was found to be 47%, 44%, 42% and 27%, respectively. For the 4 NGI blocks studied, the rock mass modulus was found to be between 49.9% and 57.5% of the intact rock Young's modulus value. The rock mass Poisson's ratio was found to be about 11-21% higher than the intact rock Poisson's ratio value. These percentages indicate the levels of weakening of the rock masses due to the presence of fractures. The 4 blocks studied can be arranged in the following order with respect to decreasing rock mass strength and increasing deformability: block # 469, block # 169, block # 5 and block # 49.

For NGI block #s 409, 169, 5 and 49 the ratio of mean major principal rock mass strength/mean minor principal rock mass strength turned out to be 1.28, 1.32, 1.21 and 1.18, respectively. The values of 1.21, 1.13, 1.15 and 1.06 were obtained for the ratio of mean major principal rock mass modulus/mean minor principal rock mass modulus for NGI block #s 409, 169, 5 and 49, respectively. Reasons are given in the report to support the statement that most probably the obtained results for anisotropy of rock mass strength and deformability are less than the actual level of anisotropy that exists in the field. The available orientation data for the project were inadequate with respect to both the quality and quantity. Therefore, the confidence level of the calculated anisotropic directions and the corresponding magnitudes for rock mass parameters is low.

Sammanfattning

Läget för bergvolymen benämnd NGI-volymen (Norges Geotekniska Institut) i Äspö Hard Rock Laboratory redovisas i Kulatilake och Um (2002). Volymen är indelad i 480 kubiska block med en kantlängd av 30 meter. Kulatilake och Um (2002) redovisar även hur fyra av blocken, alla med olika bergartssammansättning, valdes. De valda blocken är: (a) NGI block 409 -- Äspödiorit, (b) NGI block 169 -- Smålandsgranit, (c) NGI block 005 -- finkornig granit, NGI block 049 -- bestående av en blandad geologi med cirka 49% Smålandsgranit, 22% Äspödiorit, 15% grönsten och 14% finkornig granit. Ovanstående referens redogör även för framtagandet och valideringen en stokastiskt 3-D sprickmodell för vart och ett av de 4 blocken ur NGI-volymen. Denna rapport redogör för hur arbetet med att bedöma blockens tryckhållfasthet och tredimensionella deformationsegenskaper gått till samt redovisar de resultat som erhållits.

Medelvärdet för det intakta bergets tryckhållfasthet i de 4 valda blocken ur NGI-volymen ligger mellan 267 och 303 MPa vilket visar på ett hållfast berg. För NGI blocken med nummer 409, 169, 5 och 49 är kvoten mellan medelvärdet på bergmassans tryckhållfasthet/medelvärdet på det intakta bergets tryckhållfasthet 47%, 44%, 42% respektive 27%. För de 4 studerade blocken befanns bergmassans elasticitetsmodul vara mellan 49,9% och 57,5% av det intakta bergets elasticitetsmodul. Bergmassans tvärkontraktionstal befanns vara cirka 11-21% högre än tvärkontraktionstalet för det intakta berget. Ovan givna procentsatser indikerar graden av försvagning av bergmassan på grund av befintliga sprickor. De 4 studerade blocken kan delas in i följande ordning med hänsyn till sjunkande tryckhållfasthet och ökande deformationsegenskaper i bergmassan: block # 409, block # 169, block # 5 och block # 49.

För NGI blocken med nummer 409, 169, 5 och 49 befanns kvoten mellan bergmassans tryckhållfasthet i riktning med den största huvudspänningen och bergmassans tryckhållfasthet i riktning med den minsta huvudspänningen vara 1,28; 1,32; 1,21 respektive 1,18. Kvoten mellan bergmassans elasticitetsmodul i största respektive minsta huvudspänningens riktning befanns vara 1,21; 1,13; 1,15 respektive 1,06 för NGI blocken numrerade 409, 169, 5 och 49. I rapporten finns anledningar givna som stödjer påståendet att den erhållna anisotropin för bergmassans tryckhållfasthet och deformationsegenskaper är mindre än den anisotropi som kan förväntas i den verkliga bergmassan. Den tillgängliga informationen för detta projekt var inte tillräcklig med avseende på både kvalitet och kvantitet. Detta är anledningen till att anisotropiernas konfidensintervall för de beräknade parametrarnas riktningarna och magnituder är för låga.

Table of Contens

1. Introduction

The location of the NGI box in the three-dimensional (3-D) space at the ASPO Hard Rock Laboratory was shown in a previous report submitted by Kulatilake & Associates (Kulatilake and Um, 2001) using the 3-D rectangular Cartesian coordinate data provided for the NGI's (Norwegian Geotechnical Institute's) box. The NGI box was divided into 480 blocks of 30m cubes. NGI provided the 3-D coordinates for the center of each cube. The orientation and location data given for the three boreholes KAS02, KA2598A and KA2511A were used to show the location of the boreholes in the 3-D space with respect to the location of the NGI box (Kulatilake and Um, 2001). It was found that the borehole KA2511A only just touches the NGI box. The other two boreholes were found to intersect the NGI box. The lithology data provided for the boreholes KAS02 and KA2598A were used to select the following four 30m cubes from the NGI box, each having a different lithology which is given below (Kulatilake and Um, 2001): (a) NGI block number 409---Aspo diorite; (b) NGI block number 169----Smaland granite; (c) NGI block number 5---fine grained granite; (d) NGI block number 49----a mixed lithology consisting of about 49% Smaland granite, 22% Aspo diorite, 15% greenstone and 14% fine grained granite. The fracture data made available for the project were used to develop and validate a stochastic 3-D fracture network model for each of the selected 4 NGI blocks (Kulatilake and Um, 2001). This report covers the estimation of rock block strength and deformability for the selected four 30m cubes of the NGI box.

2. Principal in-situ stresses for the chosen four 30M blocks

A previous report (Kulatilake and Um, 2001) provides the cube ID number, rock unit or lithology and the location for each of the chosen four 30m blocks. This information is reproduced in Table 2.1 of this technical report. Klasson and Leijon (1989) provide the magnitudes and directions of the principal in-situ stresses resulting from the in-situ stress measurements performed in borehole number KAS02. Note that the same borehole goes through NGI's box cubic ID numbers 49, 169 and 409. Therefore, in-situ stress measurement results coming out of KAS02 borehole are ideally suited to estimate principal in-situ stresses for cubic ID numbers 49,169 and 409. Table 3 of the report by Klasson and Leijon (1989) provides the calculated vertical overburden stress, S_v, minimum horizontal stress, S_h, and maximum horizontal stress, S_H, values at depths 381m, 390m, 426m and 495m. For S_H, one value based on the first breakdown method and another value based on the second breakdown method are given. The report mentions that the value based on the second breakdown method has better accuracy than that of the first breakdown method. Therefore, for the current study, the values based on the second breakdown method are used to represent S_H at different depths. The mean depth of cubic ID number 409 is 485m. The mean S_v value at 485m depth was calculated based on the unit weight of rock calculated using the S_v value available at 495m depth. The mean S_v value estimated at 485m was then used along with the ratios of S_h/S_v and S_H/S_v available at 495m to estimate mean S_h and S_H values at 485m depth. For cubic ID numbers 49 and 169, the mean depths are respectively 395m and 425m. A procedure similar to the aforementioned was used in estimating the mean S_v, S_h and S_H at depths 395m and 425m for cubic ID numbers 49 and 169, respectively based on the S_v, S_h/S_v and S_H/S_v values available at depths 390m and 426m, respectively. Table 4 of the report by Klasson and Leijon (1989) provides the direction for S_H at depths 381m, 390m, 426m and 495m. These values do not show a clear trend for the direction of S_H with depth. Therefore, the S_H direction values available at depths 390m, 426m and 495m were used to represent the mean direction of S_H at depths 395m, 425m and 485m, respectively. Mean values for the direction of S_h at depths 395m, 425m and 485m were selected to preserve the perpendicularity between S_h and S_H directions. The aforementioned estimated mean values are given in Table 2.1. Please note that for all four cubic ID numbers considered, S_H is the major principal stress, σ_1. For depths 395m and 425m, S_v and S_h are the intermediate principal stress, σ_2, and minor principal stress, σ_3, respectively. For depth 485m, S_v and S_h are the minor principal stress and intermediate principal stress, respectively.

Table 2.1 Estimates of magnitudes and directions of principal in-situ stresses for different NGI block numbers

NGI block #		409	169	5	49
Lithology		Äspö diorite	Småland granite	Fine grained granite	Mixed lithology
Coordinates of block center	X, Northing, (m)	7283.22	7283.22	7335.78	7283.22
	Y, Easting, (m)	2087.20	2087.20	1963.76	2087.20
	Z, Depth (m)	485.00	425.00	395.00	395.00
Major principal stress, σ_1	mean magnitude (MPa)	22.75	17.73	13.38	13.38
	uncertainty (MPa)	± 3	± 3	± 3	± 2.5
	confidence level	2	2	2	2
Intermediate principal stress, σ_2	mean magnitude (MPa)	13.90	11.08	10.29	10.29
	uncertainty (MPa)	± 2	± 0.5	± 0.5	± 0.5
	confidence level	2	2	2	2
Minor principal stress, σ_3	mean magnitude (MPa)	12.64	8.86	7.20	7.20
	uncertainty (MPa)	± 0.5	± 2	± 2.5	± 2
	confidence level	2	2	2	2
Trend of σ_1, α_1	mean (degs.)	143	138	121	121
	uncertainty (degs.)	± 10	± 10	± 10	± 10
	confidence level	2	2	2	2
Plunge of σ_1, β_1	mean (degs.)	0	0	0	0
	uncertainty (degs.)	± 5	± 5	± 5	± 5
	confidence level	2	2	2	2
Trend of σ_2, α_2	mean (degs.)	53	-	-	-
	uncertainty (degs.)	± 10	± 10	± 10	± 10
	confidence level	2	2	2	2
Plunge of σ_2, β_2	mean (degs.)	0	90	90	90
	uncertainty (degs.)	± 5	± 5	± 5	± 5
	confidence level	2	2	2	2
Trend of σ_3, α_3	mean (degs.)	-	48	31	31
	uncertainty (degs.)	± 10	± 10	± 10	± 10
	confidence level	2	2	2	2
Plunge of σ_3, β_3	mean (degs.)	90	0	0	0
	uncertainty (degs.)	± 5	± 5	± 5	± 5
	confidence level	2	2	2	2

The uncertainty of S_v results from uncertainty of assumed lithology units of overburden, thickness of each lithology unit, estimated unit weight value for each lithology unit and correctness of the assumption of horizontal ground level in estimating the overburden stress. These factors are considered in coming up with the uncertainty value given for S_v in Table 2.1. Vertical direction is considered as one of the principal stress directions based on the assumption of horizontal ground level in the NGI box area. Uncertainty level of the vertical direction depends on how good this assumption is. The uncertainty values assigned in Table 2.1 for the magnitudes and directions of S_h and S_H are based on the measured values given in the report by Klasson and Leijon (1989).

The mean depth of cubic ID number 5 is 395m. Although measured in-situ stress values are available at a depth of 395m, with respect to the horizontal coordinates, in-situ stress measurements are not available very close to the location of cubic ID number 5. Also, in-situ stress values are not available to estimate spatial variation of in-situ stress on horizontal planes. Therefore, the mean in-situ stress values selected for cubic ID number 49 (at a depth of 395m) were also used to represent the mean in-situ stresses for cubic ID number 5. The uncertainty values assigned for cube ID number 5 in Table 2.1 for the magnitudes and directions of S_h and S_H are based on the measured values given in the report by Klasson and Leijon (1989) for the depth 395m plus the uncertainty resulting from lack of in-situ stress data close to the location of cube ID number 5. According to the specifications given in the report by Andersson (2001), a confidence level of 2 can be assigned for the estimated in situ stresses given in Table 2.1.

3.Estimation of rock mass mechanical parameters in three dimensions

3.1. Intact Rock Strength

The 30m cubic block was discretized into many intact rock deformable blocks. A mean value of 2765 kg/m^3 and an uncertainty of ±55 kg/m^3 (Nisca, 1988) were used to represent the density of intact rock for all four selected lithologies. Mechanical behaviour of each deformable block was represented by an isotropic linear elastic model up to the peak strength and a strain-softening model between the peak strength and the residual strength. Note that the mechanical property data are available only for Aspo diorite (Nordlund et al., 1999). Therefore, for all four NGI blocks (lithologies) considered in this report, mechanical properties were represented using the data available for Aspo diorite. Pre-peak deformation behaviour was represented by a Young's modulus, E, value of 73 ± 3 GPa and a Poisson's ratio, ν, value of 0.28 ± 0.02. The peak strength was represented by the Mohr-Coulomb criterion with a tension cut-off (cohesion, C = 49 ± 5 MPa, friction angle, ϕ = 44 ± 4 degrees, tensile strength, σ_t, value of 14.7 ± 2.0 MPa). The residual strength was represented by a cohesion value of 1.23 MPa, a friction angle of 35.2 degrees and a tensile strength of 1.05 MPa. Values used to represent intact rock of all four 30m cubes are shown in Table 3.1.

Table 3.1 Values used to represent intact rock properties for the considered 4 NGI blocks

Intact rock property	Mean value	Uncertainty
Density (kg/m^3)	2765	± 55
Pre-peak linear elastic parameters		
Young's modulus, E, (GPa)	73	± 3
Poisson's ratio, ν	0.28	± 0.02
Bulk modulus, K, (GPa)	55.3	± 3
Shear modulus, G, (GPa)	28.5	± 3
Peak strength parameters		
Cohesion, C, (MPa)	49	± 5
Friction angle, ϕ, (deg.)	44	± 4
Tensile strength, σ_t, (MPa)	14.7	± 2.0
Residual strength parameters		
Residual cohesion, C_{res}, (MPa)	1.23	-
Residual friction angle, ϕ_{res}, (deg.)	35.2	-
Residual tensile strength, $(\sigma_t)_{res}$, (MPa)	1.05	-

Table 3.2 Estimates of intact rock strength in principal in-situ stress directions for different NGI block numbers

NGI block #	Lithology	Coordinates of block center			Intact rock strength (MPa)					
					In σ_1 direction		In σ_2 direction		In σ_3 direction	
		X (m)	Y (m)	Z (m)	mean	Uncertainty: 5/95 percentiles	mean	Uncertainty: 5/95 percentiles	mean	Uncertainty: 5/95 percentiles
409	Äspö diorite	7283.2	2087.2	485	291.6	262-321	297.0	267-327	303.2	273-333
169	Småland granite	7283.2	2087.2	425	275.2	248-303	275.8	248-303	287.0	258-316
5	Fine grained granite	7335.8	1963.8	395	267.4	241-294	270.1	243-297	282.6	254-311
49	Mixed lithology	7283.2	2087.2	395	267.4	241-294	270.1	243-297	282.6	254-311

Note: Confidence level of the intact rock strength values given in the table = 2

Each 30 m block corresponding to a different lithology was subjected to the mean principal in-situ stresses given in Table 2.1. Mechanical properties of each intact material element in the block were represented by the mean values given in Table 3.1. Keeping two of the principal stresses constant, the stress in the third direction was increased by applying a constant velocity of 0.05 m/sec in that direction until the block failed. This was repeated in each of the three mean principal stress directions. These stress analyses were conducted using the 3DEC code (Itasca, 1999). The results (Table 3.2) basically provide the anisotropic mean intact rock strength values resulting from the anisotropy of the in-situ stress system. As an example, stress-strain diagrams obtained for Aspo diorite in the three mean principal in-situ stress directions are shown in Figs. 3.1a-c. Uncertainty of estimated intact rock strength arises due to the variability of the intact rock properties

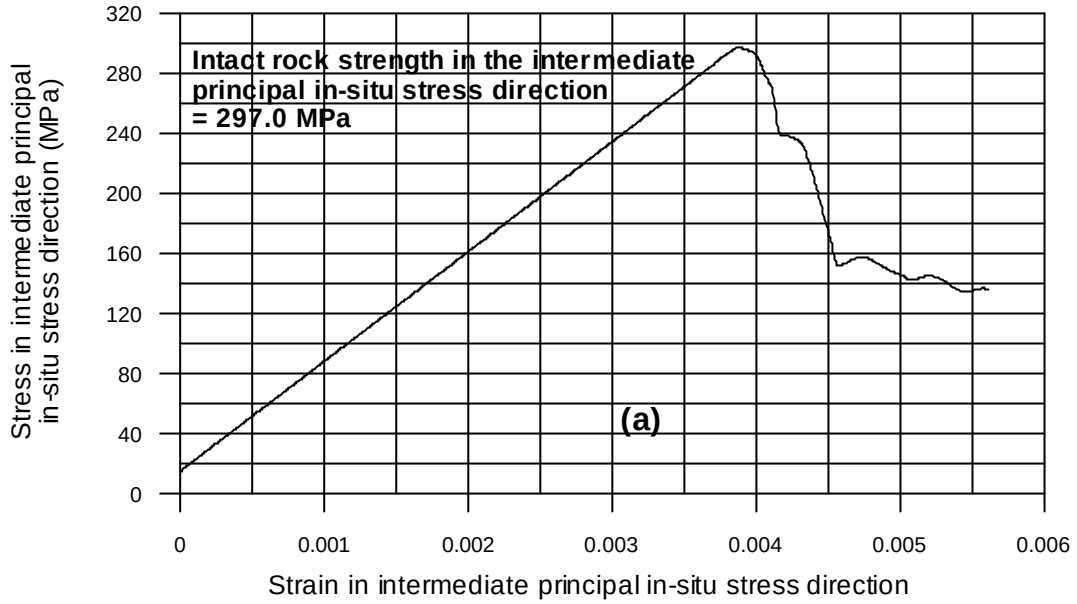

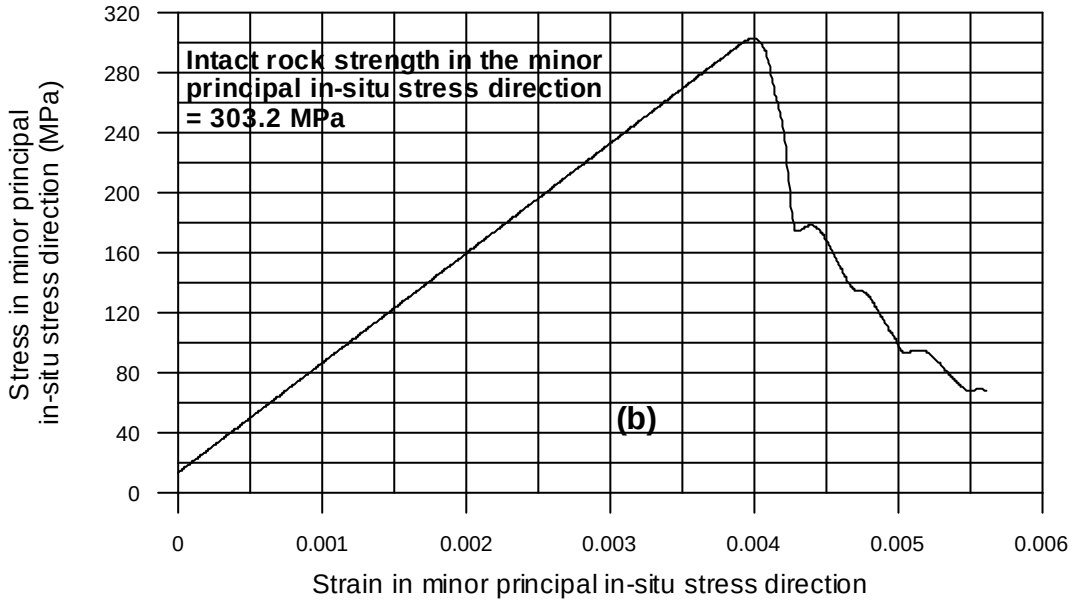

Fig. 3.1 *Intact rock strength at NGI block #409 (Äspö diorite) in the principal in-situ stress directions*

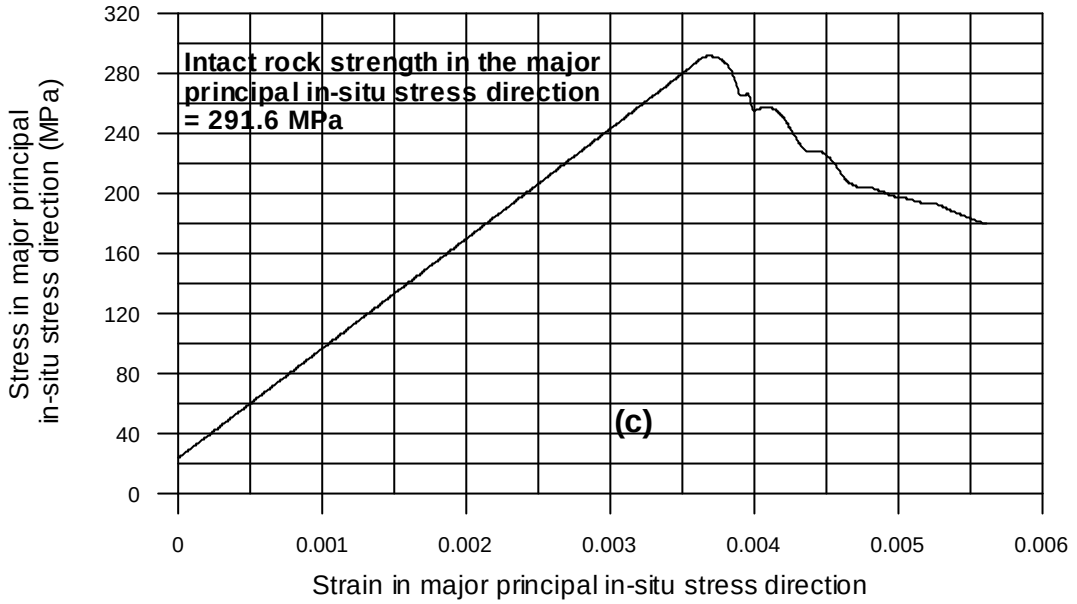

Fig. 3.1 *Continued*

and the uncertainty of principal in-situ stress values. Intact rock strength calculations in the same three directions were repeated for the following two cases: (a) using the lowest possible principal in-situ stresses combined with the lowest strength and highest deformability intact rock material properties; (b) using the highest possible principal in-situ stresses combined with the highest strength and lowest deformability intact rock material properties. The obtained results were used to estimate the uncertainty values given in Table 3.2. It seems reasonable to assign a confidence level of 2 for the intact rock strength values given in Table 3.2.

3.2. Rock Mass Strength and Deformability Estimation

3.2.1. Procedures

A previous report (Kulatilake and Um, 2001) provided the fracture network model developed for each of the four selected 30m cubic blocks. Three-dimensional intensities of 0.30, 0.23, 0.29 and 0.37 fractures per m^3 were obtained for Aspo diorite, Smaland granite, fine grained granite and mixed lithology, respectively. These three dimensional intensities produce 8100, 6210, 7830 and 9990 fractures in a 30m block of Aspo diorite, Smaland granite, fine grained granite and the mixed lithology, respectively. In addition, these fractures are of finite size. To perform stress analysis using the 3DEC code, it is necessary to discretize the entire domain into polyhedra (Cundall, 1988; Hart et al., 1988). In general, the intersection of only the finite size fractures does not discretize the domain into polyhedra. However, the needed polyhedra can be obtained by introducing fictitious joints into the considered block and combining them with the actual fractures

(Kulatilake et al., 1992) that exist in each of the 30m cubic blocks. Such a procedure creates a large number of polyhedral blocks in a 30m cube. Just one 3-D stress analysis of such a 30m block using the 3DEC code on a personal computer can easily take several months. Therefore, due to time constraints of the project, it was necessary to come up with a procedure to obtain 3D stress analyses results for a 30m cube that can capture the anisotropy in 3D within about two weeks. The stress analysis procedure given below was developed to fulfill the needed requirement.

After a few trial 3-D stress analysis runs, it was decided to perform 3-D stress analysis at a number of increasing cubic block sizes before reaching the 30m cubic size. For each of these different cubic block sizes, it was decided to limit the maximum number of fractures to 16. With this arrangement, it was possible to complete a 3-D stress analysis for a selected cubic block size in one particular direction within about 3 to 4 hours using a personal computer having the Intel Pentium IV processor with a speed of 1.5 GHz. The different block sizes needed for a particular lithology was decided as follows. First the largest 16 discontinuities that exist in the generated 30m cube was found. The size of the smallest discontinuity out of these 16 discontinuities was noted. A cubic block of this discontinuity size was then placed with its center exactly coinciding with the center of the 30m cubic block. The largest 16 discontinuities of this second block were found and the size of the smallest discontinuity out of these 16 discontinuities noted. A cubic block of the latter mentioned discontinuity size was then placed with its center coinciding with the center of the 30m cube. This procedure was repeated until a block size was found that contains less than or equal to 16 discontinuities. For example, when this procedure was applied to Aspo diorite, the following sequence of block sizes was obtained: 5.8, 7.2, 8.0, 9.6, 12.3 and 30.0m. Note that apart from the 30m cubic block, all other block sizes contain a discontinuity of size close to the size of the block. In these blocks, a significant number of discontinuities may intersect the block boundaries. On the other hand, if the discontinuities that exist inside one of these blocks are located inside the 30m block, most of them do not then intersect any of the boundaries. In order to simulate this situation in all the block sizes apart from the 30m block, all the block sizes were set to the maximum discontinuity size within the block plus the mean discontinuity size in the block. For example, with this adjustment, the following sequence of block sizes was used to perform 3-D stress analyses for Aspo diorite lithology: 9.5, 13.5, 15.5, 18.3, 21.9 and 30m. From now onwards, in the report, the different increasing block sizes used are referred to as the smallest, second, third block size so on.

For each selected lithology, the 3-D stress analysis was first performed on the smallest block size. Each of these blocks contains intact rock and actual fractures. As mentioned before, the maximum number of fractures in any block was limited to 16. Because these fractures are of finite extent, these fractures themselves do not discretize the entire block domain into polyhedra. On the other hand, to perform 3DEC stress analysis, the domain should be discretized into polyhedra. However, the needed polyhedra can be obtained by introducing fictitious joints to the block and combining them with the actual fractures. These fictitious joints should then behave as intact material elements. Kulatilake et al. (1992) developed such a procedure to estimate equivalent continuum mechanical properties for rock blocks that contain actual fractures. In addition they gave procedures

to estimate the mechanical properties of fictitious joints that are included in these blocks. The shear stress-shear displacement behaviour of fictitious joints was modeled as linear elastic up to peak shear strength and perfect plastic beyond peak shear strength. Linear elastic shear behaviour was represented by the joint shear stiffness, JKS. Kulatilake et al. (1992) suggested the expression shear modulus (G)/JKS = 0.01m to estimate the JKS value for fictitious joints. This expression was used with the mean G value of the intact rock (28.5 GPa) to obtain mean JKS as 2852 GPa/m. The perfect-plastic shear strength behaviour was modeled by the Mohr-Coulomb criterion with a tension cut-off. Because the fictitious joints should behave as intact rock material, the same C, ϕ and σ_t values as for the intact rock were used to represent the strength of fictitious joints. Normal stress-normal displacement behaviour of fictitious joints was represented by a constant joint normal stiffness, JKN. Mean JKN of fictitious joints was estimated as 7130 GPa/m using the relation JKN/JKS = 2.5 given by Kulatilake et al. (1992). Intact material parameter values given in Table 3.1 were used to represent the physical and mechanical behaviour of the intact material portion of the cubic blocks for all four lithologies.

The shear stress-shear displacement behaviour of actual fractures was modeled as linear elastic up to peak shear strength and perfect plastic beyond peak shear strength. Linear elastic shear behavior was represented by the joint shear stiffness, JKS. A report by Lanaro (2001) provides initial, peak and reloading JKS values at different normal stresses. The highest normal stress used for JKS determination was 10 MPa. The average in situ stresses of the four 30m cubic blocks considered in this report are either around 10 or greater than 10 MPa. In Lanaro's report, one set of JKS values is given for sub-horizontal fractures and another set of JKS values is given for sub-vertical fractures. Reloading JKS values given at a normal stress of 10 MPa are selected for the calculations performed in the current work. Accordingly, a mean value of 43.4 GPa/m along with a coefficient of variation of 0.26 were selected to represent JKS of sub-horizontal fractures. For sub-vertical fractures, a mean value of 45.2 GPa/m along with a coefficient of variation of 0.23 were selected to represent JKS. To be on the conservative side, the fracture shear strength was modeled by a Mohr-Coulomb criterion with a residual friction angle and zero cohesion and tensile strength. For sub horizontal fractures, a residual friction angle of 27 degrees was used (Lanaro, 2001). A residual friction angle of 32 degrees was used for sub-vertical fractures (Lanaro, 2001). The normal stress-normal displacement behaviour of actual fractures was represented by a constant joint normal stiffness, JKN. For sub-horizontal fractures, reloading JKN values (mean= 1628 GPa/m with a coefficient of variation of 0.68) available at a normal stress range of 0.5 to 30 MPa (Lanaro, 2001) were used to represent JKN of actual fractures. For sub-vertical fractures, reloading JKN values (mean= 187 GPa/m with a coefficient of variation of 0.71) available at a normal stress range of 0.5 to 15 MPa (Lanaro, 2001) were used to represent JKN of actual fractures. Table 3.3 provides the values used to represent the mechanical properties of actual fractures.

Table 3.3 Values used to represent mechanical properties of actual fractures for all four considered lithologies

Mechanical parameter	Sub-horizontal fractures		Sub-vertical fractures	
	mean value	cov	mean value	cov
Shear stiffness, JKS	43.4 (GPa)	0.26	45.2 (GPa)	0.23
Normal stiffness, JKN	1628 (GPa/m)	0.68	187 (GPa/m)	0.71
Friction angle, ϕ	27 (deg.)	-	32 (deg.)	-
Cohesion, C	0	0	0	0
Tensile strength, σ_t	0	0	0	0

Note: cov = coefficient of variation

As mentioned before, for a particular selected lithology (NGI block number), prior to performing stress analysis on the 30m cube, 3-D stress analyses were performed on several increasing cubic block sizes smaller than 30m. Due to time constraints, 3-D stress analysis was performed only in three perpendicular directions for all the cubic block sizes that were less than 30m cube. However, for the 30m cube, the stress analysis was performed in 18 directions to cover the entire 3-D space. The local coordinate system shown in Figure 3.2 was introduced to the cube to keep track of the block rotation. Note that the coordinate system shown in Figure 3.2 rotates with the rotation of the cubic block. At the zero degree rotation, the Z and X axes coincide with north and east, respectively and Y axis points in the vertical upward direction. All the block rotations are expressed with respect to the rotation of the Z axis. A clockwise rotation of Z on the horizontal plane and an upward rotation of Z on the vertical plane are assumed as positive rotations. For each of the smallest cubic blocks, physical and mechanical properties of intact rock, fictitious joints and actual fractures were assigned according to the values

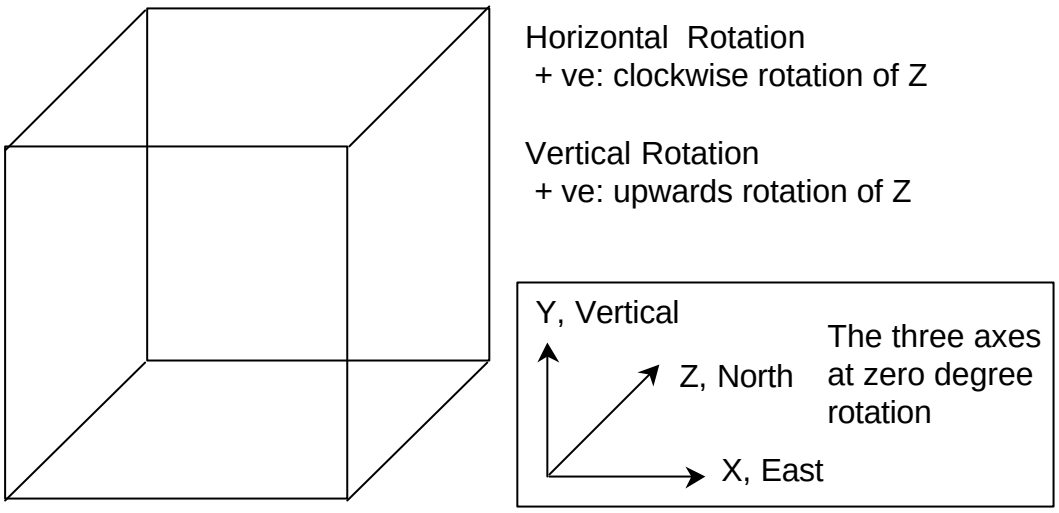

Fig. 3.2 *Co-ordinate system and conventions used to keep track of block rotation*

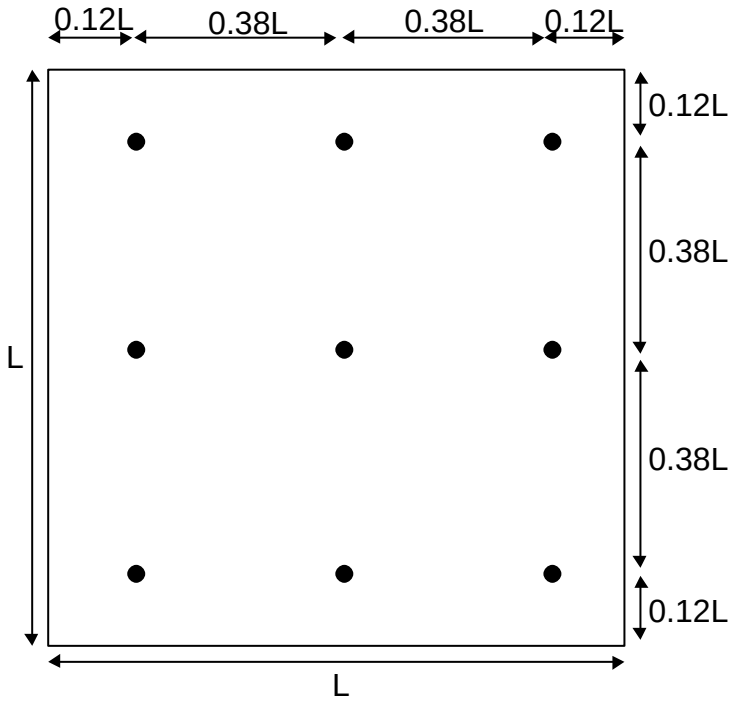

Fig. 3.3 *Location of the nine points selected on each face to monitor the stress and deformation of each block*

mentioned in the aforementioned paragraphs. On each face of the block as shown in Figure 3.3 nine points were marked to monitor deformation and stress of each block.

The in-situ stress system for the block rotation of -135 degrees on the horizontal plane and 45 degrees on the vertical plane was calculated to apply for each of the smallest cubic blocks to bring them to in-situ equilibrium stress condition in the chosen direction. Then in a direction perpendicular to one of the parallel faces, the block was subjected to a constant velocity boundary condition and monitored the deformation and stress of the block. The displacements and stresses recorded on the monitoring points on the two faces perpendicular to the direction of applied velocity were used to calculate the average stress-strain diagram of the block in the applied velocity direction. This stress-strain diagram was used to estimate the Peak shear strength and the rock mass modulus (tangent modulus at 50% peak strength level) of the block in the applied velocity direction (see Kulatilake et al., 1993 for detailed procedures). The monitored deformations of the other faces of the block were used along with the monitored deformations of the two parallel faces perpendicular to the applied velocity direction to estimate two of the six Poisson's ratios of the block (see Kulatilake et al., 1993 for detailed procedures). Similar stress analyses were performed by changing the applied velocity direction to estimate the block strength and tangent rock mass modulus perpendicular to other faces of the cube and the remaining four Poisson's ratios of the block (see Kulatilake et al., 1993 for detailed procedures).

The second block size level was considered to consist of an equivalent continuum material that represents the combined influence of intact rock and the fractures that were present in the smallest block size level, the next higher size level of actual fractures and a set of fictitious joints to form necessary polyhedra in the block. The 3 peak block strength results coming from the smallest block size were used to draw Mohr circles to estimate the new C and ϕ values that should be used to represent the peak shear strength of the equivalent continuum material for the second block size level. A significant drop of C was observed when going from the smallest block size to the next higher block size level. The value of ϕ was found to be more or less the same value used for the previous block size with a slight variation due to random variability. In going from the smallest block size to the next higher block size level, the new C and ϕ values represent the equivalent continuum material behavior of the intact rock combined with the fractures that were present in the smallest block size. Therefore, intuitively, it is reasonable to assume the same frictional component and a reduction of cohesion component to represent the equivalent shear strength behaviour of the intact rock combined with the fractures that were present in the smallest block size. It seems reasonable to apply the same assumption in going from the second block size to the next higher block size level and so on. The reduction ratio of σ_t was assumed to be the same as the reduction ratio of C to calculate the new tensile strength to represent the tensile strength behaviour of the equivalent continuum material of the second block size level that represents the tensile behaviour of the intact rock combined with the fractures of the smallest block size. This assumption was used to calculate the new σ_t for the equivalent continuum material in going from second block size to the next higher block size and so on. The residual strength parameter values of the equivalent continuum material for all the block sizes were assumed to be

same as that of the intact rock. The three values obtained for the tangent rock mass modulus for the smallest block size (provides an equivalent continuum value to represent the combined behaviour of the intact rock and fractures that were present in the smallest block size) were averaged to represent the rock mass modulus of the equivalent continuum material for the second block size level. The six values obtained for the Poisson's ratio of the rock mass for the smallest block size (provides an equivalent continuum value to represent the combined behaviour of intact rock and the fractures that were present in the smallest block size) were averaged to represent the Poisson's ratio of the equivalent continuum material for the second block size level. The same procedure was used in estimating the rock mass modulus and the Poisson's ratio values for the equivalent continuum material in going from the second block size level to the next higher block size level and so on. For block sizes second through the largest, the parameter values for fictitious joints were estimated based on the property values of the equivalent continuum material in the considered block size. The Strength of fictitious joints was represented by the C, ϕ and σ_t values obtained for the equivalent continuum material. Rock mass modulus and Poisson's ratio values obtained for the equivalent continuum material were used to calculate the G value for the equivalent continuum material. This G value along with the ratio (G)/JKS = 0.01m were used in computing the JKS value for the fictitious joints. The same discontinuity mechanical property values were used for the actual fractures irrespective of the block size. The stress analysis performed for the smallest block size was repeated for each increasing block size until the 30m cube size was obtained.

For each selected lithology the 30m cubic block size was rotated in a number of directions (Table 3.4) to obtain the corresponding actual fracture system. For each cubic block having an actual fracture system, necessary fictitious joints were introduced to discretize the cubic block into polyhedra. The property values for equivalent continuum material, fictitious joints and the actual fractures in the block were assigned as mentioned in the previous paragraph. The mean in-situ stress system was determined for each of the block rotations and the calculated values are given in Table 3.4. First, the determined mean in-situ stress was applied to each 30m block to bring it to the equilibrium in-situ stress condition. Then the 3-D stress analysis was repeated for the 30m block size as for the previous block sizes. However, note that for 30m block size 3-D stress analysis was repeated for a number of block rotations to calculate strength and deformability in 18 directions in 3-D to estimate the anisotropic properties.

3.2.2. Results

3.2.2.1. NGI Block # 409 that consists of Aspo Diorite

Table 3.5 shows the different block sizes used (apart from the smallest block size) to perform 3-D stress analysis on Aspo diorite blocks. A block size of 9.5m was used to represent the smallest block for Aspo diorite. Table 3.5 also shows how the equivalent continuum material and fictitious joint property values changed with the block size. The considered different block rotations for the 30m cube and the mean in-situ stress systems obtained for these rotations are given in Table 3.4. Typical stress-strain and strain-strain

Table 3.4 Mean in-situ stresses for different rotation of each of the selected 4 NGI blocks

NGI block #	Rotation		S_{xx}	S_{yy}	S_{zz}	S_{xy}	S_{xz}	S_{yx}
	horizontal (deg.)	vertical (deg.)						
409 (Äspö diorite)	-135	45	-22.58	-13.36	-13.36	0.86	0.86	-0.72
	0	0	-17.11	-12.64	-19.54	0.00	4.25	0.00
	-45	0	-14.07	-12.64	-22.58	0.00	-1.22	0.00
	-90	45	-19.54	-14.87	-14.87	-3.01	-3.01	-2.23
	0	135	-17.11	-16.09	-16.09	3.01	3.01	-3.45
	-45	45	-14.07	-17.61	-17.61	-0.86	-0.86	-4.97
169 (Småland granite)	-135	45	-17.71	-9.98	-9.98	0.33	0.33	1.10
	0	0	-12.83	-11.08	-13.76	0.00	4.41	0.00
	-45	0	-8.88	-11.08	-17.71	0.00	-0.46	0.00
	-90	135	-13.76	-11.96	-11.96	-3.12	-3.12	-0.88
	0	135	-12.83	-12.42	-12.42	3.12	3.12	-1.34
	-45	45	-8.88	-14.39	-14.39	-0.33	-0.33	-3.31
5 (Fine grained granite)	-135	45	-13.02	-8.93	-8.93	-1.03	-1.03	1.36
	0	0	-11.74	-10.29	-8.84	0.00	2.73	0.00
	-45	0	-7.56	-10.29	-13.02	0.00	1.45	0.00
	-90	45	-8.84	-11.02	-11.02	-1.93	-1.93	-0.73
	0	135	-11.74	-9.56	-9.56	1.93	1.93	0.73
	-45	45	-7.56	-11.65	-11.65	1.03	1.03	-1.36
49 (Mixed lithology)	-135	45	-13.02	-8.93	-8.93	-1.03	-1.03	1.36
	0	0	-11.74	-10.29	-8.84	0.00	2.73	0.00
	-45	0	-7.56	-10.29	-13.02	0.00	1.45	0.00
	-90	45	-8.84	-11.02	-11.02	-1.93	-1.93	-0.73
	0	135	-11.74	-9.56	-9.56	1.93	1.93	0.73
	-45	45	-7.56	-11.65	-11.65	1.03	1.03	-1.36

Note: Sign convention for positive stress components are given below

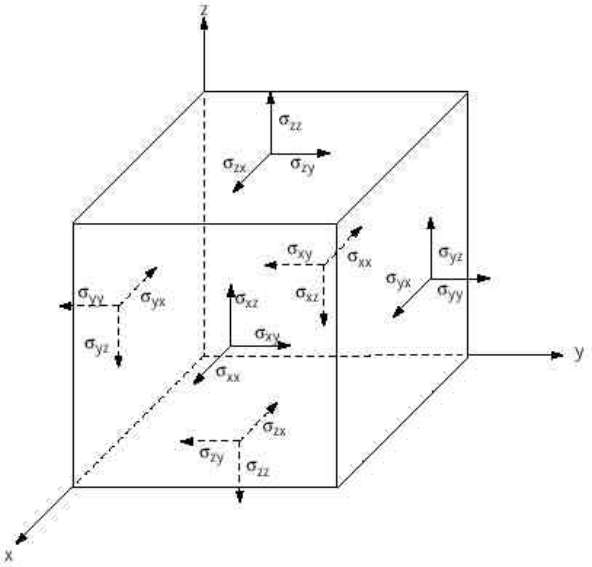

Table 3.5 Mean mechanical property values used to represent the equivalent continuum material and fictitious joints of the selected block sizes (apart from the smallest block size) for different NGI blocks

NGI block #	Block size (m^3)	Equivalent continuum material property mean values					Fictitious joint property mean values	
		C (MPa)	ϕ(deg.)	σ_t (MPa)	Rock block modulus (GPa)	Poisson's ratio of rock block	JKS (GPa/m)	JKN (GPa/m)
409 (Äspö diorite)	13.5	40.1	44	12.0	63.7	0.29	2469	6173
	15.5	31.2	44	9.4	59.0	0.30	2274	5685
	18.3	24.8	44	7.4	49.4	0.32	1878	4695
	21.9	21.1	44	6.3	42.9	0.34	1599	3998
	30.0	15.3	44	4.6	38.5	0.34	1431	3578
169 (Småland granite)	13.9	36.8	44	11.0	63.7	0.29	2467	6168
	17.4	27.8	44	8.0	58.7	0.29	2272	5680
	21.8	21.2	44	6.4	55.8	0.29	2159	5398
	30.0	19.1	44	5.7	46.9	0.31	1791	4478
5 (Fine grained granite)	12.4	35.9	44	10.8	60.2	0.28	2351	5878
	14.9	31.4	44	9.4	58.0	0.29	2254	5635
	17.6	24.3	44	7.2	52.6	0.29	2037	5093
	21.8	20.5	44	6.1	46.9	0.29	1815	4538
	30.0	15.9	44	4.8	41.4	0.30	1595	3988
49 (Mixed lithology)	12.2	39.4	44	11.8	65.9	0.28	2570	6425
	13.6	31.8	44	9.5	60.8	0.30	2346	5865
	15.0	25.7	44	7.7	56.1	0.30	2161	5403
	16.9	21.6	44	6.5	49.7	0.30	1913	4783
	19.0	10.8	44	3.2	44.5	0.30	1709	4273
	20.2	8.5	44	2.5	41.2	0.30	1582	3955
	30.0	5.6	44	1.7	39.9	0.30	1531	3828

Note:

(1) Strain softening properties for equivalent continuum material were assumed to be the same as for the intact rock material

(2) For each block size, C, ϕ, σ_t values of the fictitious joints are the same as that for equivalent continuum material

plots obtained for the 30m block for one of the rotations are shown in Figures 3.4 through 3.6. These plots were used to estimate block strengths and tangent rock mass moduli (at 50% block strength) in three directions and six Poisson's ratios. Similarly, block strengths, tangent rock mass moduli and Poisson's ratios were estimated for each of the considered rotations given in Table 3.4. All the obtained block strengths and rock mass moduli for the 30m block size are given in Tables 3.6 and 3.7, respectively. All the obtained Poisson's ratios for the 30m block size are given in Table 3.8. All these values given in Tables 3.6 through 3.8 can be considered as mean values in each direction because they were calculated using mean in-situ stresses and mean mechanical property values. Figures 3.7 and 3.8 show the anisotropy of block strength and rock mass modulus in 3-D, respectively. The calculated mean principal directions and magnitudes of principal block strengths are given in Table 3.9. The calculated mean principal directions and magnitudes of principal rock mass moduli are given in Table 3.10. These principal

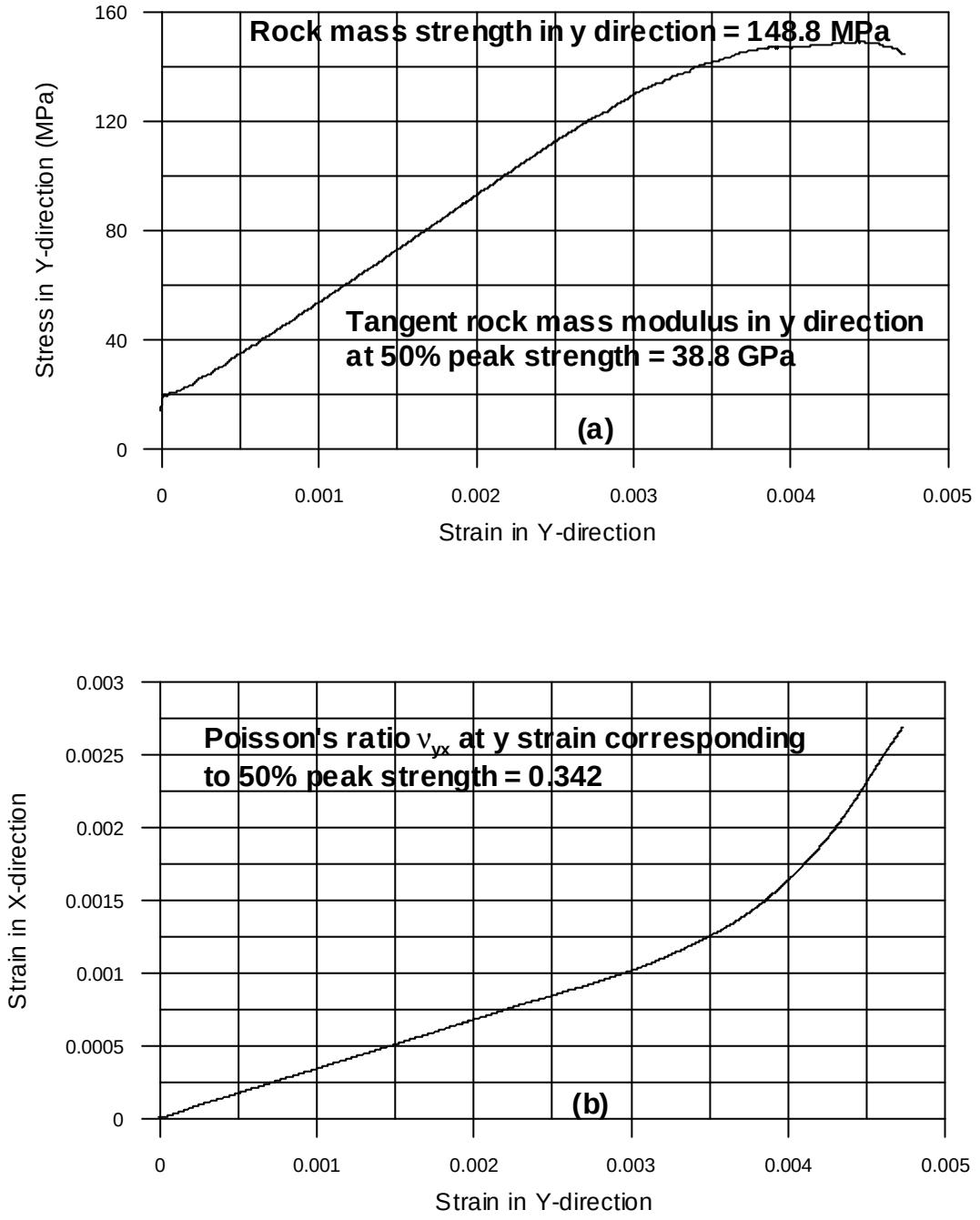

Fig. 3.4 *(a) Y stress vs. Y strain, (b) X strain vs. Y strain and (c) Z strain vs. Y strain plots obtained for 30m cubic block of Äspö diorite, having horizontal rotation = -45º and vertical rotation = 0º by application of a constant velocity of 0.05m/sec in the Y direction*

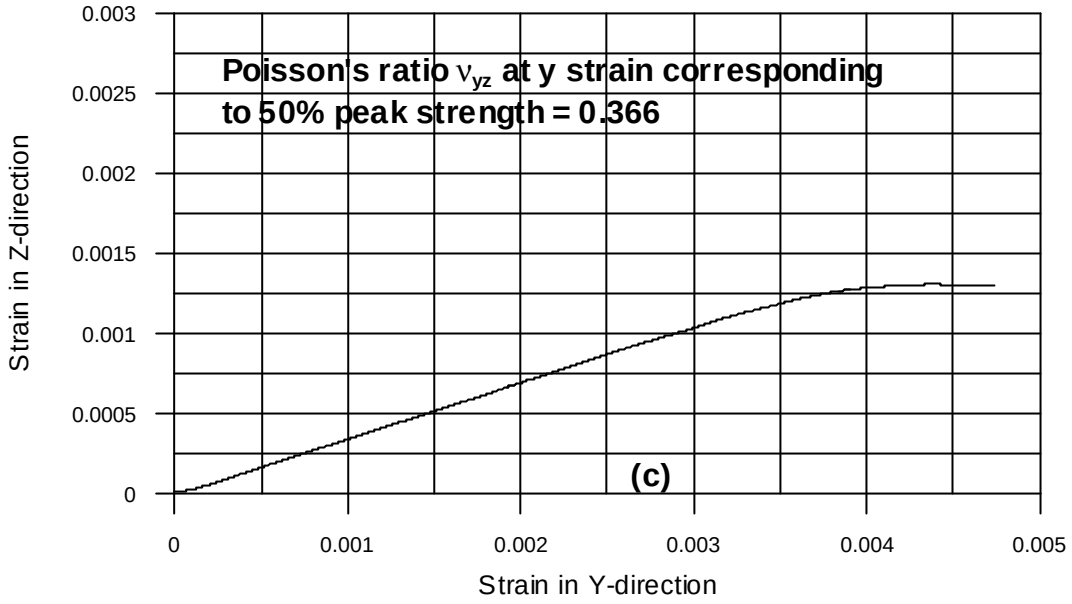

Fig. 3.4 *Continued*

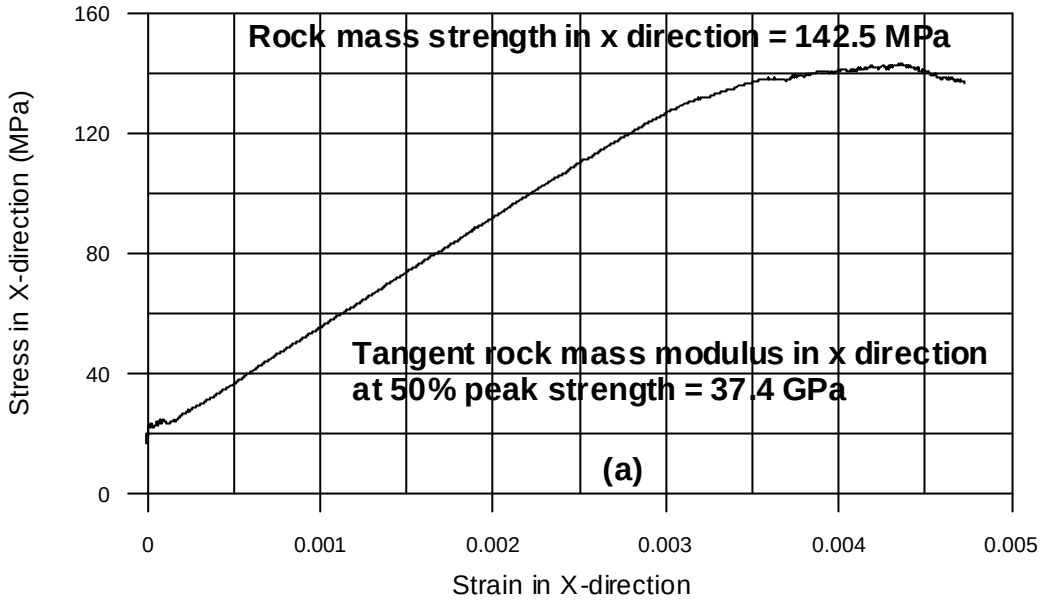

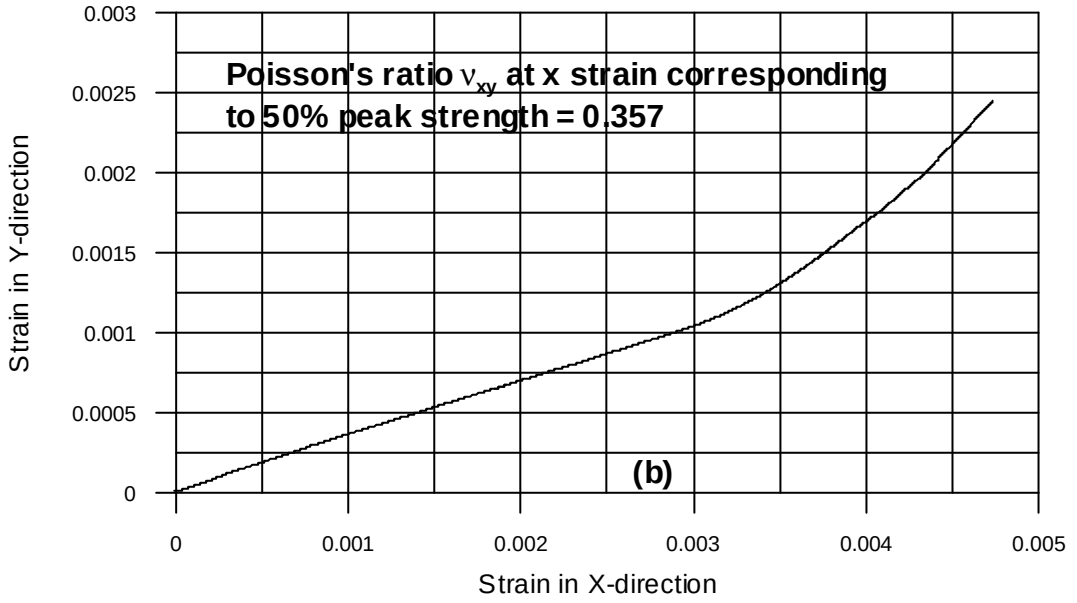

Fig. 3.5 *(a) X stress vs. X strain, (b) Y strain vs. X strain and (c) Z strain vs. X strain plots obtained for 30m cubic block of Äspö diorite, having horizontal rotation = -45º and vertical rotation = 0º by application of a constant velocity of 0.05m/sec in the X direction*

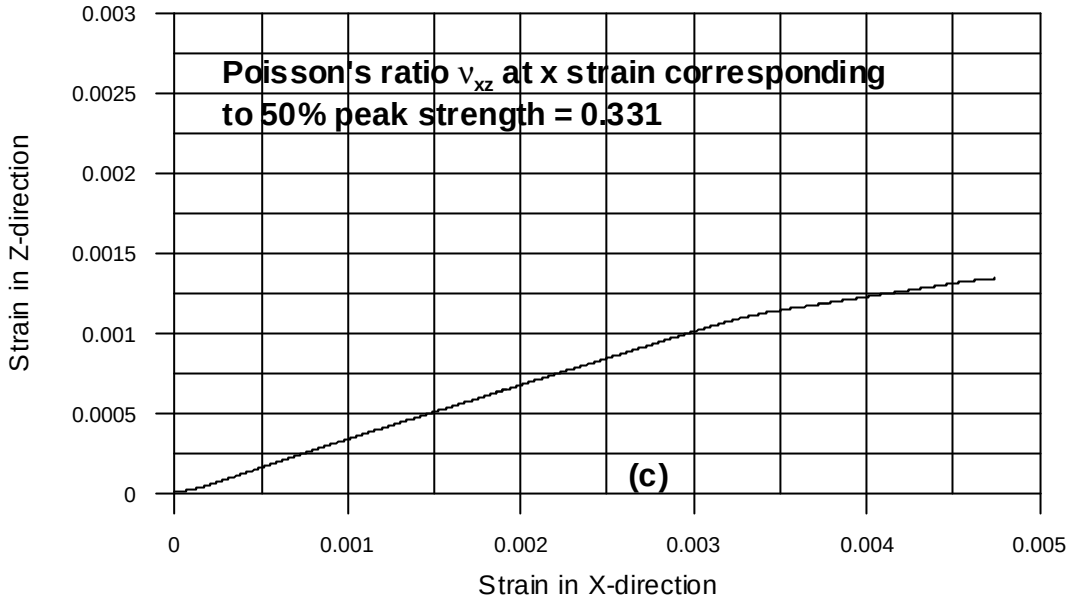

Fig. 3.5 *Continued*

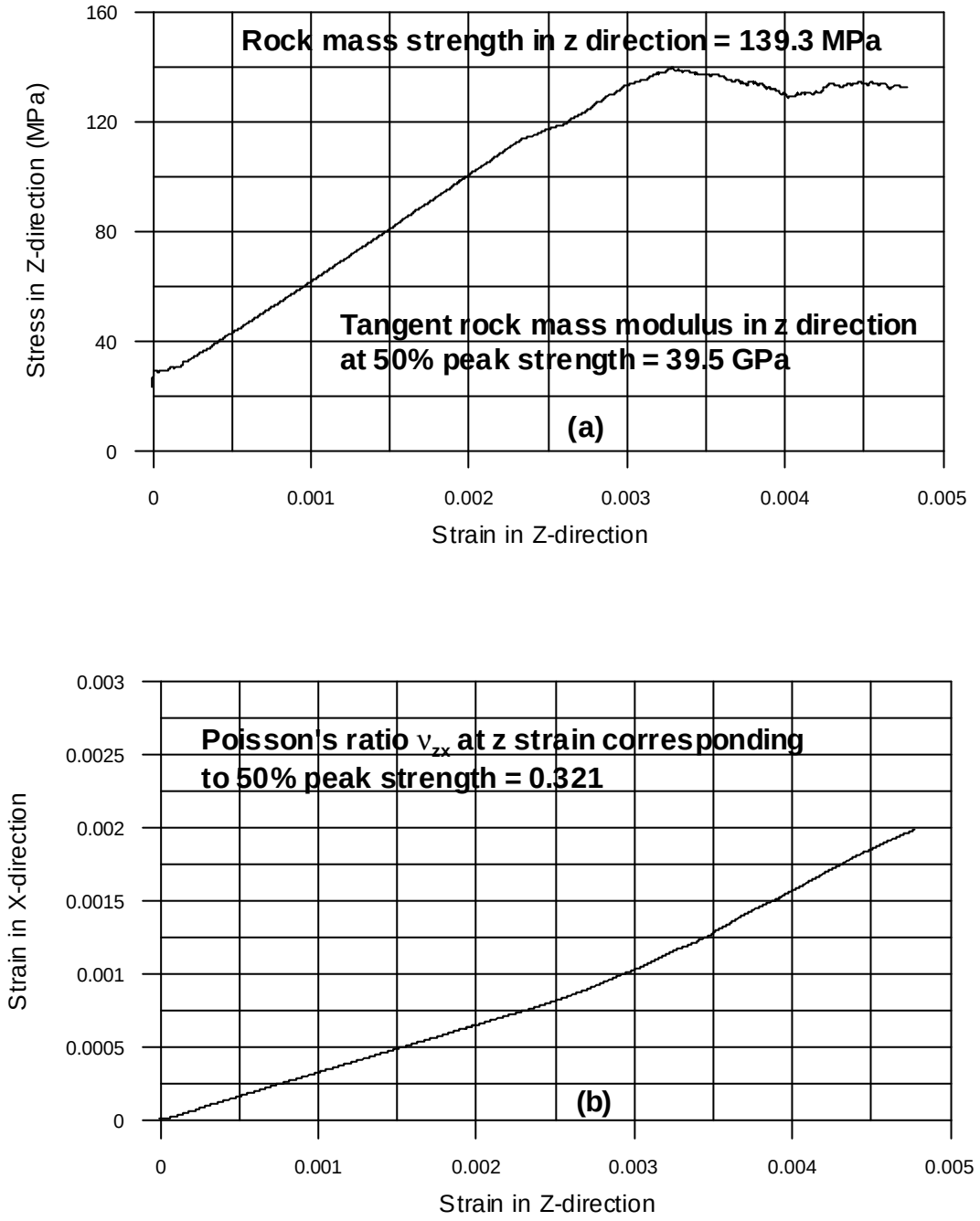

Fig. 3.6 *(a) Z stress vs. Z strain, (b) X strain vs. Z strain and (c) Y strain vs. Z strain plots obtained for 30m cubic block of Äspö diorite, having horizontal rotation = -45º and vertical rotation = 0º by application of a constant velocity of 0.05m/sec in the Z direction*

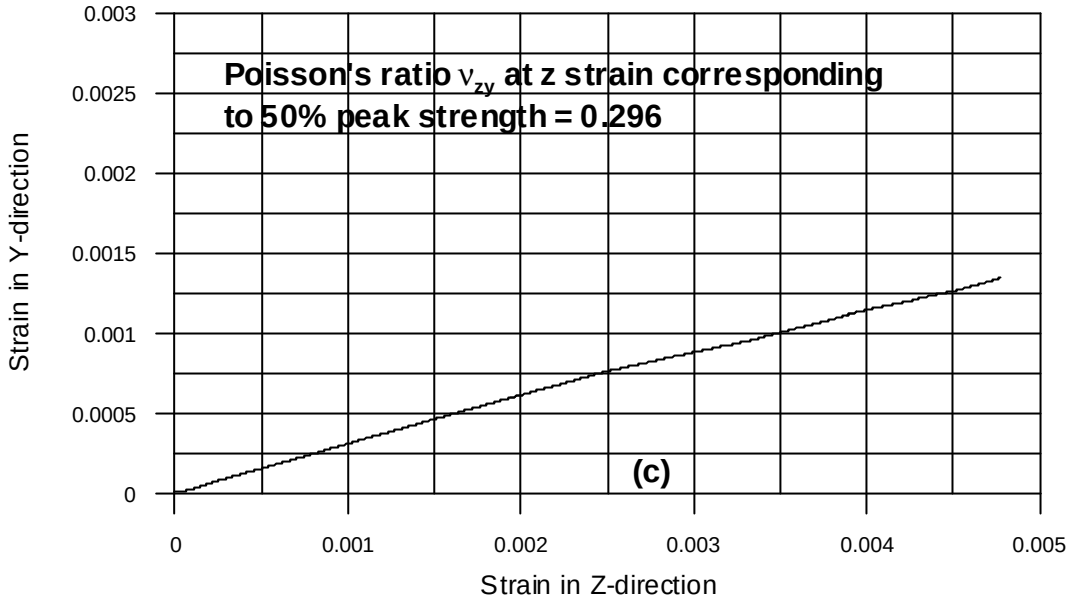

Fig. 3.6 *Continued*

Table 3.6 Calculated rock mass strength mean values in different directions in 3D for different NGI block numbers

Direction		Mean rock mass strength (MPa)			
trend (degs.)	Plunge (degs.)	NGI block #409 (Äspö diorite)	NGI block #169 (Småland granite)	NGI block #5 (Fine grained granite)	NGI block #49 (Mixed lithology)
0	-90	152.5	136.2	117.2	70.1
0	-45	113.8	123.2	115.5	71.6
0	0	129.8	141.2	122.3	80.6
0	45	140.6	93.5	123.8	81.9
45	-45	136.0	133.2	104.8	70.6
45	0	145.2	138.4	119.9	76.5
45	45	164.5	130.3	117.2	80.0
90	-45	142.3	130.7	106.5	74.5
90	0	153.0	125.6	105.9	79.8
90	45	131.5	117.6	121.5	76.5
135	-45	135.0	113.4	104.6	70.2
135	0	139.5	108.6	117.4	69.0
135	45	137.5	120.7	110.2	73.9
180	-45	140.6	93.5	123.8	81.9
180	0	129.8	141.2	122.3	80.6
180	45	113.8	123.2	115.5	71.6
180	90	152.5	136.2	117.2	70.1
225	-45	164.5	130.3	117.2	80.0
225	0	145.2	138.4	119.9	76.5
225	45	136.0	133.2	104.8	70.6
270	-45	131.5	129.3	121.5	76.5
270	0	153.0	119.8	105.9	79.8
270	45	142.3	130.7	106.5	74.5
315	-45	137.5	120.7	110.2	73.9
315	0	139.5	108.6	117.4	69.0
315	45	135.0	113.4	104.6	70.2

Note: downward plunge +ve

Table 3.7 Calculated rock mass modulus mean values in 3D for different NGI block numbers

Direction		Mean rock mass modulus (GPa)			
trend (degs.)	Plunge (degs.)	NGI block #409 (Äspö diorite)	NGI block #169 (Småland granite)	NGI block #5 (Fine grained granite)	NGI block #49 (Mixed lithology)
0	-90	38.2	42.2	38.0	37.1
0	-45	34.2	40.0	35.5	34.5
0	0	35.7	45.1	39.3	35.6
0	45	41.1	43.5	38.1	36.0
45	-45	32.8	42.0	32.7	36.3
45	0	36.2	43.7	38.8	37.2
45	45	39.9	37.9	35.0	37.5
90	-45	40.5	42.4	36.5	35.0
90	0	39.0	42.6	36.1	36.6
90	45	39.0	40.1	34.5	37.2
135	-45	34.5	43.2	36.5	35.5
135	0	38.8	42.5	38.3	37.1
135	45	34.2	40.8	34.2	37.2
180	-45	41.1	43.5	38.1	36.0
180	0	35.7	45.1	39.3	35.6
180	45	34.2	40.0	35.5	34.5
180	90	38.2	42.2	38.0	37.1
225	-45	39.9	37.9	35.0	37.5
225	0	36.2	43.7	38.8	37.2
225	45	32.8	42.0	32.7	36.3
270	-45	39.0	40.1	34.5	37.2
270	0	39.0	42.6	36.1	36.6
270	45	40.5	42.4	36.5	35.0
315	-45	34.2	40.8	34.2	37.2
315	0	38.8	42.5	38.3	37.1
315	45	34.5	43.2	36.5	35.5

Note: downward plunge +ve

Table 3.8 Calculated rock mass Poisson's ratio mean values in 3D for different NGI block numbers

NGI block #	30m block axis directions						Mean Poisson's ratio					
	X		*Y*		*Z*		n_{xy}	n_{xz}	n_{yx}	n_{yz}	n_{zx}	n_{zy}
	trend (degs.)	Plunge (degs.)	trend (degs.)	Plunge (degs.)	trend (degs.)	Plunge (degs.)						
409 (Äspö diorite)	315	0	45	-45	225	-45	0.35	0.37	0.32	0.33	0.35	0.32
	90	0	0	-90	0	0	0.33	0.33	0.34	0.33	0.40	0.29
	45	0	0	-90	315	0	0.36	0.33	0.34	0.37	0.32	0.30
	0	0	90	-45	270	-45	0.37	0.35	0.38	0.31	0.33	0.28
	90	0	180	45	180	-45	0.28	0.39	0.34	0.32	0.35	0.28
	45	0	135	-45	315	-45	0.32	0.36	0.34	0.33	0.32	0.36
169 (Småland granite)	315	0	45	-45	225	-45	0.29	0.31	0.29	0.29	0.31	0.37
	90	0	0	-90	0	0	0.32	0.31	0.30	0.36	0.30	0.29
	45	0	0	-90	315	0	0.31	0.29	0.33	0.30	0.33	0.29
	0	0	90	45	90	-45	0.36	0.29	0.31	0.30	0.31	0.38
	90	0	180	45	180	-45	0.31	0.29	0.28	0.31	0.33	0.39
	45	0	135	-45	315	-45	0.28	0.32	0.28	0.33	0.34	0.28
5 (Fine grained granite)	315	0	45	-45	225	-45	0.35	0.32	0.28	0.36	0.30	0.33
	90	0	0	-90	0	0	0.28	0.31	0.28	0.29	0.32	0.28
	45	0	0	-90	315	0	0.29	0.30	0.30	0.30	0.31	0.30
	0	0	90	-45	270	-45	0.29	0.31	0.28	0.32	0.28	0.35
	90	0	180	45	180	-45	0.28	0.31	0.28	0.28	0.29	0.31
	45	0	135	-45	315	-45	0.28	0.34	0.31	0.32	0.31	0.32
49 (Mixed lithology)	315	0	45	-45	225	-45	0.36	0.37	0.29	0.28	0.31	0.31
	90	0	0	-90	0	0	0.31	0.28	0.29	0.28	0.34	0.30
	45	0	0	-90	315	0	0.32	0.32	0.30	0.30	0.31	0.30
	0	0	90	-45	270	-45	0.37	0.32	0.30	0.30	0.29	0.29
	90	0	180	45	180	-45	0.33	0.33	0.28	0.29	0.34	0.28
	45	0	135	-45	315	-45	0.29	0.28	0.33	0.31	0.28	0.33

Note: downward plunge +ve

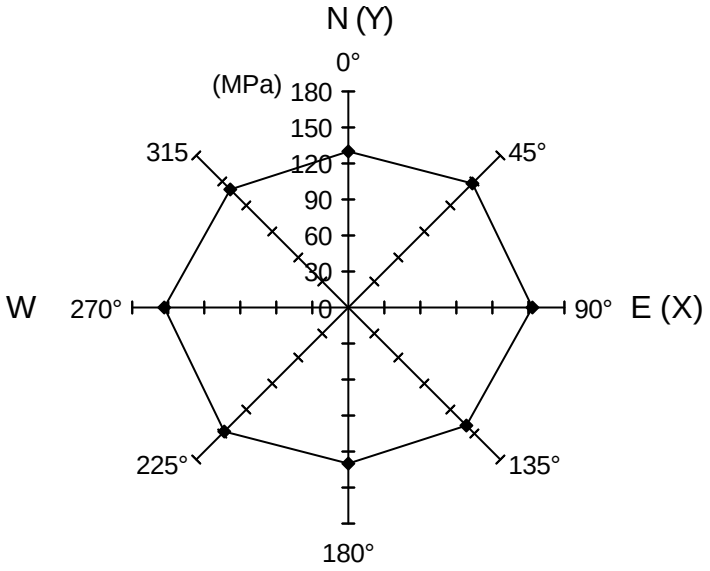

Fig. 3.7a *Variation of directional rock mass strength on the horizontal plane for NGI block #409 (Äspö diorite)*

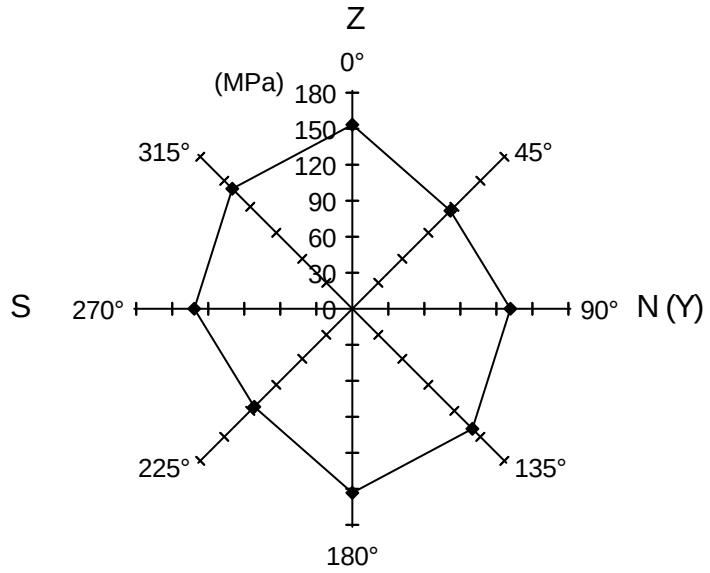

Fig. 3.7b *Variation of directional rock mass strength on the vertical plane striking N – S for NGI block #409 (Äspö diorite)*

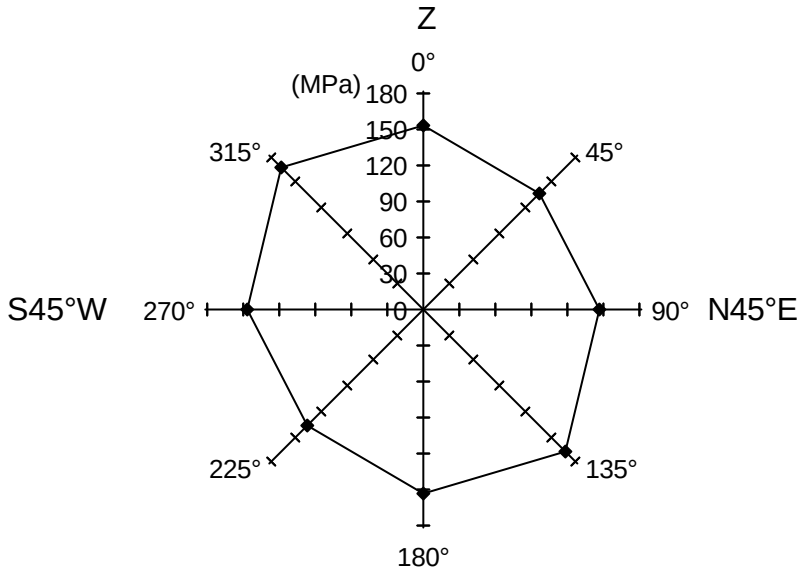

Fig. 3.7c *Variation of directional rock mass strength on the vertical plane striking N45°E for NGI block #409 (Äspö diorite)*

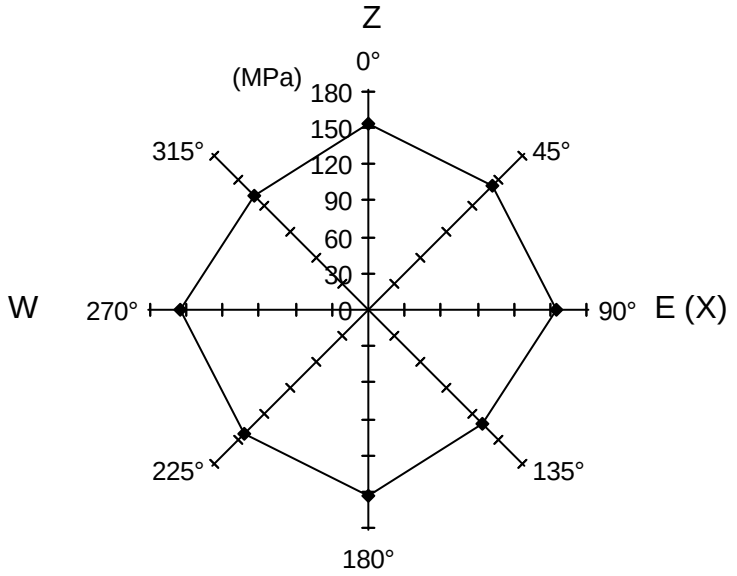

Fig. 3.7d *Variation of directional rock mass strength on the vertical plane striking E – W for NGI block #409 (Äspö diorite)*

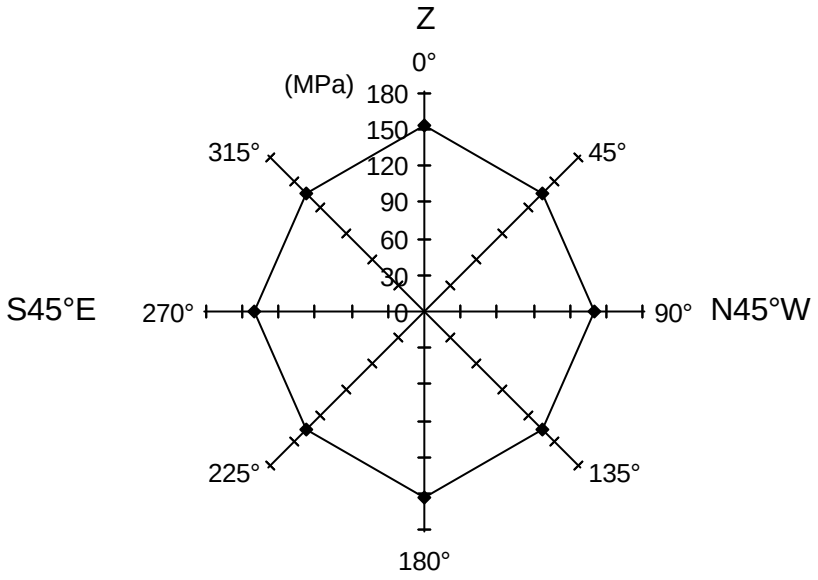

Fig. 3.7e *Variation of directional rock mass strength on the vertical plane striking N45°W for NGI block #409 (Äspö diorite)*

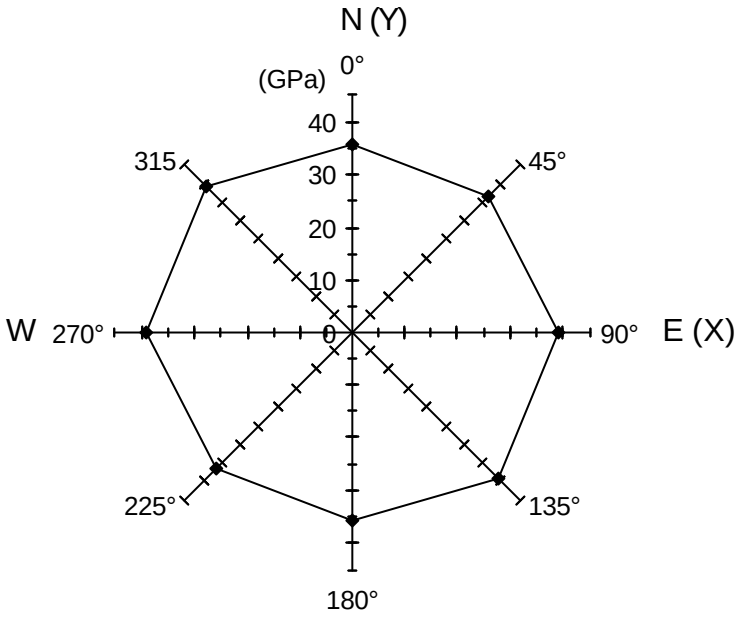

Fig. 3.8a *Variation of directional rock mass modulus on the horizontal plane for NGI block #409 (Äspö diorite)*

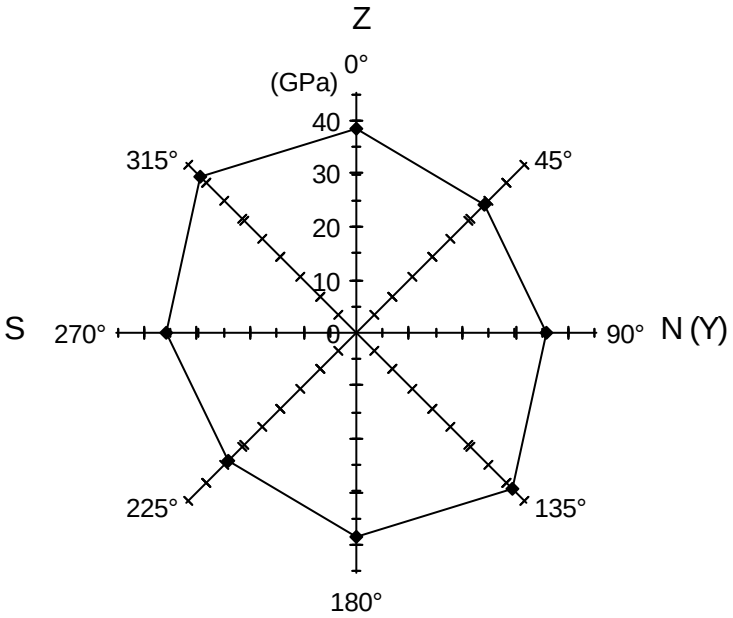

Fig. 3.8b *Variation of directional rock mass modulus on the vertical plane striking N – S for NGI block #409 (Äspö diorite)*

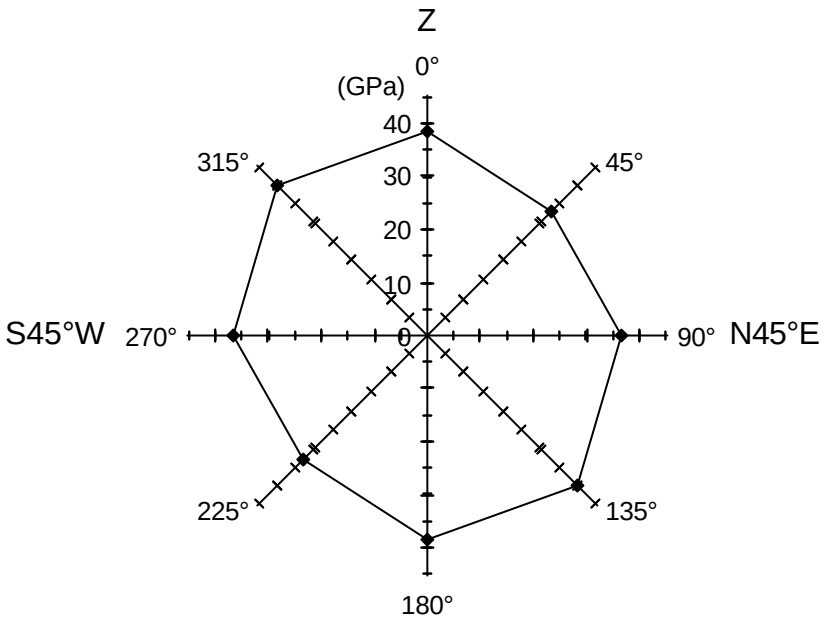

Fig. 3.8c *Variation of directional rock mass modulus on the vertical plane striking N45°E for NGI block #409 (Äspö diorite)*

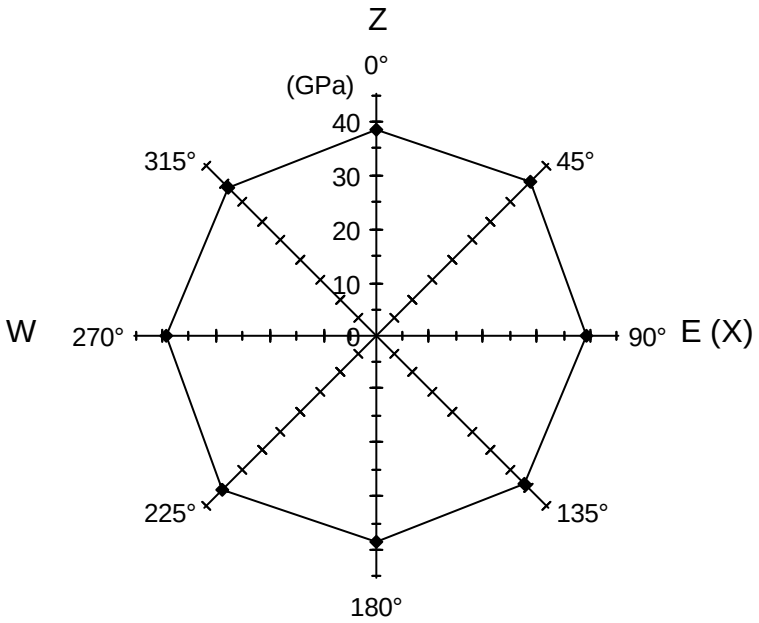

Fig. 3.8d *Variation of directional rock mass modulus on the vertical plane striking E – W for NGI block #409 (Äspö diorite)*

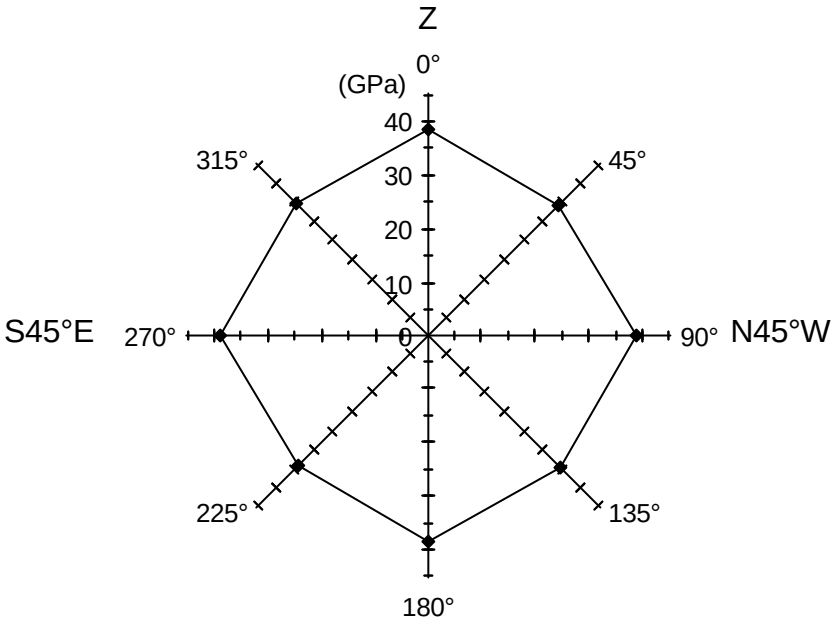

Fig. 3.8e *Variation of directional rock mass modulus on the vertical plane striking N45°W for NGI block #409 (Äspö diorite)*

Table 3.9 Principal rock mass strength mean magnitudes and their directions for different NGI block numbers

NGI block #	Lithology	First principal direction			Second principal direction			Third principal direction		
		trend (deg.)	plunge (deg.)	mag. (MPa)	trend (deg.)	plunge (deg.)	mag. (MPa)	trend (deg.)	plunge (deg.)	mag. (MPa)
409	Äspö diorite	063	29	155.2	295	48	143.6	170	27	121.1
169	Småland granite	221	22	142.6	090	58	122.5	320	22	107.7
5	Fine grained granite	017	24	124.8	133	45	115.7	269	35	103.1
49	Mixed lithology	039	23	82.5	309	2	73.3	215	67	70.0

Note: mag. = magnitude
downward plunge +ve

Table 3.10 Principal rock mass modulus mean magnitudes and their directions for different NGI block numbers

NGI Block #	Lithology	First principal direction			Second principal direction			Third principal direction		
		trend (deg.)	plunge (deg.)	mag. (GPa)	trend (deg.)	plunge (deg.)	mag. (GPa)	trend (deg.)	plunge (deg.)	mag. (GPa)
409	Äspö diorite	051	45	39.9	296	23	38.7	188	37	33.1
169	Småland granite	340	16	44.3	242	27	42.8	098	58	39.3
5	Fine grained granite	352	19	39.4	258	11	35.9	139	68	34.4
49	Mixed lithology	078	35	37.8	339	13	35.8	232	52	35.5

Note: mag. = magnitude
downward plunge +ve

directions and magnitudes are calculated according to a procedure developed by Kulatilake et al. (1999). Based on the calculated 3-D rock block strength and deformability values for the 30m block size, the mean estimations are given for rock block strength (Table 3.11), rock mass modulus (Table 3.12) and Poisson's ratio (Table 3.12) for NGI block # 409 that consists of Aspo diorite. Due to time constraints no stress analysis was performed to evaluate the fracture network, and intact rock and fracture mechanical property variability on rock mass strength and deformability. However, in Tables 3.11 and 3.12 values are assigned for coefficient of variation (cov) of the rock mass strength, rock mass modulus and rock mass Poisson's ratio. When the possible variabilities of fracture network and fracture mechanical properties are considered, the values assigned for cov can be considered as fairly low estimates. Using these low cov estimates and the mean values given in Tables 3.11 and 3.12, and assuming normal distributions for rock mass strength, rock mass modulus and Poisson's ratio 5^{th} and 95^{th} percentiles were estimated for the three rock mass parameters. The obtained 5^{th} and 95^{th} percentiles are given in Tables 3.11 and 3.12.

Table 3.11 Estimates of rock mass strength for different NGI block numbers

NGI block #	Lithology	Coordinates of cube center			Rock mass Strength			
		X (m)	Y (m)	Z (m)	mean (MPa)	5/95 percentiles (MPa)	coefficient of variation	confidence level
409	Äspö diorite	7283.2	2087.2	485	140.1	83 – 198	0.25	2
169	Småland granite	7283.2	2087.2	425	124.3	73 – 175	0.25	2
5	Fine grained granite	7335.8	1963.8	395	114.4	68 – 161	0.25	2
49	Mixed lithology	7283.2	2087.2	395	75.0	44 – 106	0.25	2

Table 3.12 Estimates of rock mass deformability parameters for different NGI block numbers

NGI block #	Lithology	Coordinates of cube center			Rock mass modulus				Poisson's ratio			
		X (m)	Y (m)	Z (m)	mean (GPa)	5/95 percentiles (GPa)	cov	conf	mean	5/95 percentiles	cov	conf
409	Äspö diorite	7283.2	2087.2	485	37.2	25--49	0.20	2	0.34	0.28 - 0.42	0.15	2
169	Småland granite	7283.2	2087.2	425	42.0	28--56	0.20	2	0.32	0.28 - 0.40	0.15	2
5	Fine grained granite	7335.8	1963.8	395	36.4	24--48	0.20	2	0.31	0.28 - 0.39	0.15	2
49	Mixed lithology	7283.2	2087.2	395	36.4	24--48	0.20	2	0.32	0.28 - 0.39	0.15	2

Note: cov = coefficient of variation
conf = confidence level

3.2.2.2. NGI block # 169 that consists of Smaland granite

Table 3.5 shows the different block sizes used (apart from the smallest block size) to perform 3-D stress analysis on Smaland granite blocks. A block size of 10m was used to represent the smallest block for Smaland granite. Table 3.5 also shows how the equivalent continuum material and fictitious joint property values changed with the block size. The considered different block rotations for the 30m cube and the mean in-situ stress systems obtained for these rotations are given in Table 3.4. Typical stress-strain and strain-strain plots obtained for the 30m block for one of the rotations are shown in Figures 3.9 through 3.11. As for the 30m Aspo diorite blocks, block strengths, tangent rock mass moduli and Poisson's ratios were estimated for each 30m Smaland granite cube for each of the considered rotations given in Table 3.4. All the obtained block strengths and rock mass moduli for the 30m cube are given in Tables 3.6 and 3.7, respectively. All the obtained Poisson's ratios for the 30m block size are given in Table 3.8. All these values given in Tables 3.6 through 3.8 can be considered as mean values in each direction because they were calculated using mean in-situ stresses and mean mechanical property values. Figures 3.12 and 3.13 show the anisotropy of block strength and rock mass modulus in 3-D, respectively. The calculated mean principal directions and magnitudes of principal block strengths are given in Table 3.9. The calculated mean principal directions and magnitudes of principal rock mass moduli are given in Table 3.10. Based on the calculated 3-D rock block strength and deformability values for the 30m block size, the mean estimations are given for rock block strength (Table 3.11), rock mass modulus (Table 3.12) and Poisson's ratio (Table 3.12) for NGI block # 169 that consists of Smaland granite. As for Aspo diorite, 5^{th} and 95^{th} percentiles were estimated for the three rock mass parameters of Smaland granite. The obtained 5^{th} and 95^{th} percentiles are given in Tables 3.11 and 3.12.

3.2.2.3. NGI block # 5 that consists of fine grained granite

Table 3.5 shows the different block sizes used (apart from the smallest block size) to perform 3-D stress analysis on fine grained granite blocks. A block size of 8.7m was used to represent the smallest block for fine grained granite. Table 3.5 also shows how the equivalent continuum material and fictitious joint property values changed with the block size. The considered different block rotations for the 30m cube and the mean in-situ stress systems obtained for these rotations are given in Table 3.4. Typical stress-strain and strain-strain plots obtained for the 30m block for one of the rotations are shown in Figures 3.14 through 3.16. As for the 30m Aspo diorite blocks, block strengths, tangent rock mass moduli and Poisson's ratios were estimated for each 30m fine grained granite cube for each of the considered rotations given in Table 3.4. All the obtained block strengths and rock mass moduli for the 30m cube are given in Tables 3.6 and 3.7, respectively. All the obtained Poisson's ratios for the 30m block size are given in Table 3.8. All these values given in Tables 3.6 through 3.8 can be considered as mean values in each direction because they were calculated using mean in-situ stresses and mean mechanical property values. Figures 3.17 and 3.18 show the anisotropy of block strength and rock mass modulus in 3-D, respectively. The calculated mean principal directions and magnitudes of principal block strengths are given in Table 3.9. The calculated mean

principal directions and magnitudes of principal rock mass moduli are given in Table 3.10. Based on the calculated 3-D rock block strength and deformability values for the 30m block size, the mean estimations are given for rock block strength (Table 3.11), rock mass modulus (Table 3.12) and Poisson's ratio (Table 3.12) for NGI block # 5 that consists of fine grained granite. As for Aspo diorite, 5^{th} and 95^{th} percentiles were estimated for the three rock mass parameters of fine grained granite. The obtained 5^{th} and 95^{th} percentiles are given in Tables 3.11 and 3.12.

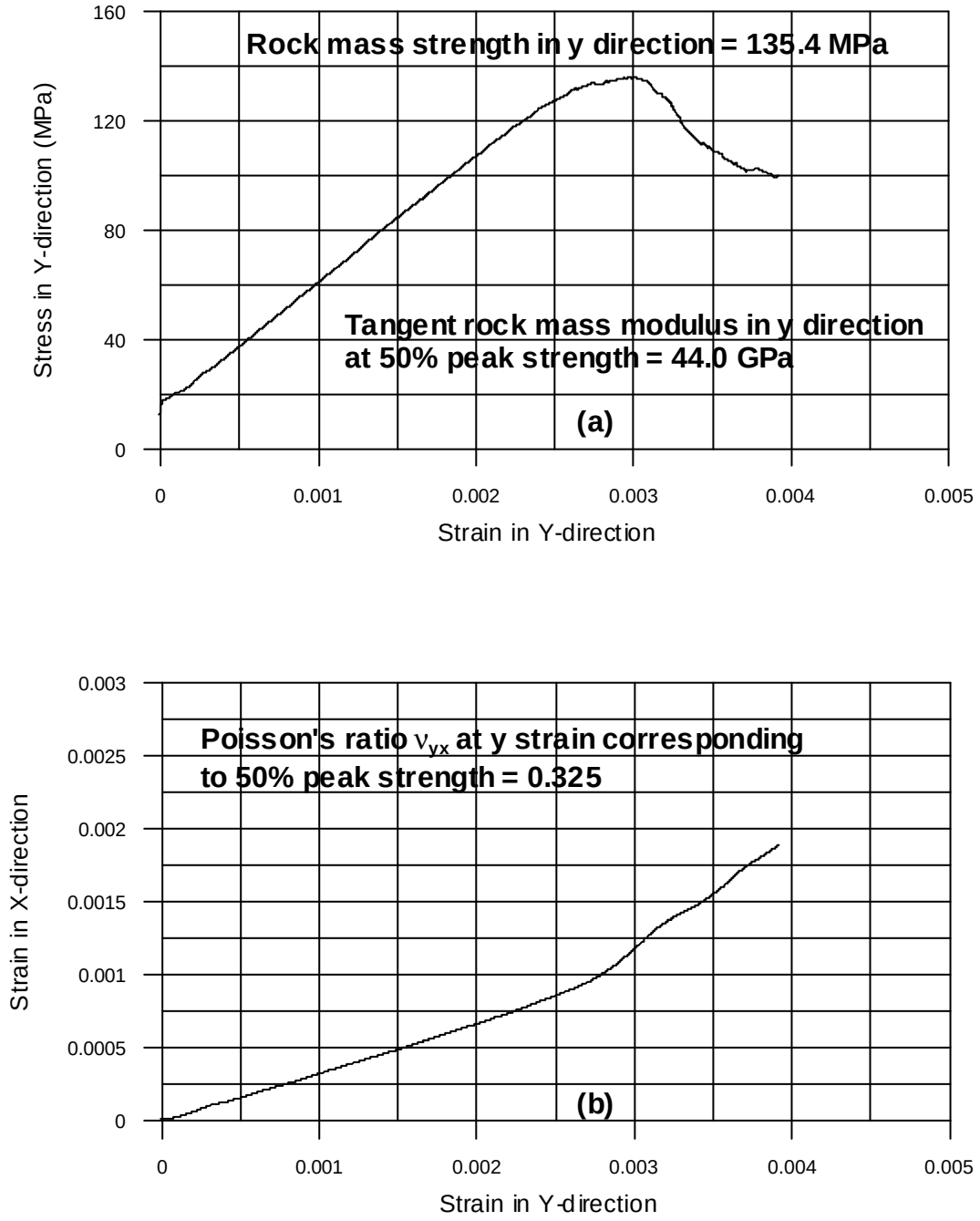

Fig. 3.9 (a) Y stress vs. Y strain, (b) X strain vs. Y strain and (c) Z strain vs. Y strain plots obtained for 30m cubic block of Småland granite, having horizontal rotation = -45º and vertical rotation = 0º by application of a constant velocity of 0.05m/sec in the Y direction

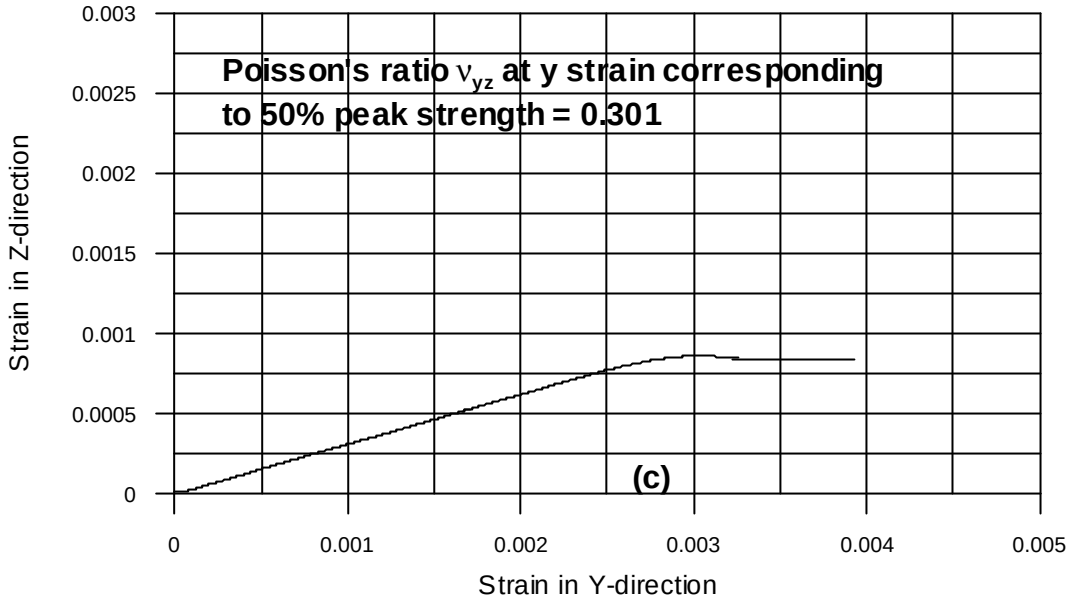

Fig. 3.9 *Continued*

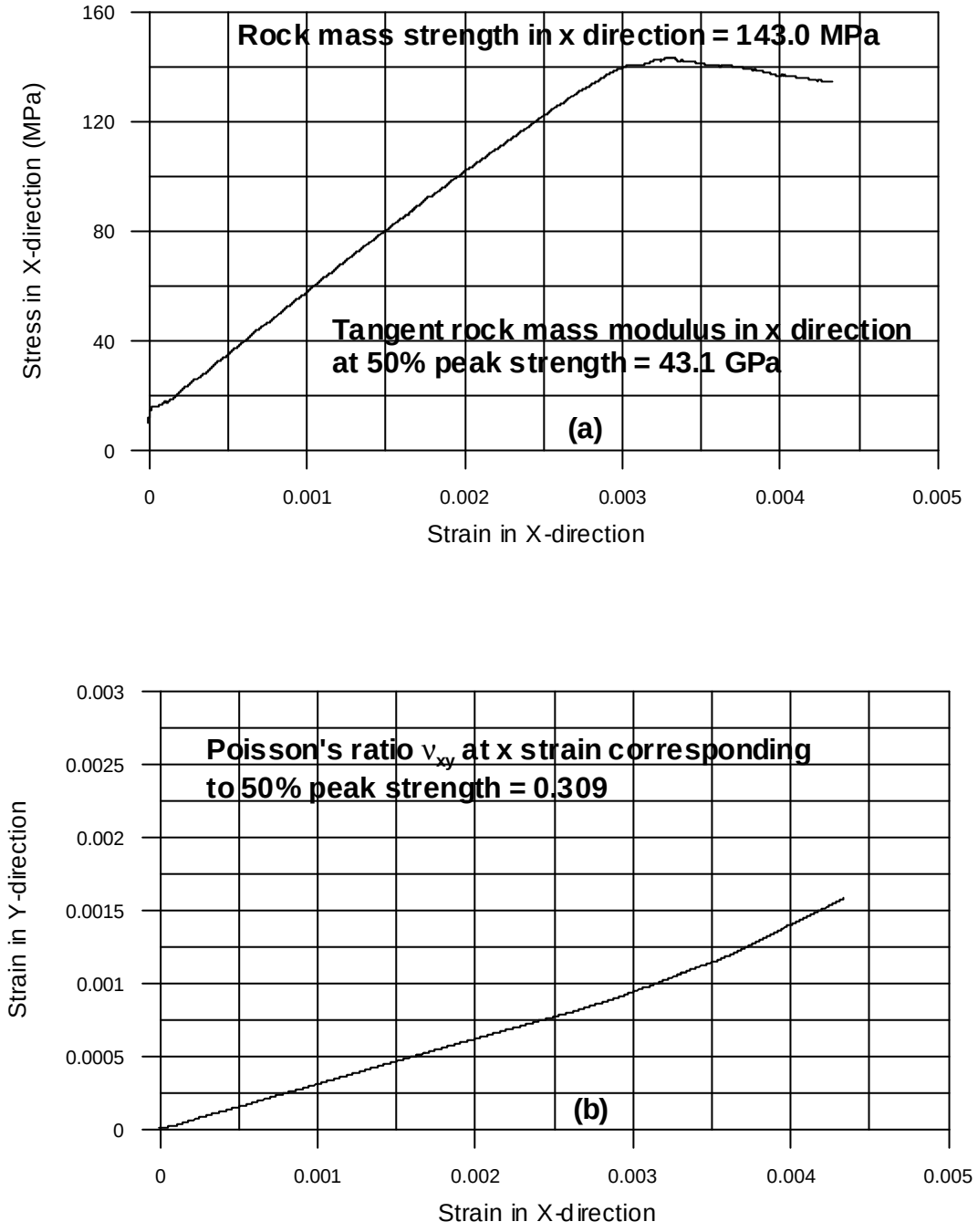

Fig. 3.10 *(a) X stress vs. X strain, (b) Y strain vs. X strain and (c) Z strain vs. X strain plots obtained for 30m cubic block of Småland granite, having horizontal rotation = -45º and vertical rotation = 0º by application of a constant velocity of 0.05m/sec in the X direction*

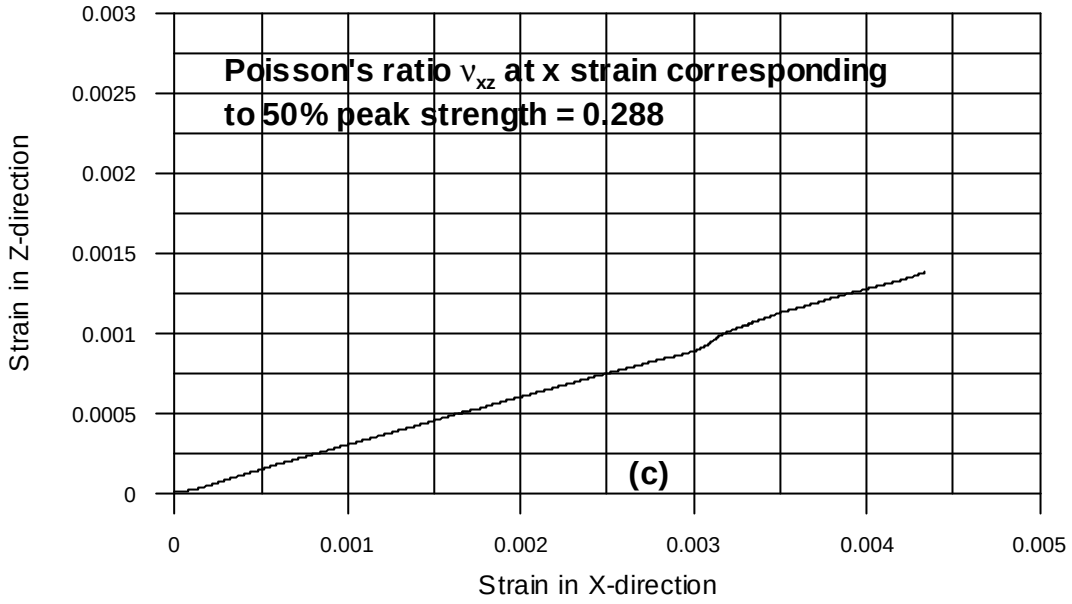

Fig. 3.10 *Continued*

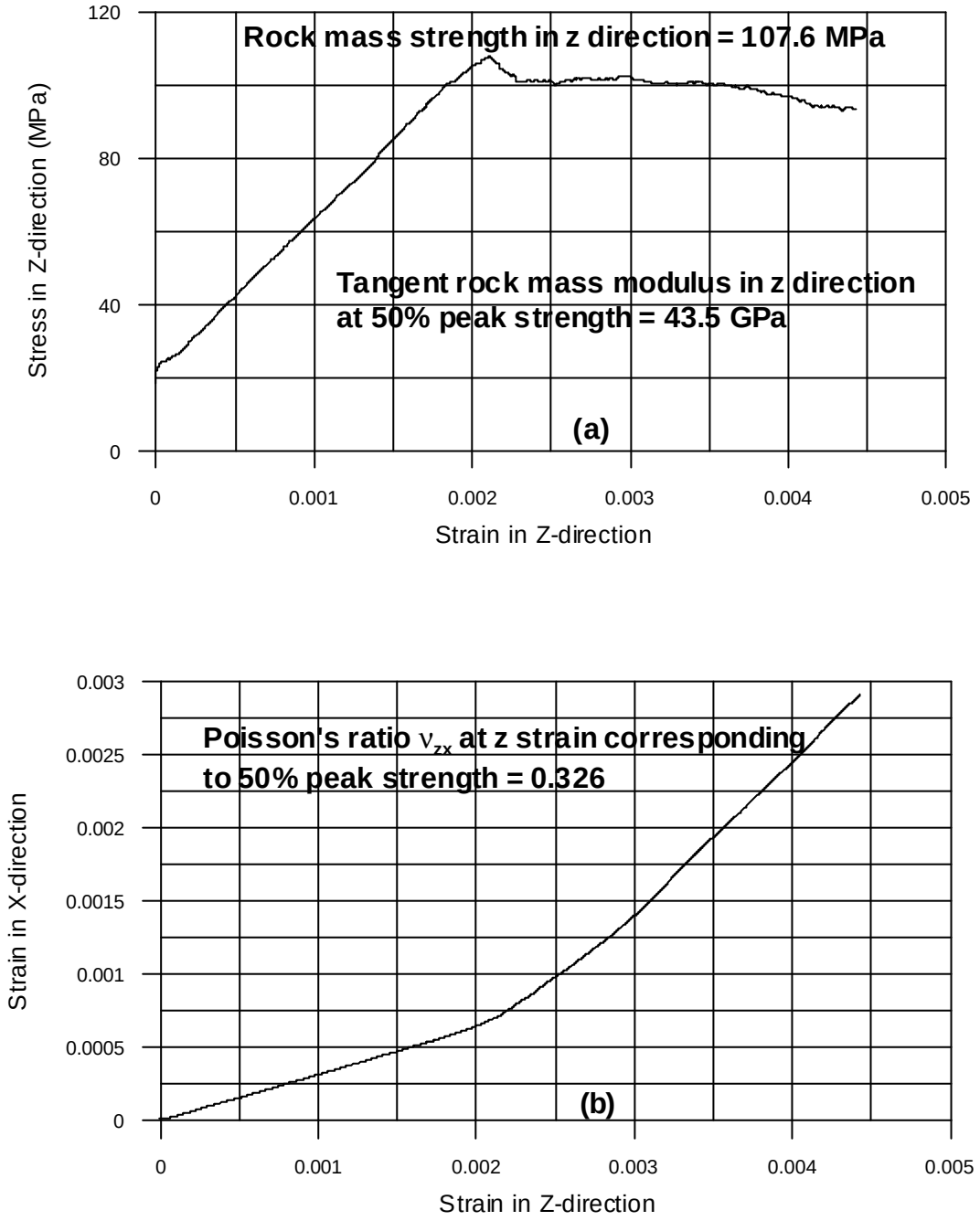

Fig. 3.11 *(a) Z stress vs. Z strain, (b) X strain vs. Z strain and (c) Y strain vs. Z strain plots obtained for 30m cubic block of Småland granite, having horizontal rotation = -45º and vertical rotation = 0º by application of a constant velocity of 0.05m/sec in the Z direction*

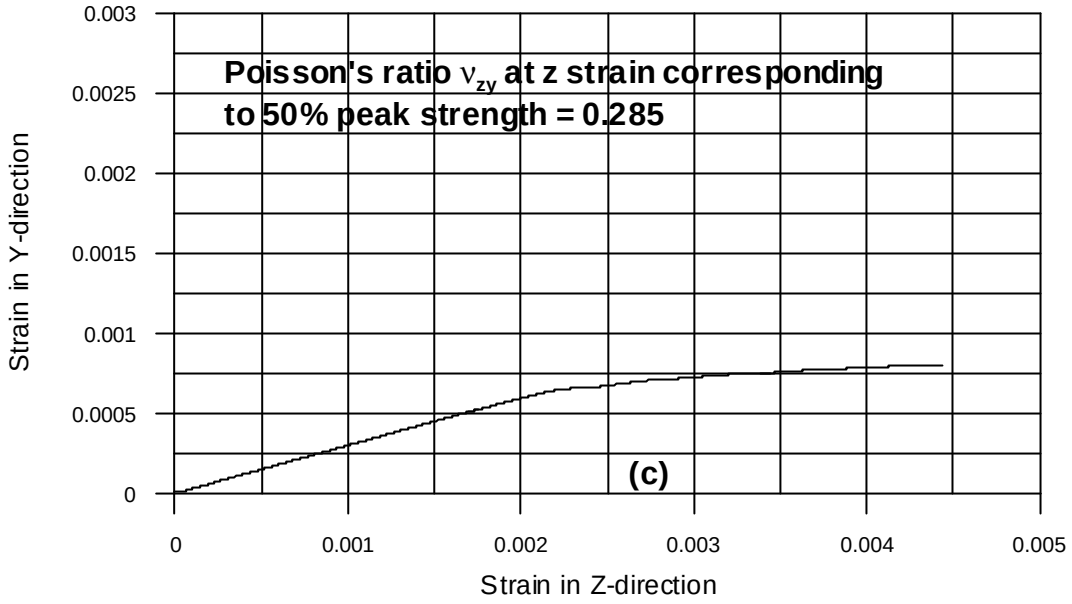

Fig. 3.11 *Continued*

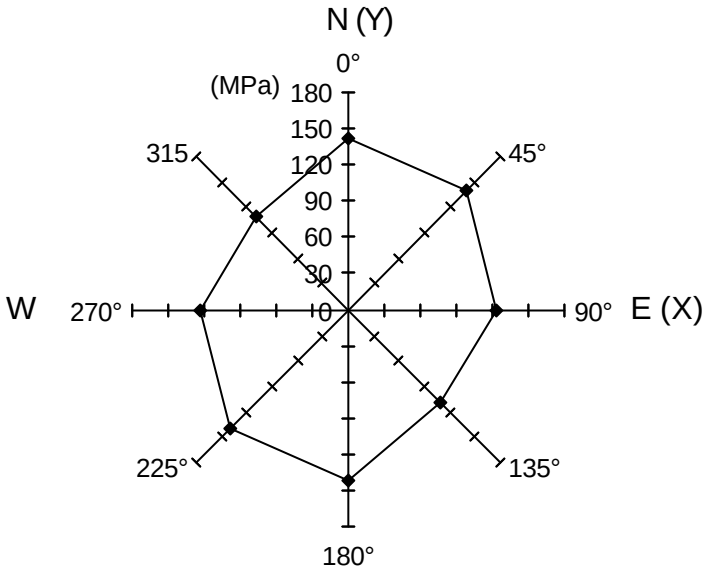

Fig. 3.12a *Variation of directional rock mass strength on the horizontal plane for NGI block #169 (Småland granite)*

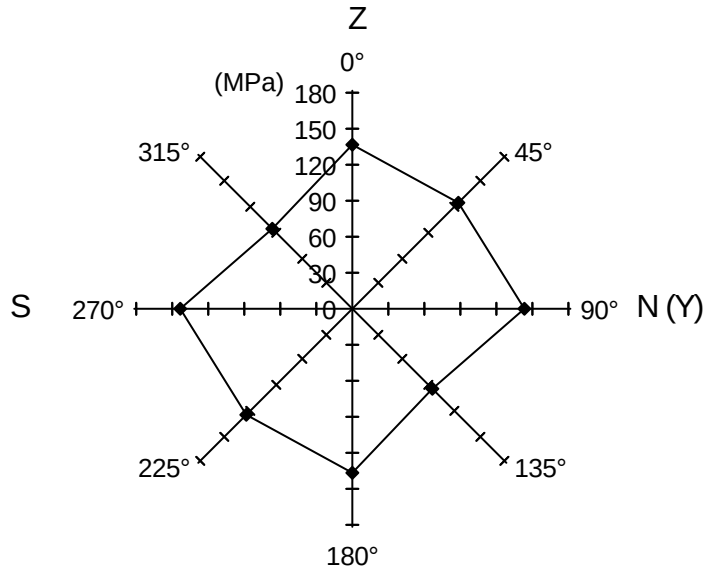

Fig. 3.12b *Variation of directional rock mass strength on the vertical plane striking N – S for NGI block #169 (Småland granite)*

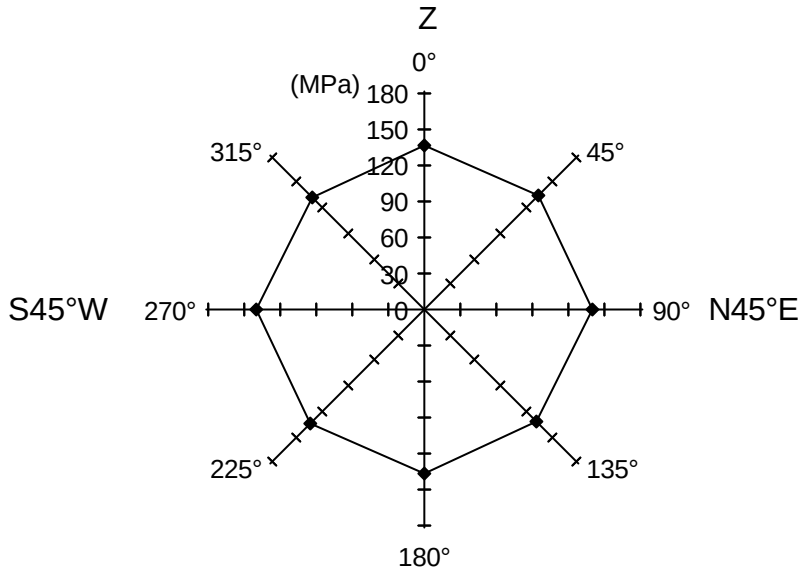

Fig. 3.12c *Variation of directional rock mass strength on the vertical plane striking N45°E for NGI block #169 (Småland granite)*

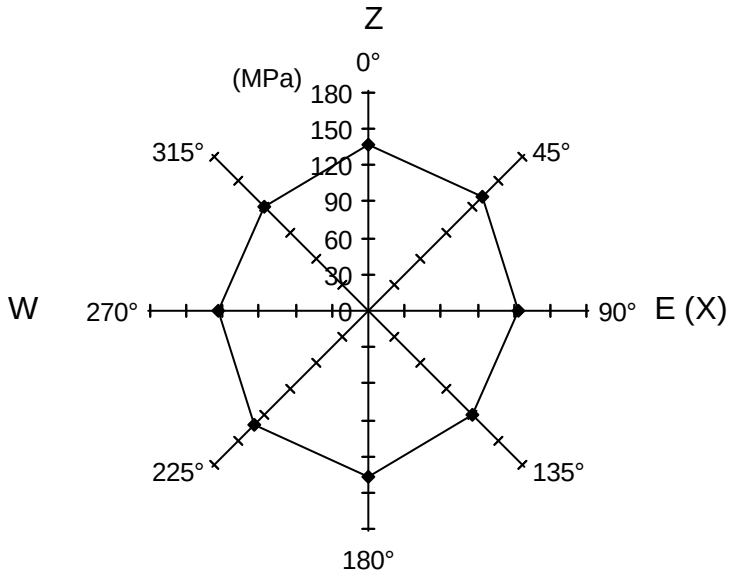

Fig. 3.12d *Variation of directional rock mass strength on the vertical plane striking E – W for NGI block #169 (Småland granite)*

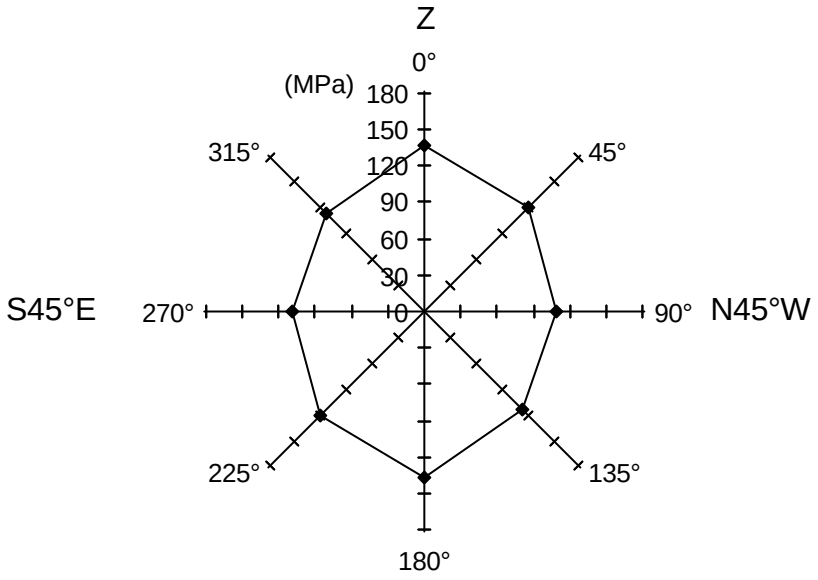

Fig. 3.12e *Variation of directional rock mass strength on the vertical plane striking N45°W for NGI block #169 (Småland granite)*

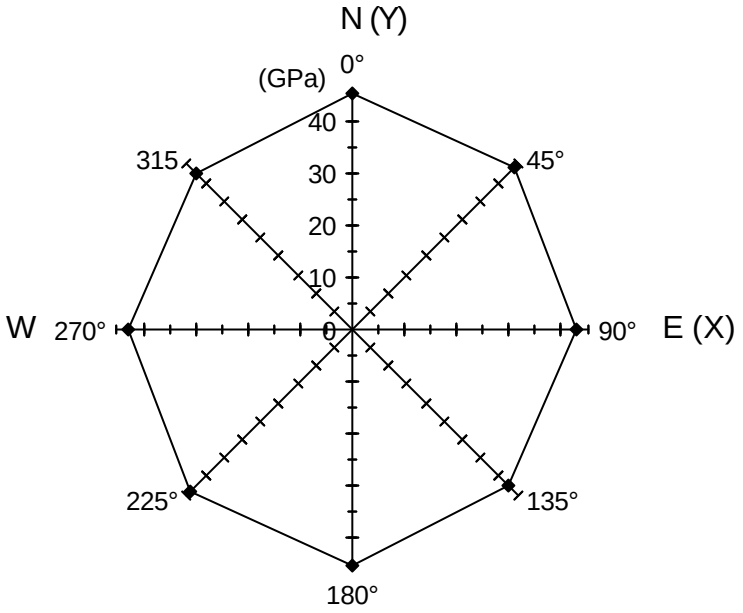

Fig. 3.13a *Variation of directional rock mass modulus on the horizontal plane for NGI block #169 (Småland granite)*

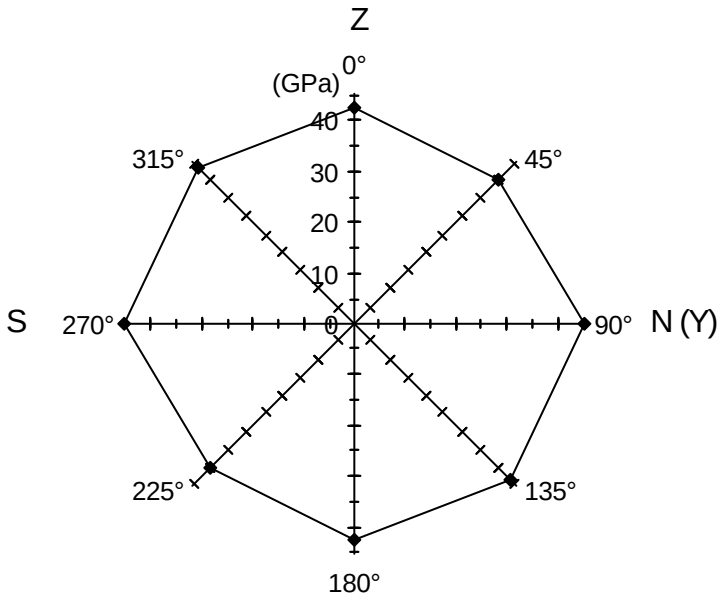

Fig. 3.13b *Variation of directional rock mass modulus on the vertical plane striking N – S for NGI block #169 (Småland granite)*

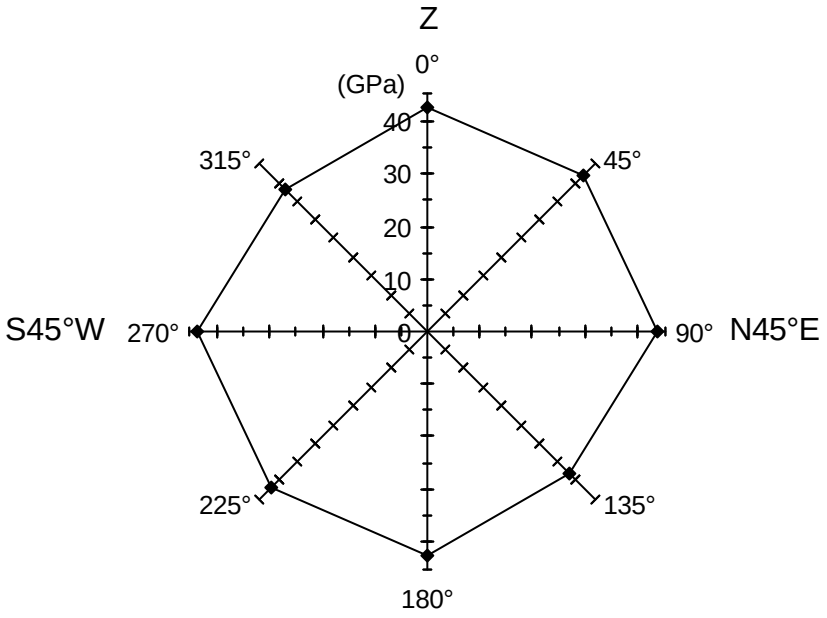

Fig. 3.13c *Variation of directional rock mass modulus on the vertical plane striking N45°E for NGI block #169 (Småland granite)*

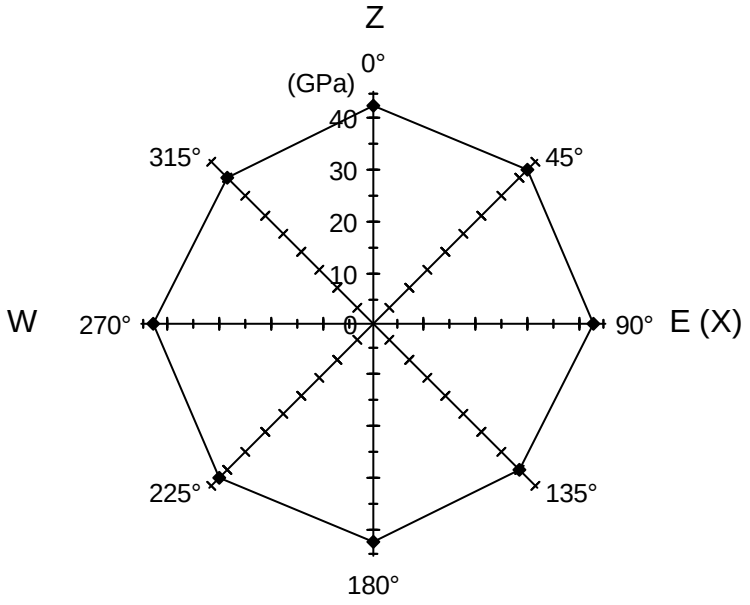

Fig. 3.13d *Variation of directional rock mass modulus on the vertical plane striking E – W for NGI block #169 (Småland granite)*

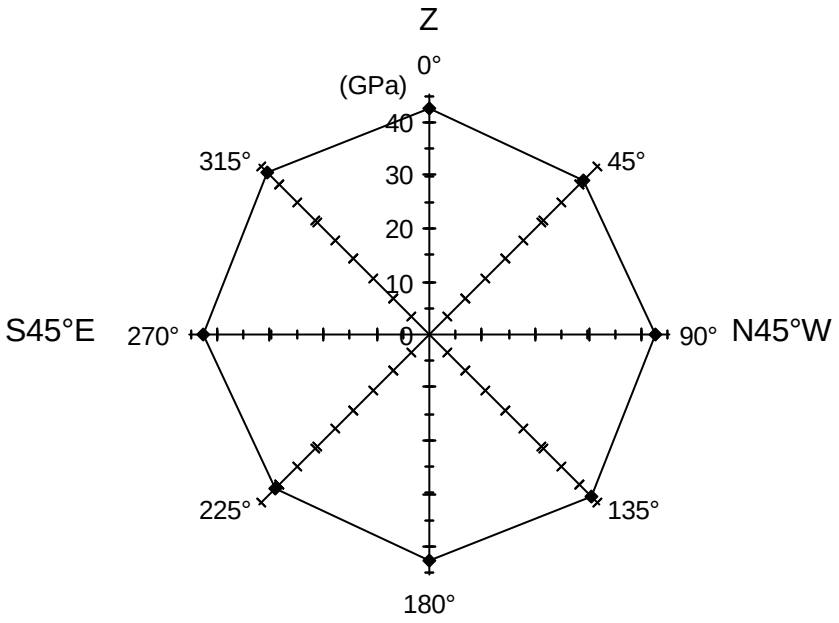

Fig. 3.13e *Variation of directional rock mass modulus on the vertical plane striking N45°W for NGI block #169 (Småland granite)*

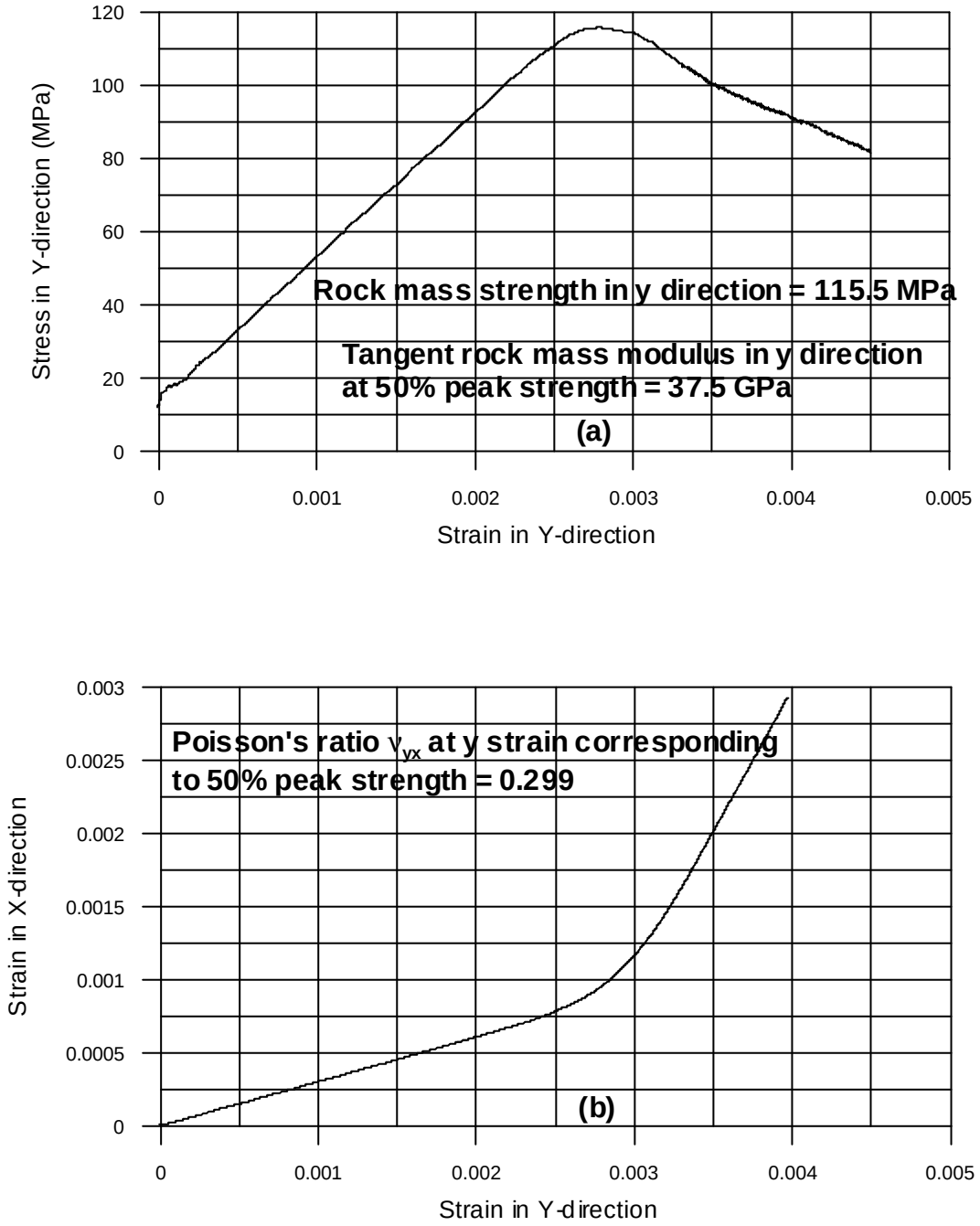

Fig. 3.14 *(a) Y stress vs. strain, (b) X strain vs. Y strain and (c) Z strain vs. Y strain plots obtained for 30m cubic block of fine grained granite, having horizontal rotation = -45º and vertical rotation = 0º by application of a constant velocity of 0.05m/sec in the Y direction*

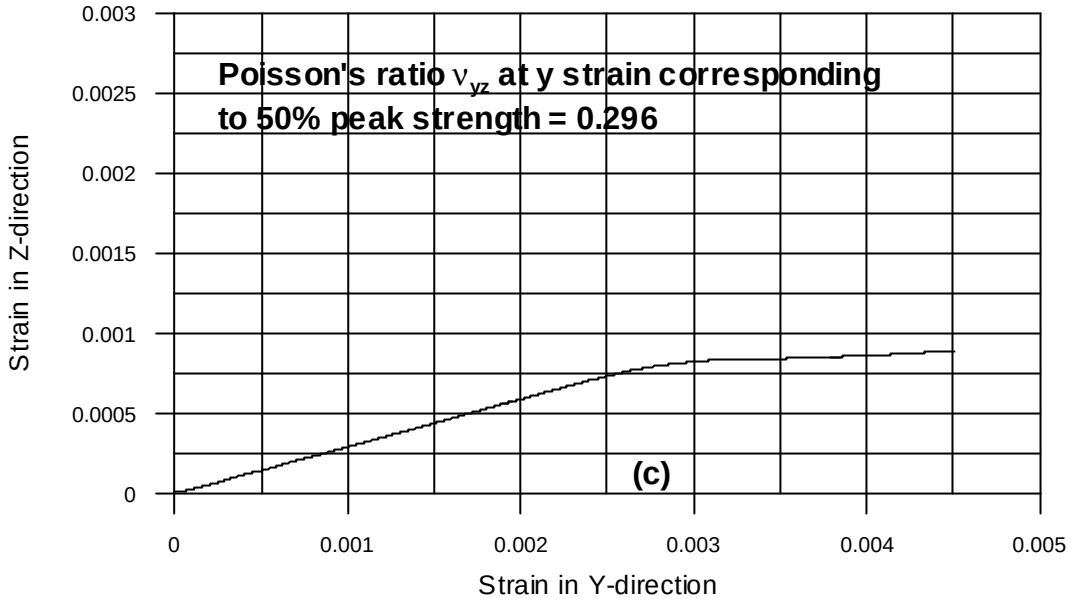

Fig. 3.14 *Continued*

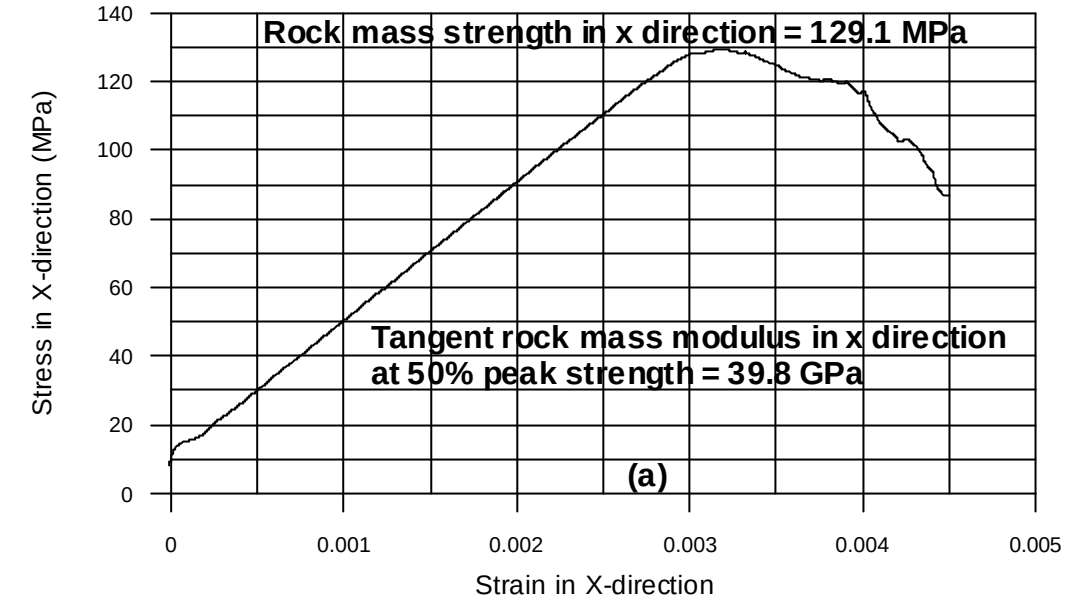

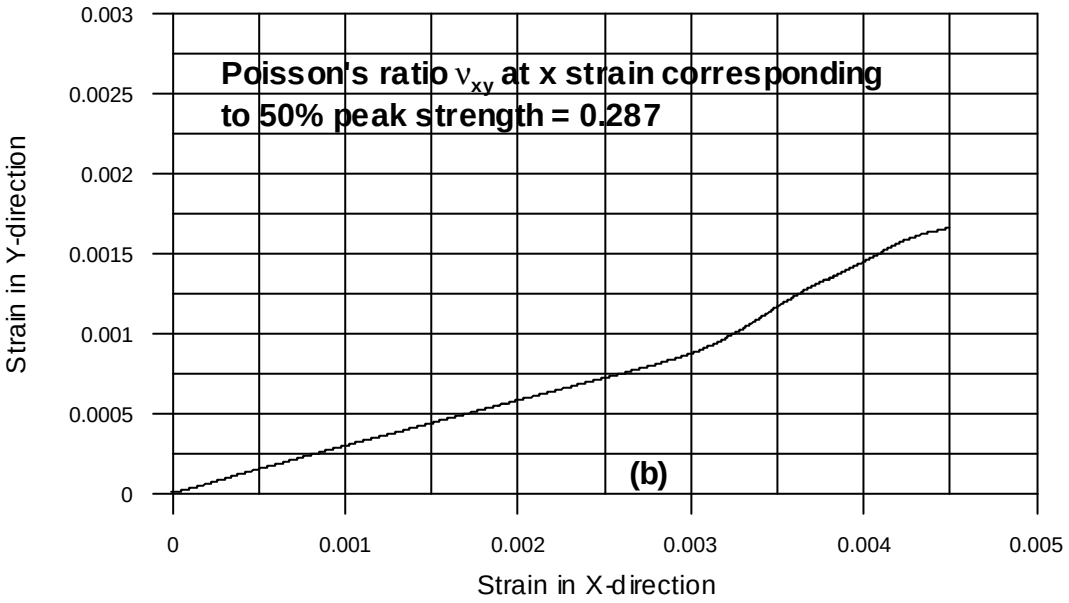

Fig. 3.15 *(a) X stress vs. X strain, (b) Y strain vs. X strain and (c) Z strain vs. X strain plots obtained for 30m cubic block of fine grained granite, having horizontal rotation = -45º and vertical rotation = 0º by application of a constant velocity of 0.05m/sec in the X direction*

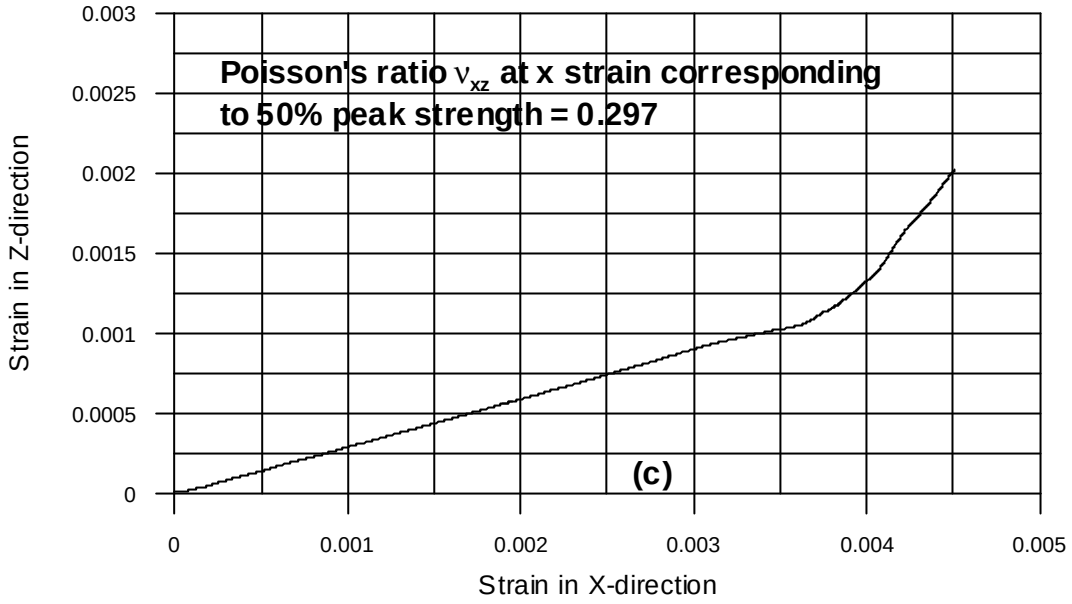

Fig. 3.15 *Continued*

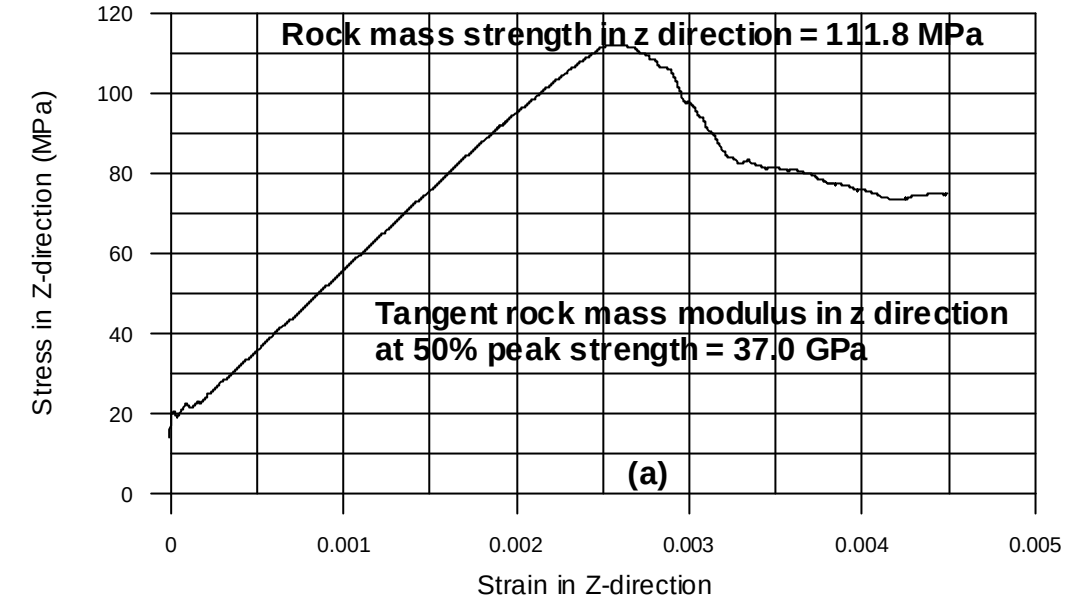

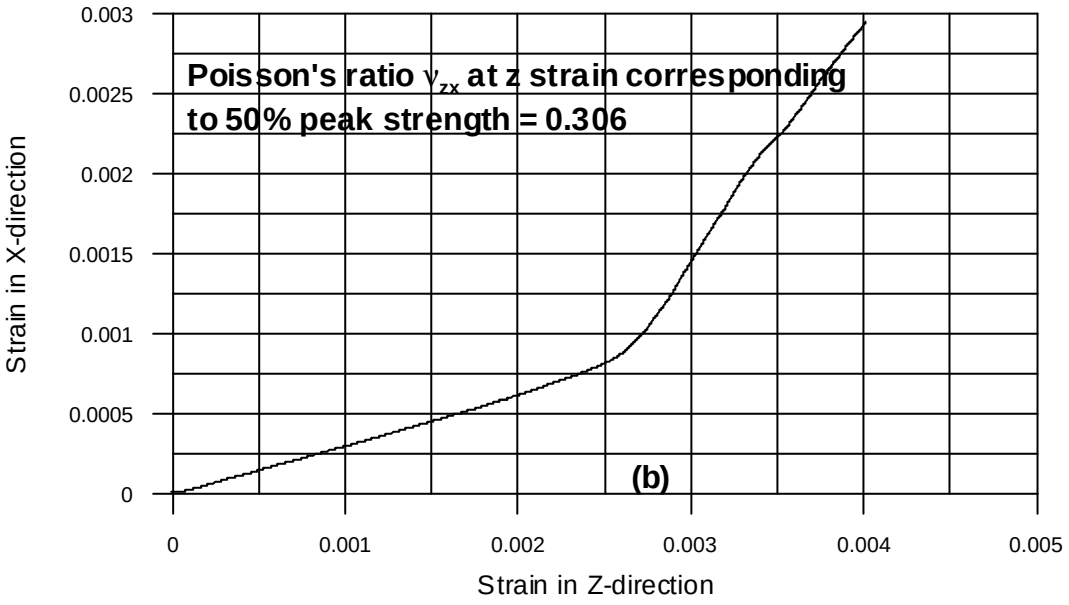

Fig. 3.16 *(a) Z stress vs. Z strain, (b) X strain vs. Z strain and (c) Y strain vs. Z strain plots obtained for 30m cubic block of fine grained granite, having horizontal rotation = -45º and vertical rotation = 0º by application of a constant velocity of 0.05m/sec in the Z direction*

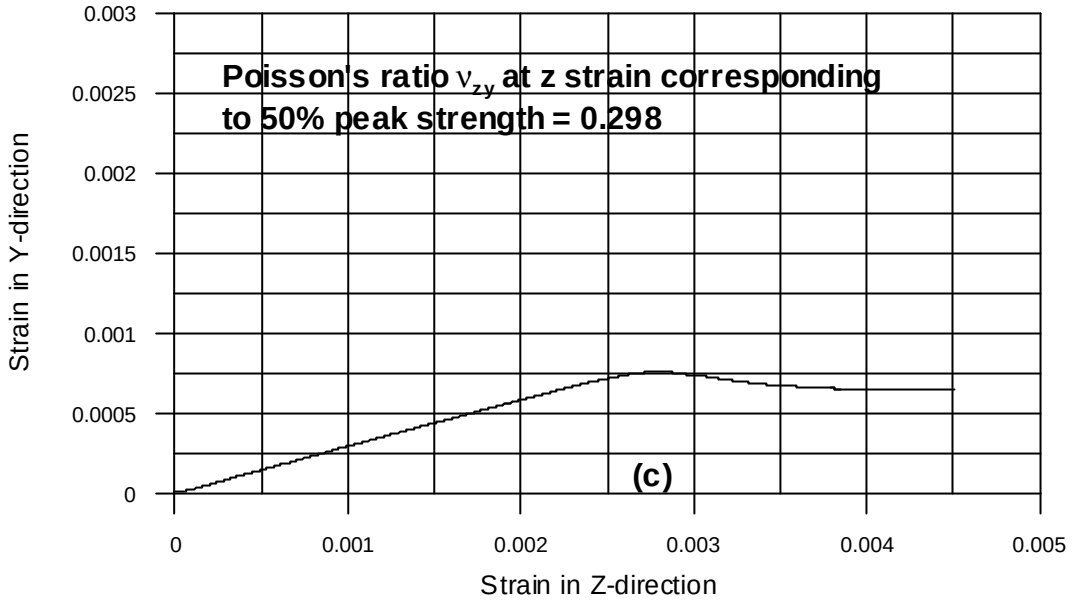

Fig. 3.16 *Continued*

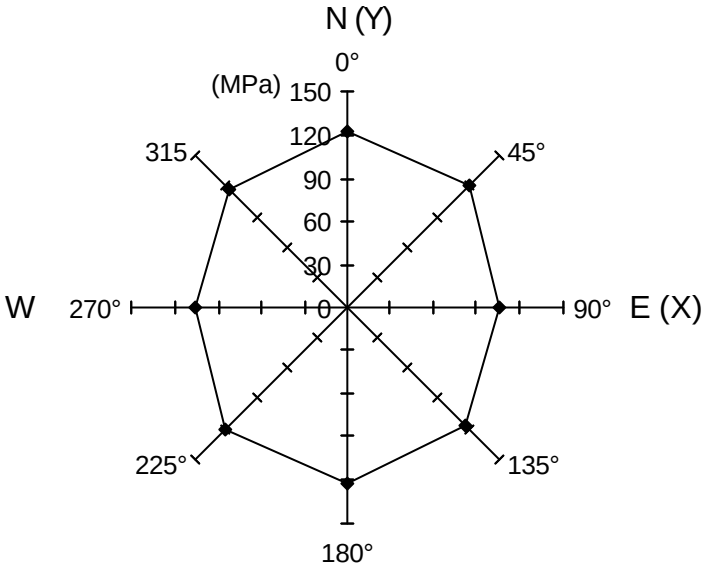

Fig. 3.17a *Variation of directional rock mass strength on the horizontal plane for NGI box #5 (fine grained granite)*

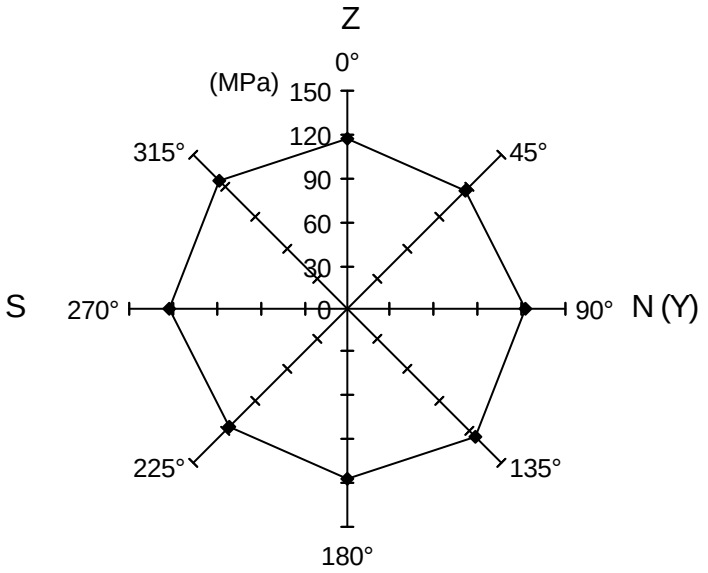

Fig. 3.17b *Variation of directional rock mass strength on the vertical plane striking N – S for NGI box #5 (fine grained granite)*

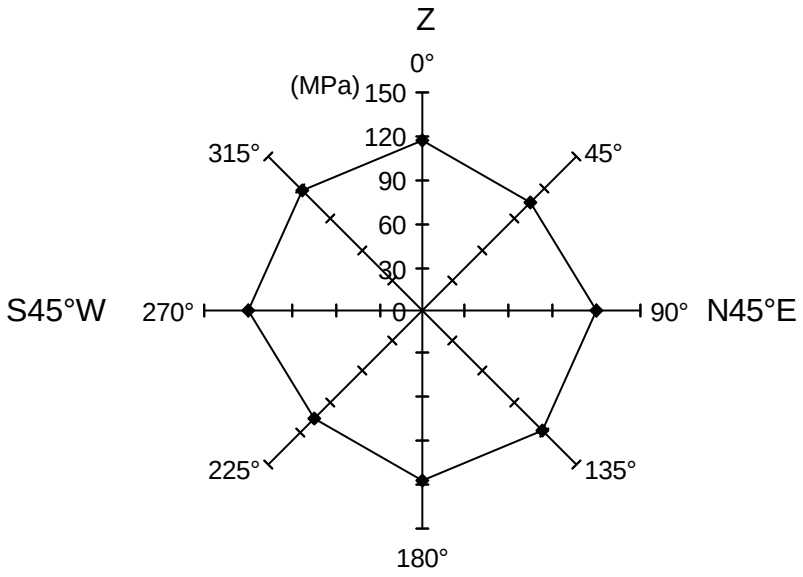

Fig. 3.17c *Variation of directional rock mass strength on the vertical plane striking N45°E for NGI box #5 (fine grained granite)*

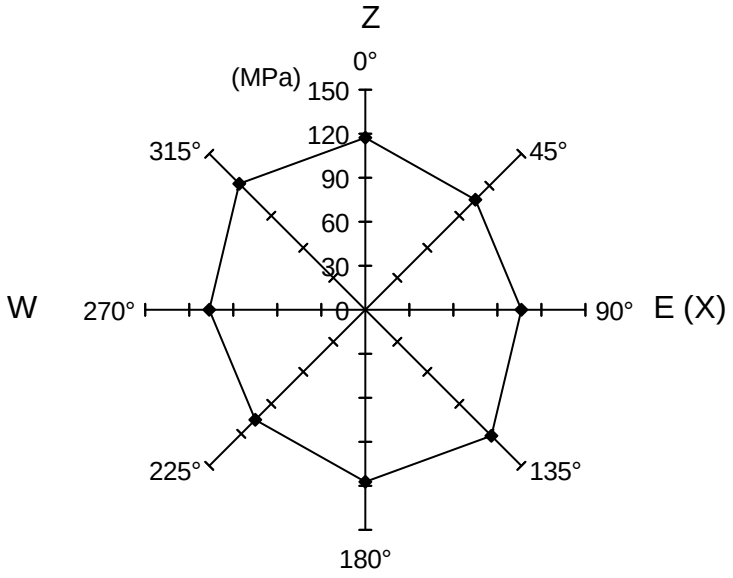

Fig. 3.17d *Variation of directional rock mass strength on the vertical plane striking E – W for NGI box #5 (fine grained granite)*

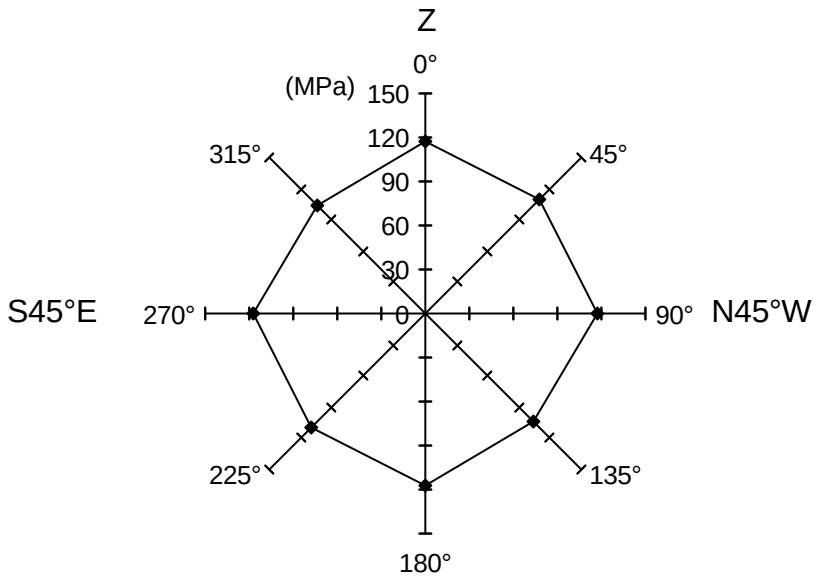

Fig. 3.17e *Variation of directional rock mass strength on the vertical plane striking N45°W for NGI box #5 (fine grained granite)*

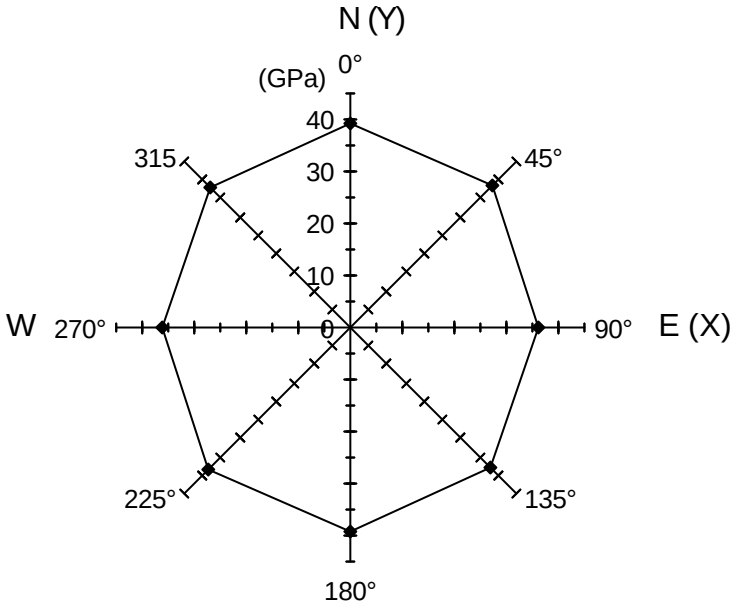

Fig. 3.18a *Variation of directional rock mass modulus on the horizontal plane for NGI box #5 (fine grained granite)*

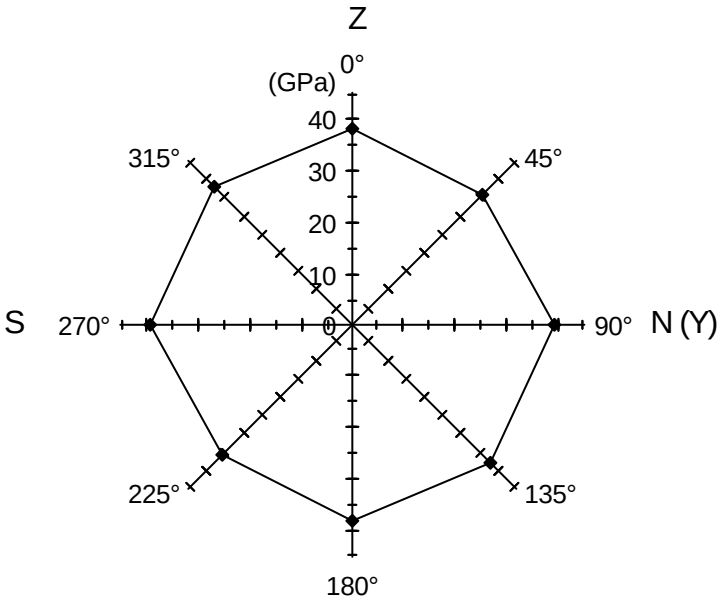

Fig. 3.18b *Variation of directional rock mass modulus on the vertical plane striking N – S for NGI box #5 (fine grained granite)*

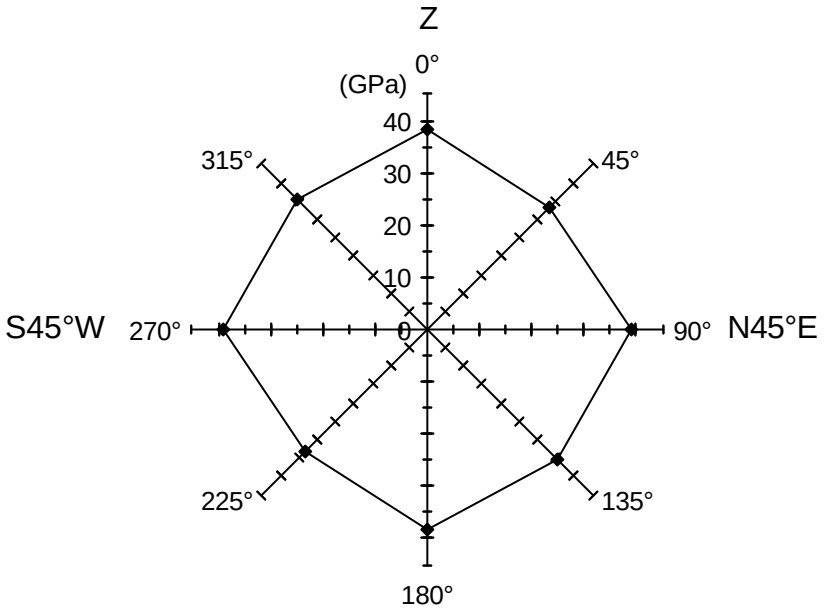

Fig. 3.18c *Variation of directional rock mass modulus on the vertical plane striking N45°E for NGI box #5 (fine grained granite)*

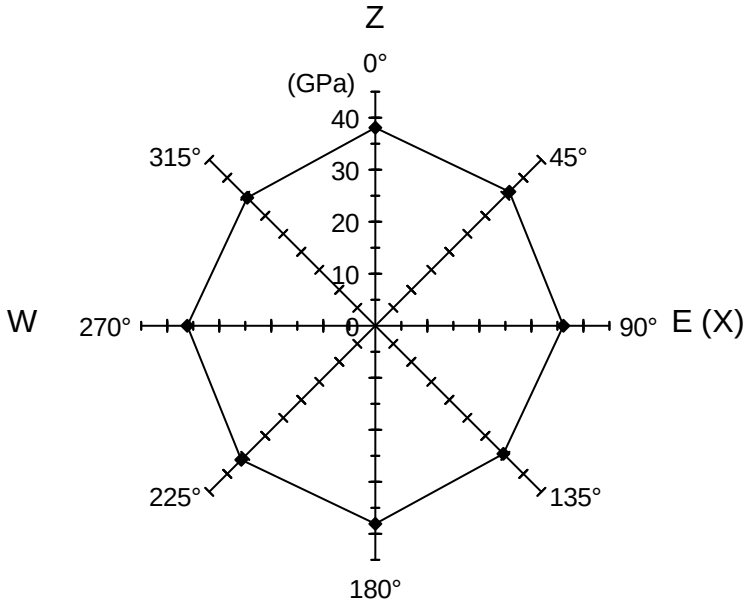

Fig. 3.18d *Variation of directional rock mass modulus on the vertical plane striking E – W for NGI box #5 (fine grained granite)*

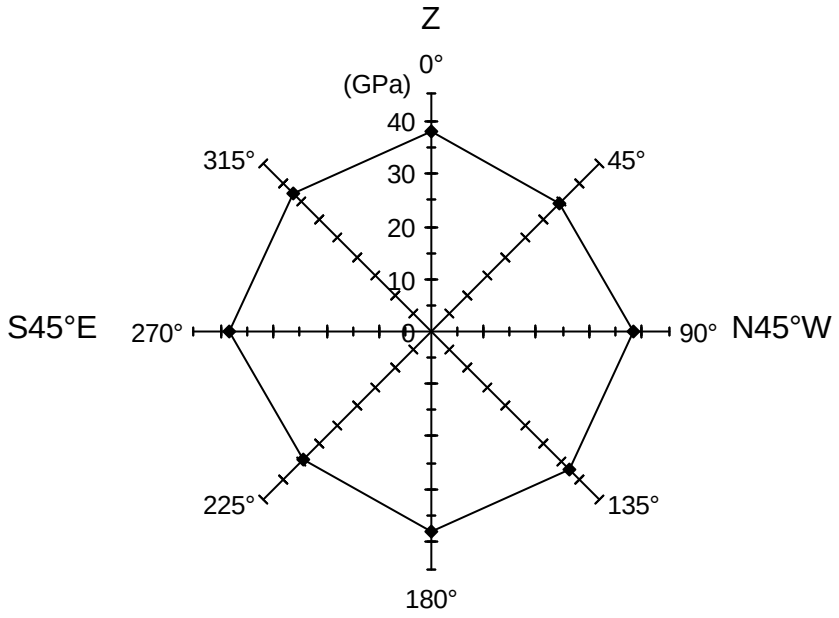

Fig. 3.18e *Variation of directional rock mass modulus on the vertical plane striking N45°W for NGI box #5 (fine grained granite)*

3.2.2.4. NGI block # 49 that consists of a mixed lithology

Table 3.5 shows the different block sizes used (apart from the smallest block) to perform 3-D stress analysis on blocks having the mixed lithology. A block size of 10.1m was used to represent the smallest block for mixed lithology. Table 3.5 also shows how the equivalent continuum material and fictitious joint property values changed with the block size. The considered different block rotations for the 30m cube and the mean in-situ stress systems obtained for these rotations are given in Table 3.4. Typical stress-strain and strain-strain plots obtained for the 30m block for one of the rotations are shown in Figures 3.19 through 3.21. As for the 30m Aspo diorite blocks, block strengths, tangent rock mass moduli and Poisson's ratios were obtained for each 30m block size that consists of the selected mixed lithology for each of the considered rotations given in Table 3.4. All the obtained block strengths and rock mass moduli for the 30m block size are given in Tables 3.6 and 3.7, respectively. All the obtained Poisson's ratios for the 30m block size are given in Table 3.8. All these values given in Tables 3.6 through 3.8 can be considered as mean values in each direction because they were calculated using mean in-situ stresses and mean mechanical property values. Figures 3.22 and 3.23 show the anisotropy of block strength and rock mass modulus in 3-D, respectively. The calculated mean principal directions and magnitudes of principal block strengths are given in Table 3.9. The calculated mean principal directions and mean magnitudes of principal rock mass moduli are given in Table 3.10. Based on the calculated 3-D rock block strength and deformability values for the 30m block size, the mean estimations are given for rock block strength (Table 3.11), rock mass modulus (Table 3.12) and Poisson's ratio (Table 3.12) for NGI block # 49 that consists of the mixed lithology. As for Aspo diorite, 5^{th} and 95^{th} percentiles were estimated for the three rock mass parameters of the mixed lithology. The obtained 5^{th} and 95^{th} percentiles are given in Tables 3.11 and 3.12.

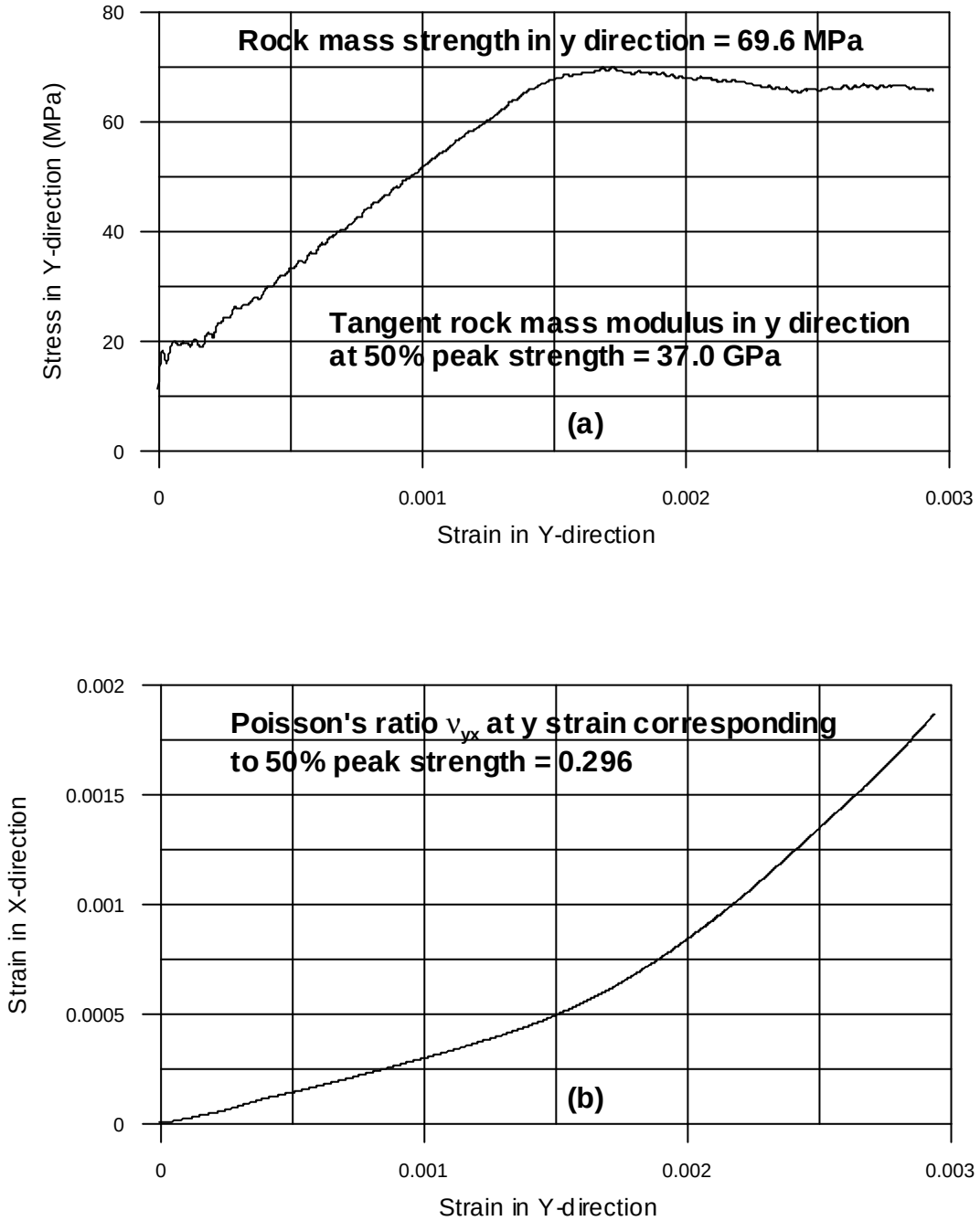

Fig. 3.19 *(a) Y stress vs. Y strain, (b) X strain vs. Y strain and (c) Z strain vs. Y strain plots obtained for 30m cubic block of a mixed lithology, having horizontal rotation = -45º and vertical rotation = 0º by application of a constant velocity of 0.05m/sec in the Y direction*

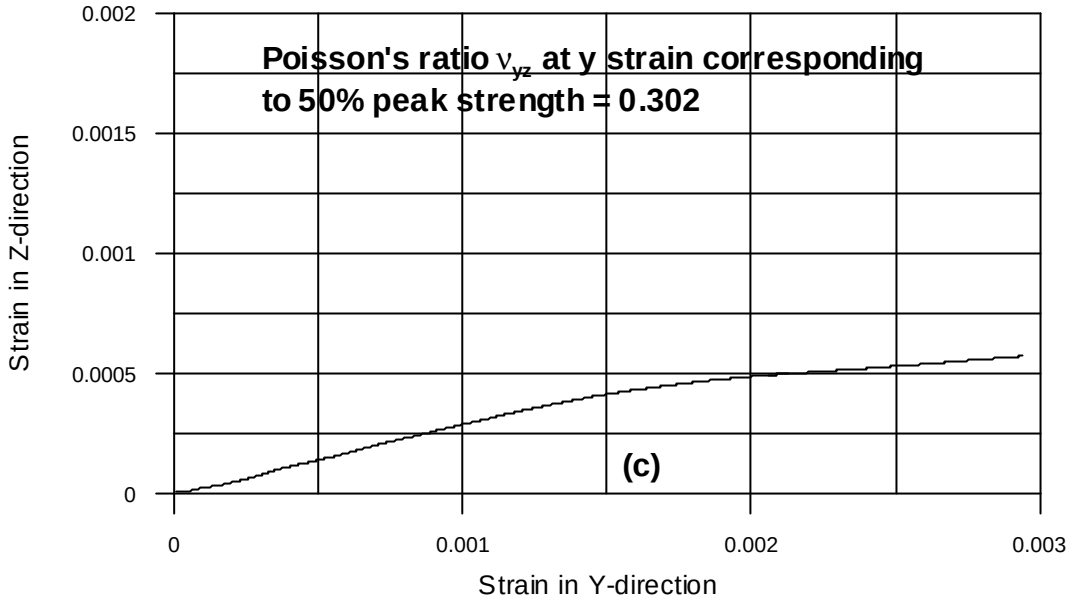

Fig. 3.19 *Continued*

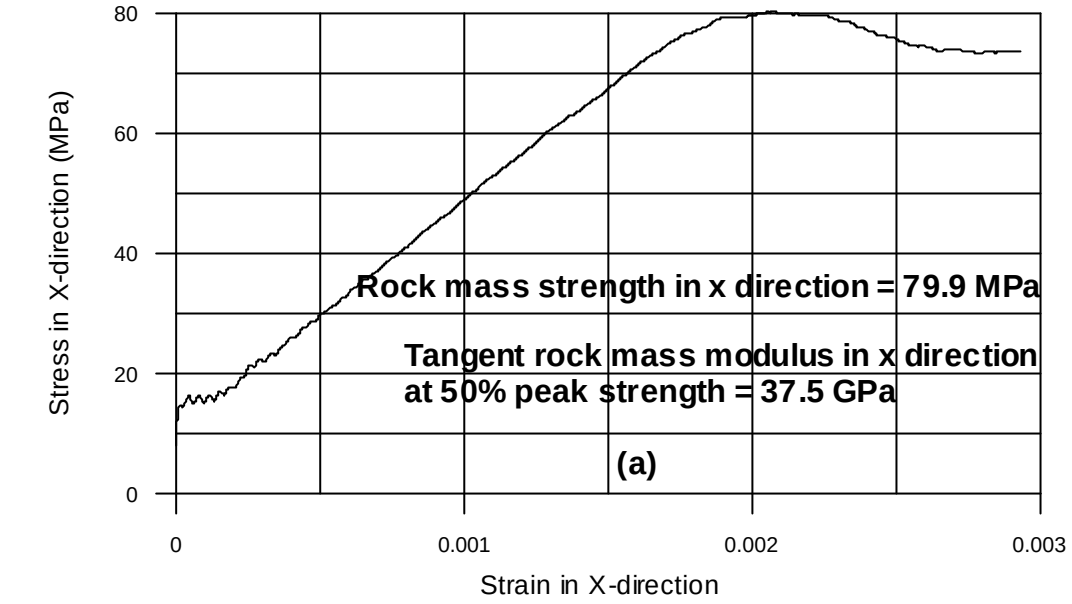

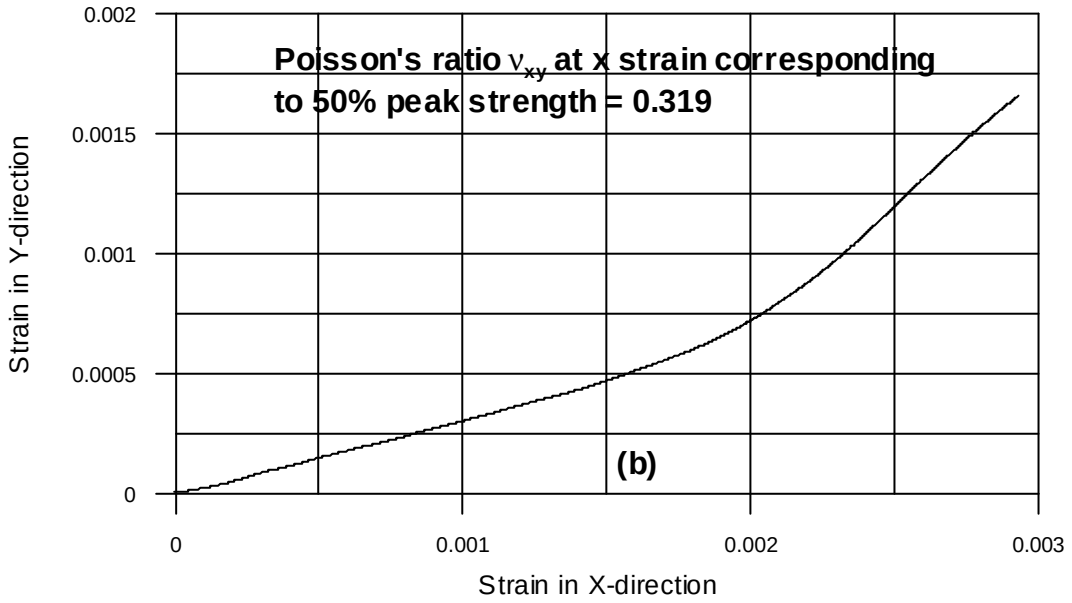

Fig. 3.20 *(a) X stress vs. X strain, (b) Y strain vs. X strain and (c) Z strain vs. X strain plots obtained for 30m cubic block of a mixed lithology, having horizontal rotation = -45º and vertical rotation = 0º by application of a constant velocity of 0.05m/sec in the X direction*

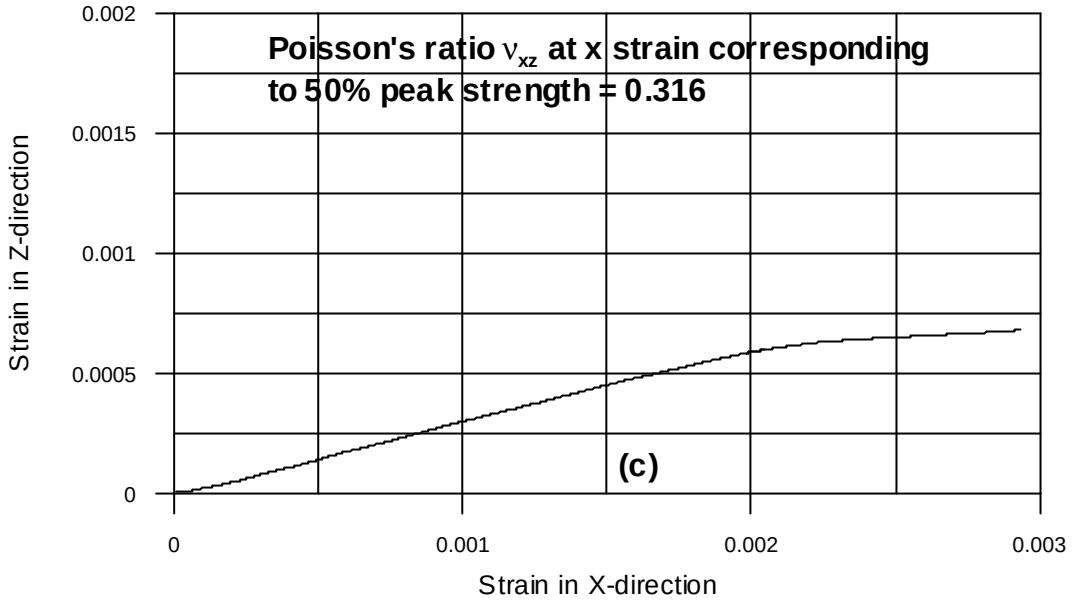

Fig. 3.20 *Continued*

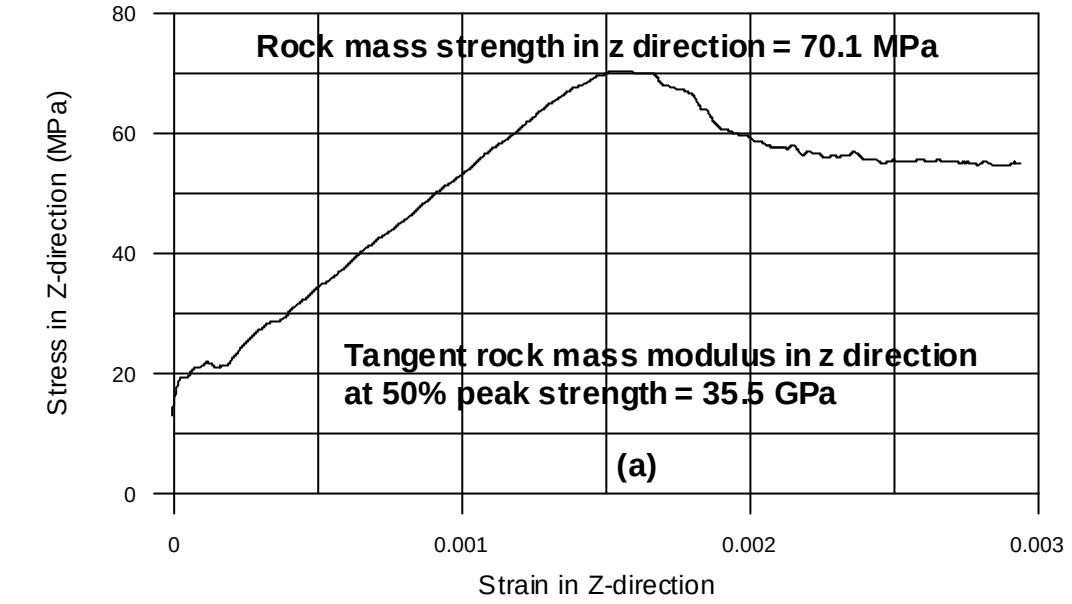

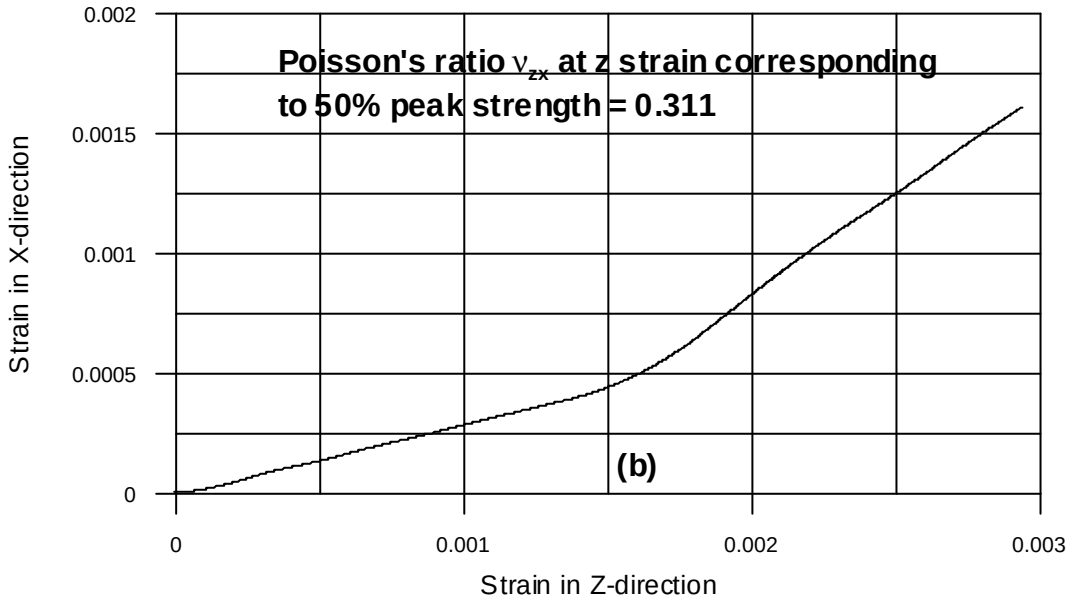

Fig. 3.21 *(a) Z stress vs. Z strain, (b) X strain vs. Z strain and (c) Y strain vs. Z strain plots obtained for 30m cubic block of a mixed lithology, having horizontal rotation = -45º and vertical rotation = 0º by application of a constant velocity of 0.05m/sec in the Z direction*

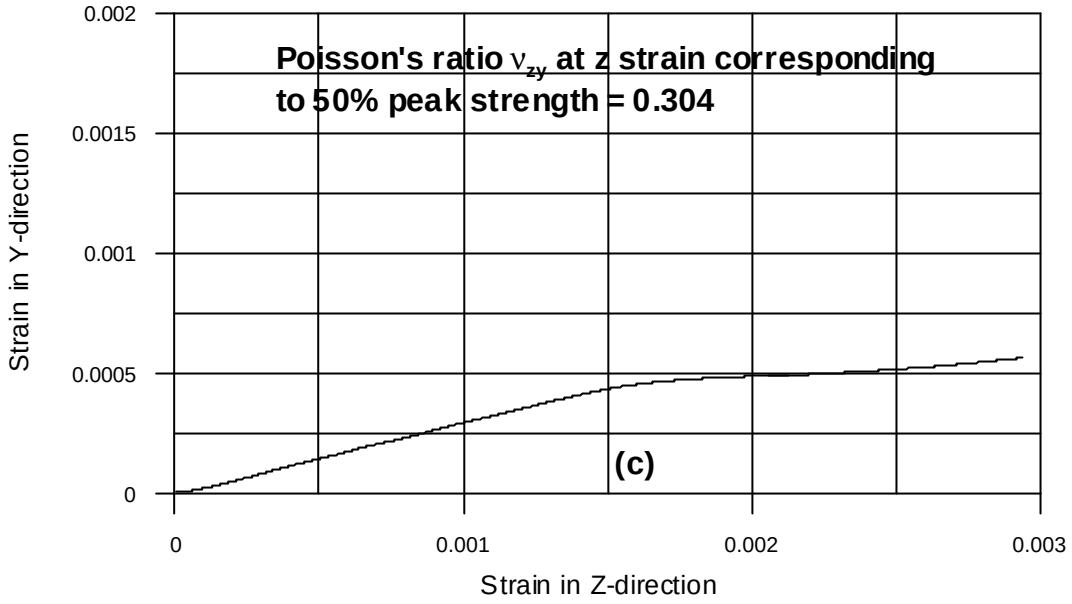

Fig. 3.21 *Continued*

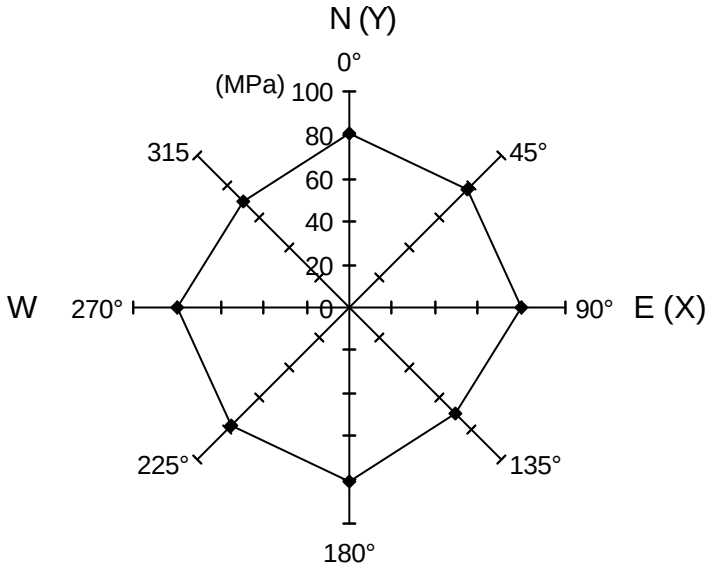

Fig. 3.22a *Variation of directional rock mass strength on the horizontal plane for NGI box #49 (mixed lithology)*

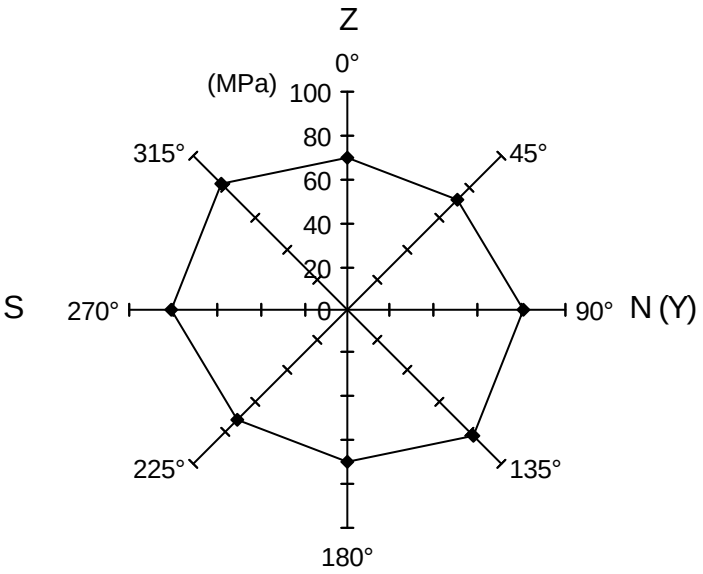

Fig. 3.22b *Variation of directional rock mass strength on the vertical plane striking N – S for NGI box #49 (mixed lithology)*

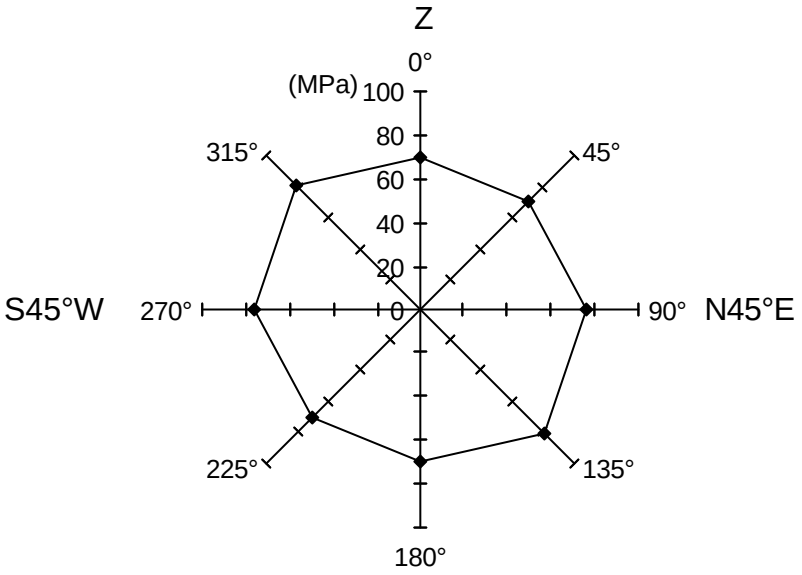

Fig. 3.22c *Variation of directional rock mass strength on the vertical plane striking N45°E for NGI box #49 (mixed lithology)*

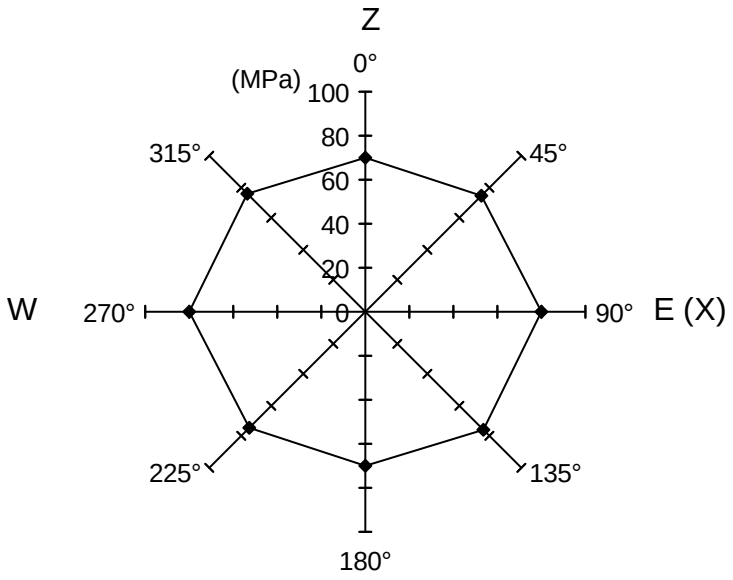

Fig. 3.22d *Variation of directional rock mass strength on the vertical plane striking E – W for NGI box #49 (mixed lithology)*

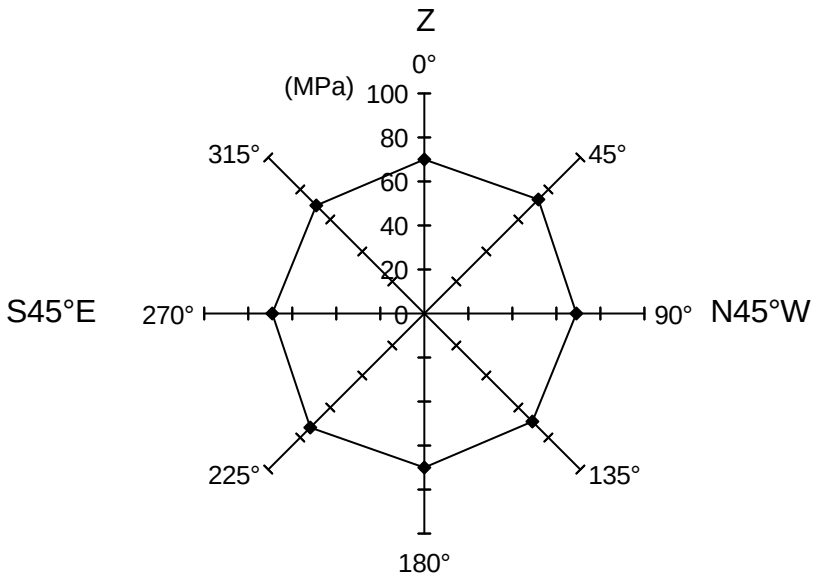

Fig. 3.22e *Variation of directional rock mass strength on the vertical plane striking N45°W for NGI box #49 (mixed lithology)*

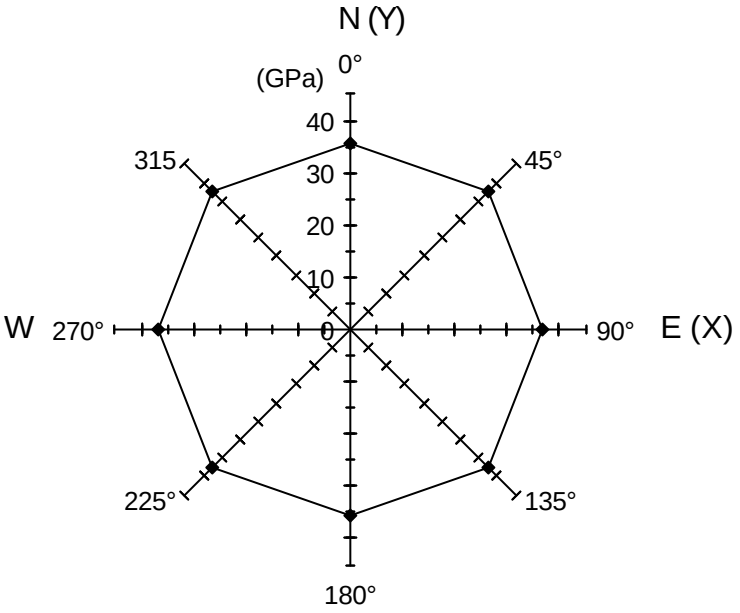

Fig. 3.23a *Variation of directional rock mass modulus on the horizontal plane for NGI box #49 (mixed lithology)*

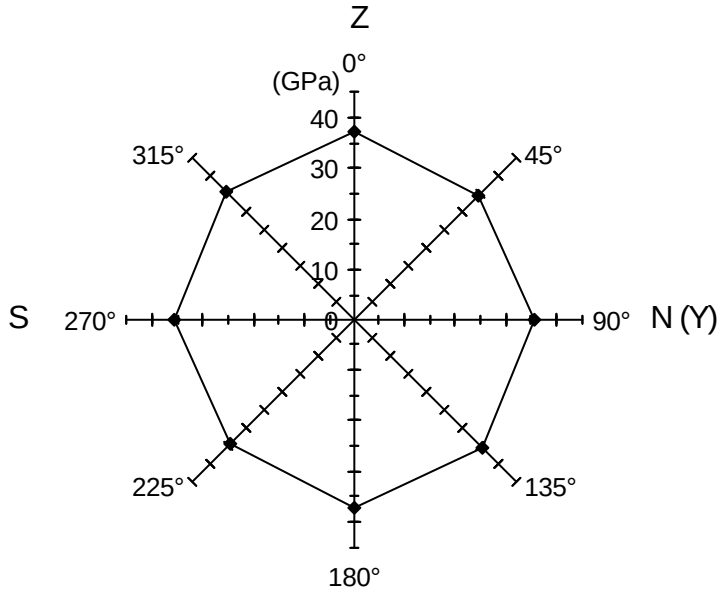

Fig. 3.23b *Variation of directional rock mass modulus on the vertical plane striking N – S for NGI box #49 (mixed lithology)*

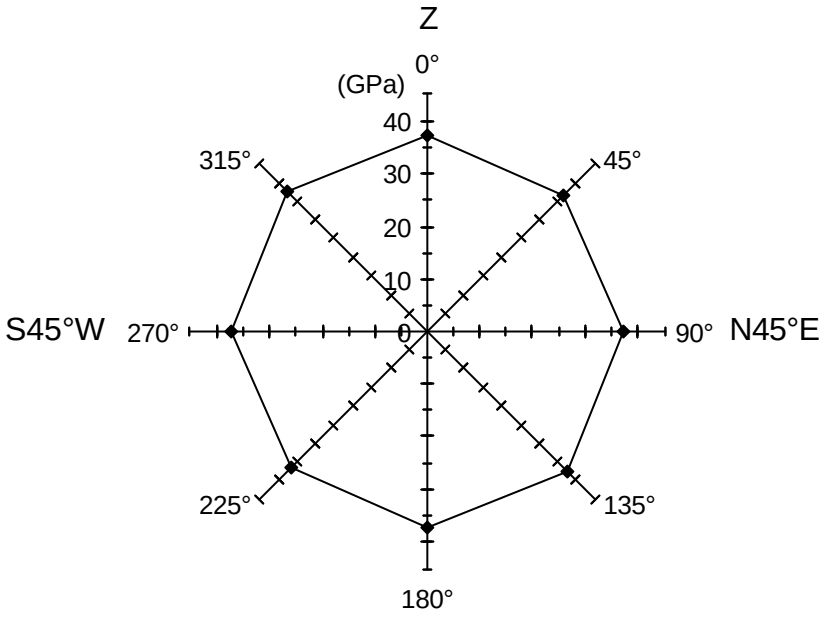

Fig. 3.23c *Variation of directional rock mass modulus on the vertical plane striking N45°E for NGI box #49 (mixed lithology)*

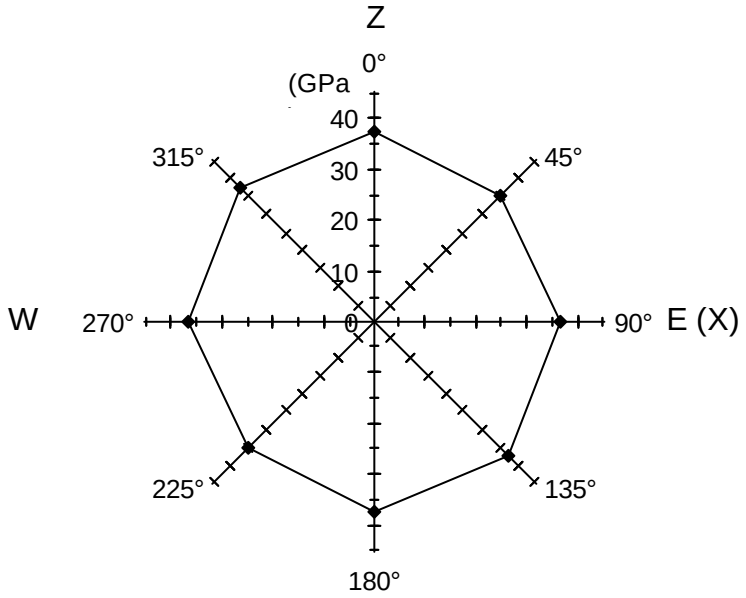

Fig. 3.23d *Variation of directional rock mass modulus on the vertical plane striking E – W for NGI box #49 (mixed lithology)*

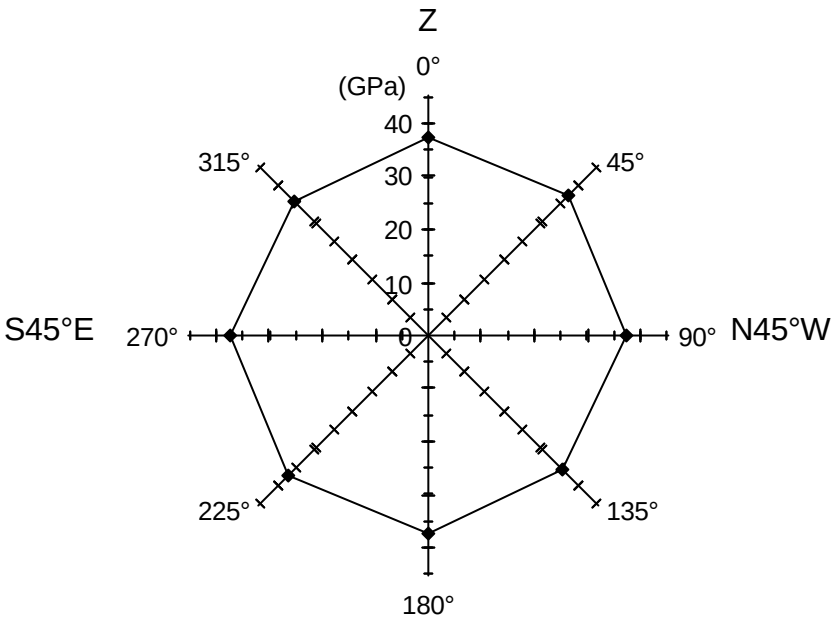

Fig. 3.23e *Variation of directional rock mass modulus on the vertical plane striking N45°W for NGI box #49 (mixed lithology)*

4. Discussion and conclusions

Note that the mechanical property data were available only for Aspo diorite. These property values were used to represent the mechanical property values for all the 4 selected lithologies. Therefore, the differences obtained for rock block strength and deformability properties of the 4 selected NGI blocks reflect the differences of the fracture systems and in situ stress system at different depths. In Table 2.1, a confidence level of 2 was assigned to the principal in-situ stress values used in the calculations performed in this project. With respect to the fracture systems, it is important to note that due to lack of fracture size data for different lithologies, the same probability distribution was assumed to represent the fracture size of each lithology considered. In a previous report submitted by Kulatilake & Associates (Kulatilake and Um, 2001), it was mentioned that both the quality and quantity of the available orientation data for the project were inadequate. Therefore, the confidence level of the calculated anisotropic directions and corresponding magnitudes is low (level 3 according to the specifications given in the report by Andersson, 2001). However, with respect to the mean estimations of rock block strength and deformability, it is reasonable to assign a confidence level of 2.

Note that the lowest in-situ stresses were obtained for NGI block #s 5 and 49. The highest 3-D fracture intensity was obtained for NGI block # 49. Therefore, intuitively, NGI block # 49 should have the lowest strength and highest deformability. The in-situ stress at NGI block number 169 is higher than that at NGI block # 5. The 3-D fracture frequency of NGI block # 169 is lower than that at NGI block number 5. Therefore, intuitively, NGI block # 5 should show a lower strength and higher deformability than NGI block number 169. The in-situ stresses at NGI block #s 5 and 49 are the same. However, the 3-D fracture frequency of NGI block number 5 is lower than that of NGI block number 49. Therefore, intuitively, NGI block # 5 should show a higher strength and lower deformability than NGI block number 49. NGI block #s 409 and 5 have almost the same 3-D fracture intensity. However, the in-situ stress at NGI block number 409 is considerably higher than that at NGI block number 5. Therefore, intuitively, NGI block # 5 should show a lower strength and higher deformability than NGI block number 409.The obtained rock mass block strength and deformability results agree very well with these intuitions.

The intact rock strength at the 4 NGI blocks studied lie between 267 and 303 MPa. These values indicate that the intact rock is strong. For NGI block #s 409, 169, 5 and 49 the ratio of mean rock mass strength/mean intact rock strength was found to be 47%, 44%, 42% and 27%, respectively. For the 4 NGI blocks studied, the rock mass modulus was found to be between 49.9% and 57.5% of the intact rock Young's modulus value. The rock mass Poisson's ratio was found to be about 11-21% higher than the intact rock Poisson's ratio value. These percentages indicate the levels of weakening of the rock masses due to the presence of fractures.

Each 30m NGI block considered had more than 6000 fractures. Therefore, it was not realistic to perform 3-D stress analysis on a 30m block directly considering each block to consist of intact rock, actual fractures and fictitious joints. To estimate strength and deformability of 30m blocks, it was necessary to perform stress analysis on several increasing block sizes before performing the stress analysis on the 30m block size. In going from second block size to the third, and third block size to the fourth so on, the equivalent continuum material was considered as isotropic. However, it is strictly anisotropic. At present, the 3DEC code does not have the capability of accommodating anisotropic equivalent continuum material properties. Due to this reason, most probably the obtained results for anisotropy of rock mass strength and deformability may be less than the actual level of anisotropy that exists in the field. From the calculations performed, for NGI block #s 409, 169, 5 and 49 the ratio of mean major principal rock mass strength/mean minor principal rock mass strength turned out to be 1.28, 1.32, 1.21 and 1.18, respectively. The performed calculations provided values of 1.21, 1.13, 1.15 and 1.06 for the ratio of mean major principal rock mass modulus/mean minor principal rock mass modulus for NGI block #s 409, 169, 5 and 49, respectively.

References

Andersson, J., 2001. Format for the submission of the Test Case individual and combined predictions.

Cundall, P.A., 1988. Formulation of a Three-Dimensional Distinct Element Model - Part 1. A Scheme to Detect and Represent Contacts in a System Composed of Many Polyhedral Blocks. International Journal of Rock Mech. Min. Sci. Vol. 25, No.3, pp. 107-116.

Hart, R., Cundall, P.A. and Lemos, J., 1988. Formulation of a Three-Dimensional Distinct Element Model-Part II: Mechanical Calculations for Motion and Interaction of a System Composed of Many Polyhedral Blocks. International Journal of Rock Mech. & Min. Sci, Vol.25, pp. 117-126.

ITASCA Consulting Group Inc., 1999. 3DEC Version 2 Users Guide.

Klasson, H. and Leijon, B., 1989. Hydrofracturing stress measurements in borehole KAS02, Aspo. A Part of SKB Progress Report 25-89-17.

Kulatilake, P.H.S.W., Liang, J. and Gao, H., 2001.Experimental and numerical simulations of jointed rock block strength under uniaxial loading. ASCE Jour. of Engineering Mechanics, Vol. 127, No. 12, pp. ??-??, 2001.

Kulatilake, P.H.S.W., Ucpirti, H., Wang, S., Radberg, G. and Stephansson, O., 1992. Use of the Distinct Element Method to Perform Stress Analysis in Rock with Non-Persistent Joints and to Study the Effect of Joint Geometry Parameters on the Strength and Deformability of Rock Masses. Rock Mechanics and Rock Engineering, Vol. 25, pp. 253-274.

Kulatilake, P.H.S.W. and Um, J., 2002. Fracture network models In three dimensions for four 30m cubes located at a depth region of 400-500m at Äspö HRL. International Progress Report, IPR-02-12. Swedish Nuclear Fuel and Waste Management Company, Stockholm, Sweden.

Kulatilake, P.H.S.W., Wang, M. and Um, J.1999. Estimation of REV size and three dimensional (3D) hydraulic conductivity tensor for the metamorphic rock mass of the Arrowhead East Tunnel Site, Inland Feeder project through 3D discrete fracture fluid flow modeling. Technical Report submitted to Metropolitan Water District of Southern California.

Kulatilake, P.H.S.W., Wang, S. and Stephansson, O., 1993. Effect of finite size joints on the deformability of jointed rock in three dimensions. Int. J. Rock Mech. Min. Sci. & Geomech. Abstr. v. 30, pp. 479-501.

Lanaro, F., 2001. Determination of the normal and shear stiffness of rock joints: geometry, normal and shear stiffness. A report submitted to SKB.

Nisca, D.H., 1988. Geophysical laboratory measurements on core samples from KLX01, Laxemar and KAS02, Aspo. SKB Progress Report 25-88-06.

Nordlund, E., Li, Chunlin and Carlsson, B., 1999. Mechanical properties of the diorite in the prototype repository at Aspo HRL. SKB International Progress Report 99-25.

Wang, S. and Kulatilake, P.H.S.W., 1993. Linking Between Joint Geometry Models and a Distinct Element Method in Three Dimensions to Perform Stress Analyses in Rock Masses Containing Finite Size Joints. Soils and Foundations, Vol. 33, No. 4, pp. 88-98.

Appendix

Rock mass strength and rock mass modulus summarized in histograms for NGI block #s 409, 169, 5 and 49.

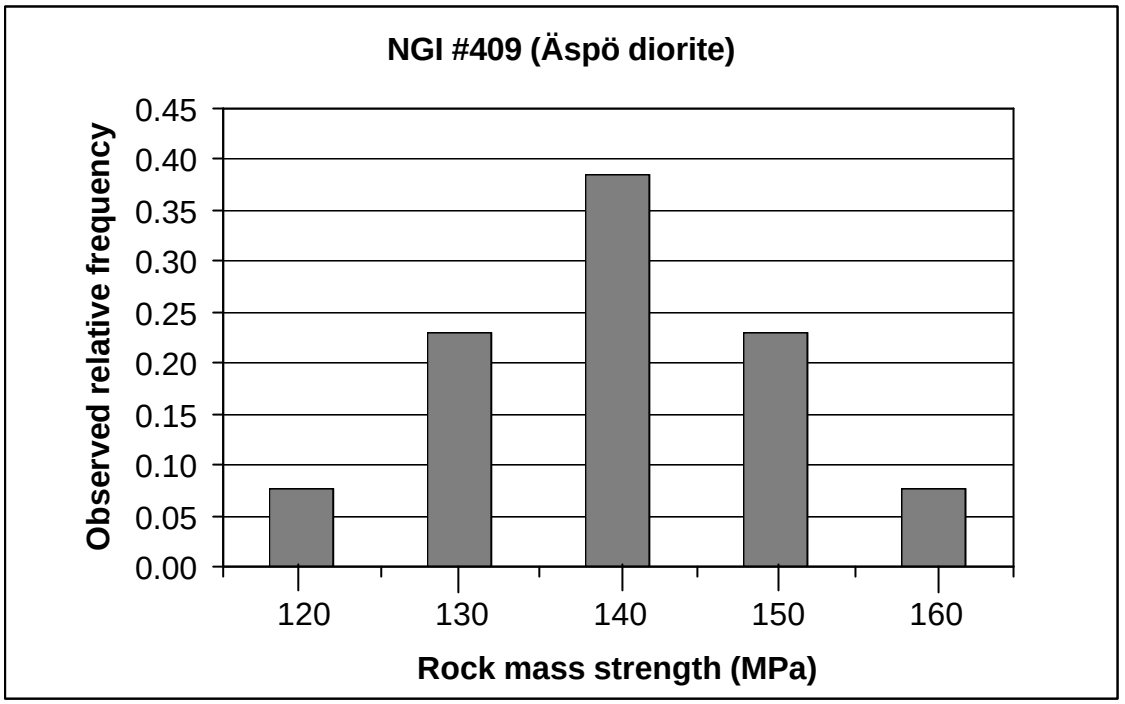

Mean (MPa)	Standard deviation (MPa)	Coefficient of variation
140.09	12.23	0.09

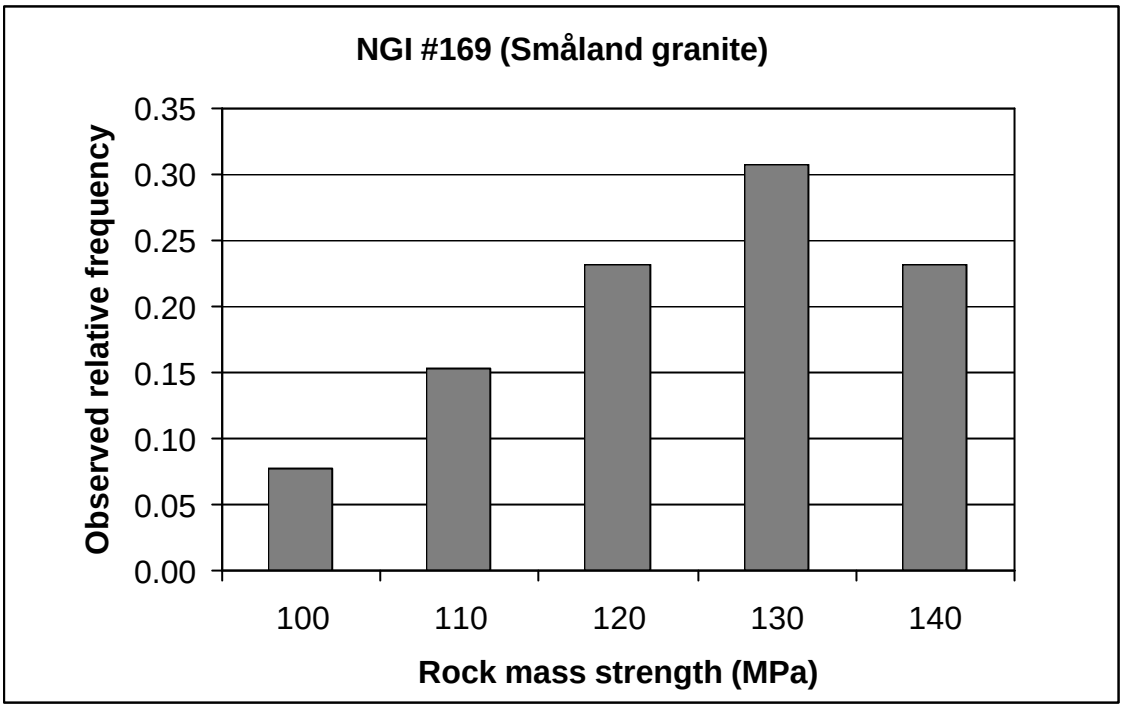

Mean (MPa)	Standard deviation (MPa)	Coefficient of variation
124.27	13.13	0.11

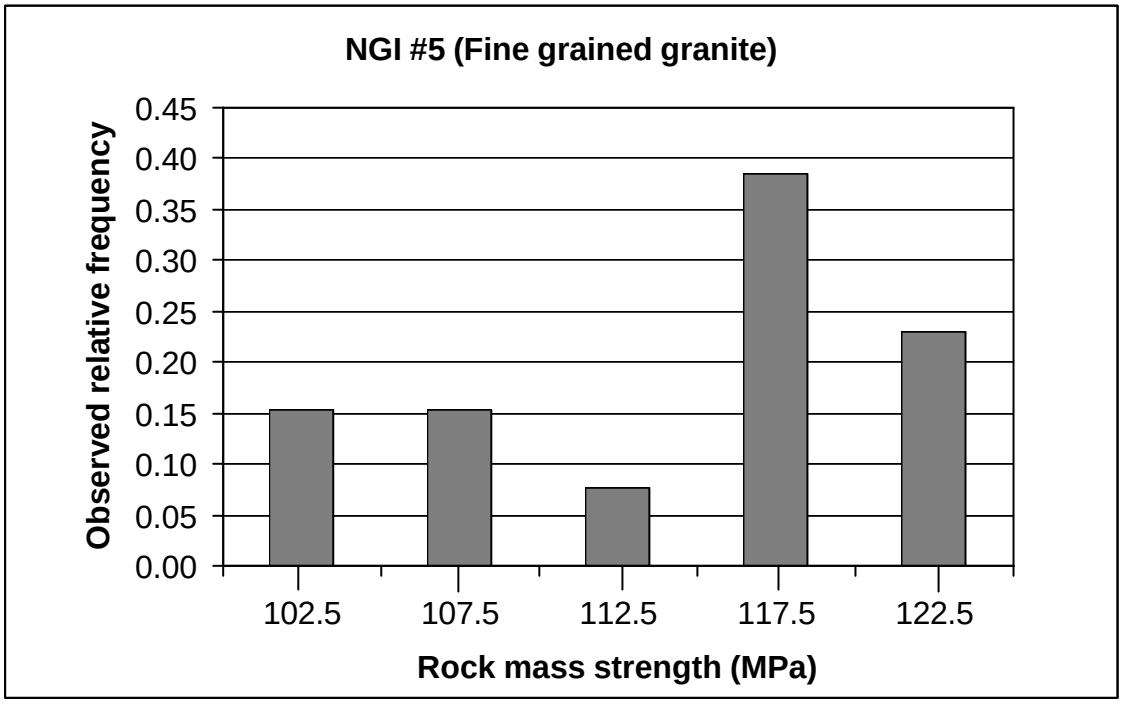

Mean (MPa)	Standard deviation (MPa)	Coefficient of variation
114.37	6.92	0.06

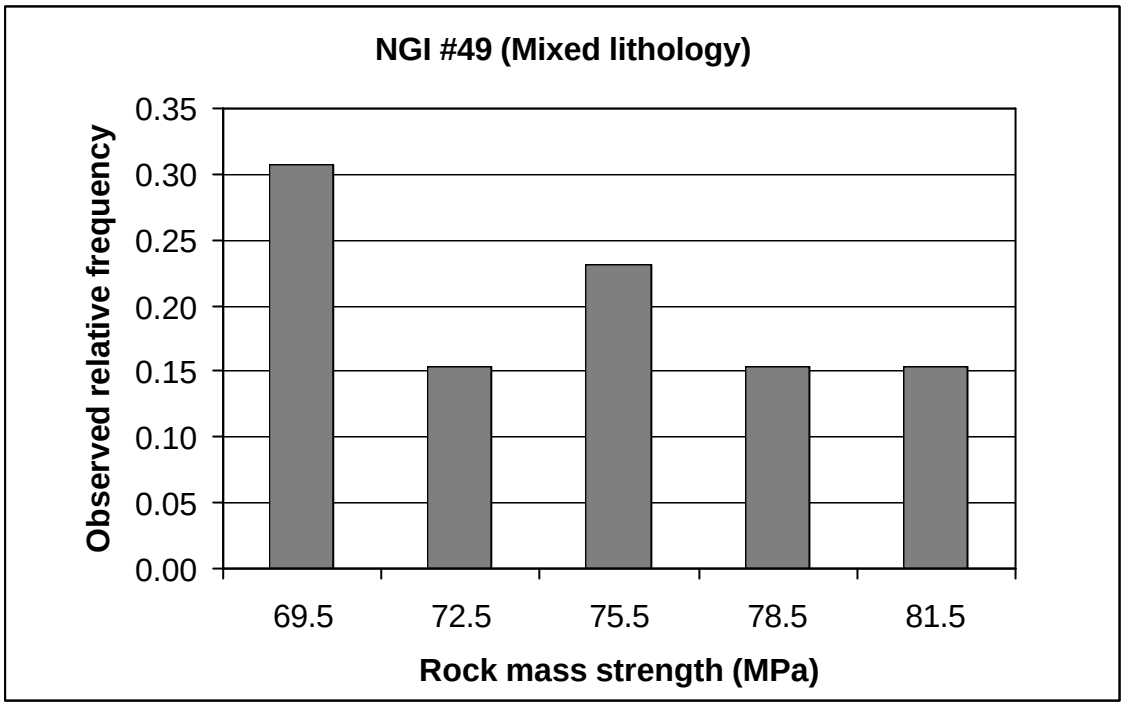

Mean (MPa)	Standard deviation (MPa)	Coefficient of variation
75.02	4.44	0.06

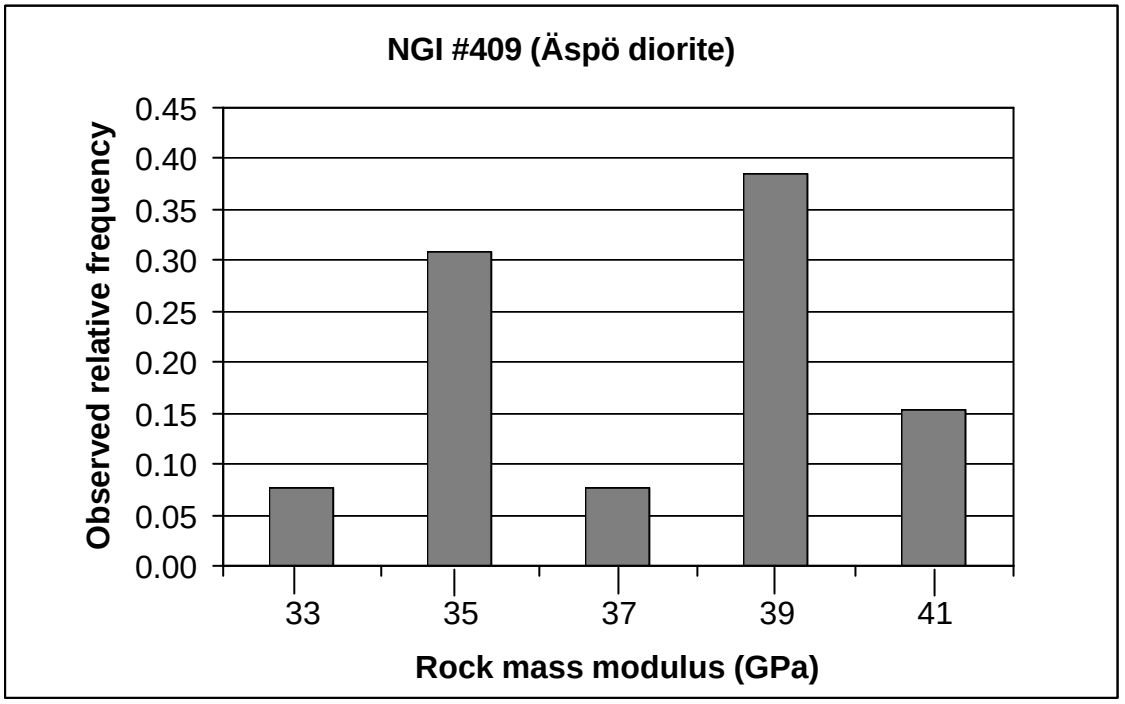

Mean (GPa)	Standard deviation (GPa)	Coefficient of variation
37.24	2.70	0.07

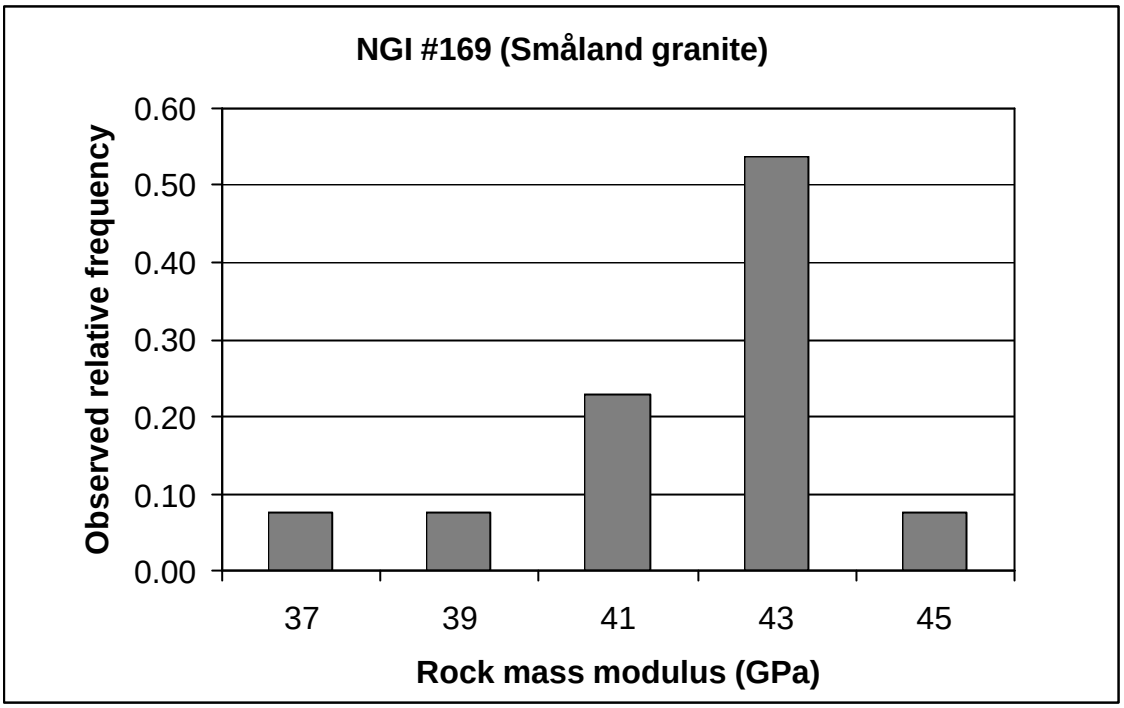

Mean (GPa)	Standard deviation (GPa)	Coefficient of variation
42.00	1.85	0.04

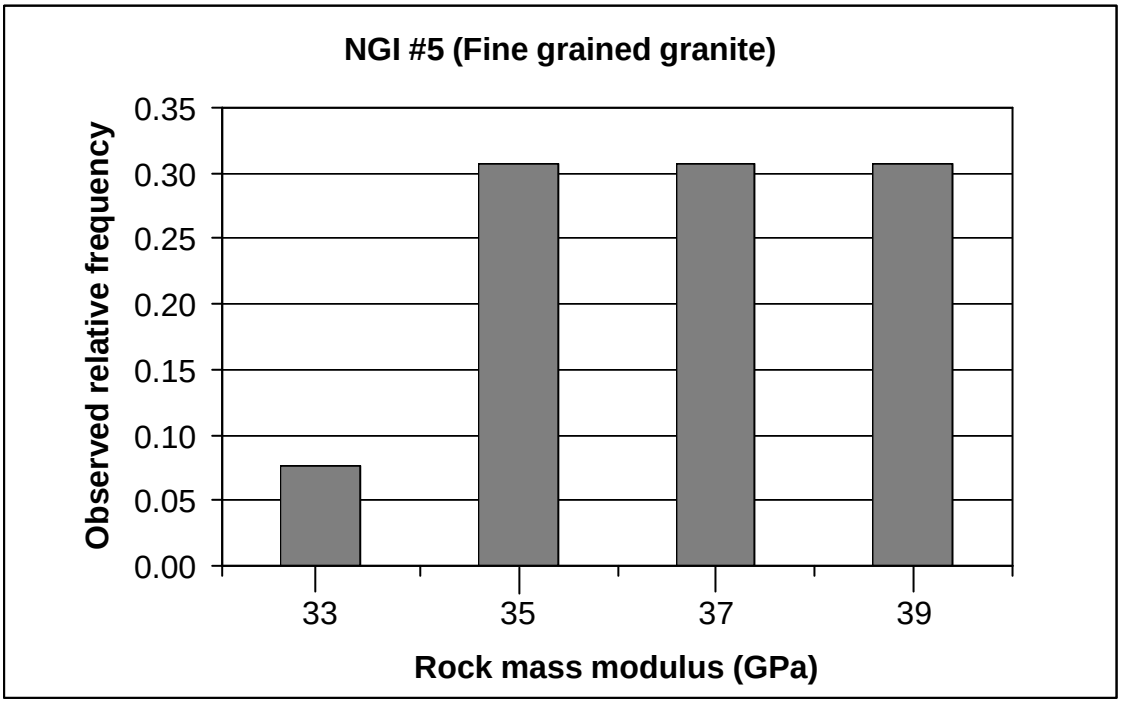

Mean (GPa)	Standard deviation (GPa)	Coefficient of variation
36.42	1.96	0.05

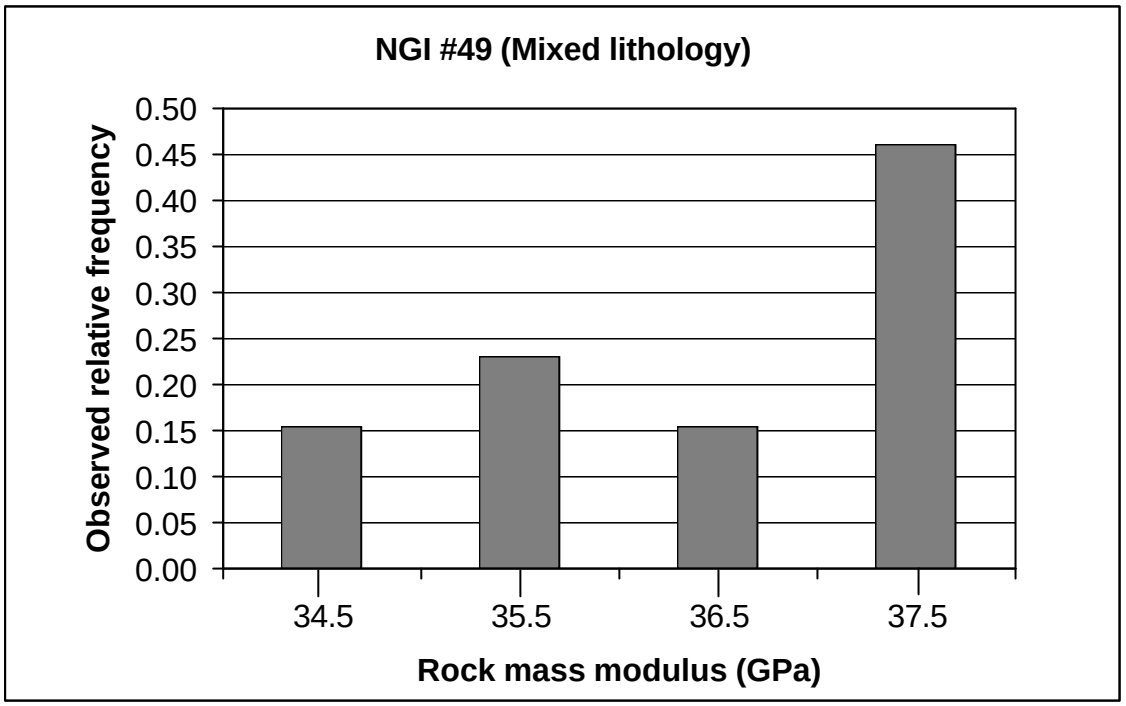

Mean (GPa)	Standard deviation (GPa)	Coefficient of variation
36.37	0.95	0.03